Aus dem Institut für Physiologie
der Medizinischen Fakultät Charité – Universitätsmedizin Berlin

DISSERTATION

In silico and in vitro investigations on the antiproliferative
efficacy of novel tyrosine kinase inhibitors in hepatocellular
carcinoma

zur Erlangung des akademischen Grades
Doctor medicinae (Dr. med.)

vorgelegt der Medizinischen Fakultät
Charité – Universitätsmedizin Berlin

von

Lisa Chiara Gosch

Aus Graz, Österreich

Datum der Promotion: 04.03.2022

Preface

Partial results of the present work were published in:

Schaller E, Ma A, Gosch LC, Klefenz A, Schaller D, Goehringer N, Kaps L, Schuppan D, Volkamer A, Schobert R, Biersack B, Nitzsche B, Höpfner M. **New 3-Aryl-2-(2-thienyl)acrylonitriles with High Activity Against Hepatoma Cells.** International Journal of Molecular Sciences. 2021;22(5):2243.

Partial results of the present work have been presented on a conference poster:

Gosch LC, Schmitt F, Biersack B, Volkamer A, Höpfner M. **Bioinformatic and functional evaluation of novel EGFR-TKIs for the treatment of hepatocellular carcinoma.** Frankfurt Cancer Conference. 2018.

Table of Contents

I.   List of Figures

II. List of Tables

III. List of Abbreviations

(P/T)KI	(Protein/Tyrosine) Kinase Inhibitor
@TOME	@utomatic Threading Optimization Modelling and Evaluation
ADMET	Absorption – Distribution – Metabolism – Excretion – Toxicity
AGC	PKA, PKG and PKC Containing Families (Kinase Group)
ATP	Adenosine Triphosphate
CADD	Computer-Aided Drug Discovery
CAMK	Calcium/Calmodulin-Dependent Protein Kinase (Kinase Group)
ChEMBL	Chemical Database of the European Molecular Biology Laboratory
CK1	Casein Kinase 1 (Kinase Group)
CLK1	Dual Specificity Protein Kinase CLK1 (CDC-like Kinase 1)
CMGC	CDK, MAPK, GSK3 and CLK Containing Families (Kinase Group)
DFG	D: Aspartate, F: Phenylalanine, G: Glycine
EGFR	Epidermal Growth Factor Receptor
ES5D	Electroshape 5D
FDA	Food and Drug Administration
HCC	Hepatocellular Carcinoma
HYDE	HYdrogen Bond and DEhydration
IC50	Inhibitory Concentration needed to reduce activity to 50%
iRAISE	inverse RApid Index-based Screening Engine
KIT / cKit	Mast/Stem Cell Growth Factor Receptor
LIST	Large-scale Inverse Screening Tool
LPE	Ligand Position Error
MACCS	Molecular ACCess System
MD	Molecular Dynamics
PDB	Protein Data Bank
PDGFR	Platelet-derived Growth Factor Receptor
Pim-1	Serine/Threonine-Protein Kinase Pim-1
Pim-2	Serine/Threonine-Protein Kinase Pim-2
pKd	Predicted Dissociation Constant

RGC	Receptor Guanylate Cyclase (Kinase Group)
SAR	Structure-Activity Relationship
SDF	Spatial Data Files
SMARTS	SMiles ARbitrary Target Specification
SMILES	Simplified Molecular Input Line Entry Specification
STE	Homologues of Yeast Sterile 7, 11, 20 Kinases (Kinase Group)
TK	Tyrosine Kinases (Kinase Group)
TKL	Tyrosine-like Kinase (Kinase Group)
VEGFR1 / FLT1	Vascular Endothelial Growth Factor Receptor 1
VEGFR2 / KDR	Vascular Endothelial Growth Factor Receptor 2

IV. Abstract

IV.I Abstract *(English)*

Introduction. Hepatocellular carcinoma (HCC) is one of the most common cancers worldwide and still lacks effective treatment for its advanced stages. While kinase inhibitors (KIs) have had first successes as systemic therapies, they only provide moderately improved prognosis compared to the best palliative care. Discovering more effective drugs – especially for targeted therapies – is a time-consuming and costly process. In recent decades, computational methods have therefore been increasingly integrated into drug research and development.

The aim of this thesis was to determine the kinase inhibitory and anticancer effects of a panel of new potential tyrosine kinase inhibitors (thiophenes and bromobenzenes) using a combined *in silico* and *in vitro* approach.

Methods. Three computational ligand- (SwissTargetPrediction) and structure-based (@TOME, iRAISE) target prediction methods were applied for the most promising thiophene (**Thio-Iva**). Correlated results (with additional targets relevant for HCC) were verified with a radiometric kinase activity assay (Eurofins KinaseProfiler^{TM}). Docking studies (SeeSAR) were performed to investigate the binding mode and structure-activity relationship of all the novel compounds to **Thio-Iva's** identified main target VEGFR2. Additional molecular dynamics simulations (Desmond) were performed for **Thio-Iva** to verify the binding hypothesis. Potential toxicities and ADME properties of **Thio-Iva** and the most promising bromobenzene **Briva** were investigated with predictive computational webservices (eMolTox, SwissADME). Cell culture experiments were performed with HCC cell lines (HepG2, Huh-7) to investigate **Thio-Iva's** and **Briva's** growth inhibitory effects (crystal violet assay), acute unspecific toxicity (LDH release measurement) and activation of apoptotic pathways (caspase-3 activity assay).

Results and discussion. Six out of the 43 kinase targets selected for *in vitro* evaluation showed inhibition by **Thio-Iva** of over 50% (VEGFR1, VEGFR2, Pim-1, Pim-2, CLK1 and c-Kit). These results indicate some selectiveness, but most importantly the high inhibitory activity of **Thio-Iva** on VEGFR2 (89% at 10 µM) and VEGFR1 (75%). Docking studies with VEGFR2 showed a stable binding pose of **Thio-Iva** with a hydrogen bond at the important hinge region of VEGFR2. This pose stayed consistent over a molecular dynamics simulation of 100 ns, rationalizing the biological activity observed on this target.

There were few predicted toxic properties of **Thio-Iva** and **Briva**, which was complemented by the low toxicity measured in the wet lab experiments. Cell culture experiments also showed pronounced growth inhibitory effects and the induction of apoptosis by the two compounds on HCC cells. Overall, these results indicate that **Thio-Iva** in particular could be a promising lead compound for VEGFR2/multikinase inhibitors with strong anticancer activity.

IV.II   Abstract (German)

Einleitung. Das hepatozelluläre Karzinom (HCC) ist eine der häufigsten Krebsformen weltweit, und es fehlt immer noch an effektiven Therapien für fortgeschrittene Stadien. Zwar konnten Kinase-Inhibitoren (KIs) erste Erfolge als systemische Therapien erzielen, jedoch bieten sie nur eine moderat verbesserte Prognose im Vergleich zur besten palliativen Versorgung. Die Suche nach effektiveren Medikamenten – insbesondere für zielgerichtete Therapien (Targeted Therapies) – ist ein zeitaufwändiger und kostspieliger Prozess. In den letzten Jahrzehnten wurden daher zunehmend computergestützte Methoden in die Arzneimittelforschung und -entwicklung integriert.

Ziel dieser Arbeit war es, die kinaseinhibitorische und krebshemmende Wirkung eines Panels neuer potentieller Tyrosinkinase-Inhibitoren (Thiophene und Brombenzole) mit einem kombinierten Ansatz aus *in silico* und *in vitro* Methoden zu bestimmen.

Methoden. Zur Target-Vorhersage wurden drei bioinformatische liganden- (SwissTargetPrediction) und strukturbasierte (@TOME, iRAISE) Methoden für das vielversprechendste Thiophen **Thio-Iva** eingesetzt. Korrelierte Ergebnisse (mit zusätzlichen Targets mit Relevanz für HCC) wurden mit einem radiometrischen Kinase-Aktivitätsassay (Eurofins KinaseProfiler™) verifiziert. Um den Bindungsmodus und die Struktur-Aktivitäts-Beziehung der neuen Moleküle zu **Thio-Ivas** identifiziertem Haupt-Target VEGFR2 zu untersuchen, wurden Docking Studien (SeeSAR) durchgeführt. Für **Thio-Iva** wurden zusätzliche molekulardynamische Simulationen (Desmond) zur Verifikation der Bindungshypothese eingesetzt. Potentielle Toxizitäten und ADME-Eigenschaften der Moleküle wurden anhand des Thiophens **Thio-Iva** und des vielversprechendsten Brombenzols **Briva** mit prädiktiven bioinformatischen Webservern (eMolTox, SwissADME) untersucht. Zellkulturexperimente zur biologischen Validierung der beiden Moleküle **Thio-Iva** und **Briva** hinsichtlich Wachstumsinhibition (Kristallviolett-

Assay), Apoptose (Caspase-3 Aktivitätsassay) und unspezifischer Toxizität (LDH-Freisetzungs-Assay) wurden an HCC-Zelllinen (HepG2, Huh-7) durchgeführt.

Ergebnisse und Diskussion. Sechs der 43 Kinase-Targets, die für die *in vitro* Evaluierung ausgewählt wurden, zeigten eine Inhibition durch **Thio-Iva** von über 50% (VEGFR1, VEGFR2, Pim-1, Pim-2, CLK1 und c-Kit). Diese Ergebnisse weisen auf eine gewisse Selektivität, aber insbesondere auf eine hohe inhibitorische Aktivität von **Thio-Iva** gegen VEGFR2 (89% bei 10 µM) und VEGFR1 (75%) hin. Docking Studien mit VEGFR2 zeigten einen stabilen Bindungsmodus von **Thio-Iva**, mit einer Wasserstoffbrückenbindung and der wichtigen Hinge-Region von VEGFR2. Dieser Bindungsmodus blieb auch über eine molekulardynamische Simulation von 100 ns konsistent, was mit der beobachteten biologischen Aktivität an diesem Target übereinstimmt. Sowohl für **Thio-Iva** als auch für **Briva** wurden nur wenige toxische Eigenschaften vorhergesagt, was durch die geringe unspezifischen Toxizität in den eigenen Zellkultur-Untersuchungen ergänzt wurde. Zellkulturexperimente zeigten auch eine starke wachstumsinhibierende und Apoptose-induzierende Wirkung der beiden Moleküle in HCC Zelllinien. Insgesamt zeigten diese Ergebnisse, dass insbesondere **Thio-Iva** eine vielversprechende Leitstruktur für VEGFR2/Multikinase-Inhibitoren mit starker Antitumor-Wirkung darstellen könnte.

1 Introduction

1.1 *Hepatocellular Carcinoma*

1.1.1 Epidemiology and Etiology

Hepatocellular carcinoma (HCC) accounts for approximately 75% of primary liver cancers (1), which are considered the sixth most common cancer type worldwide, with rising incidence rates over the past few decades (2). Incidence for HCC is particularly rising in North America, Europe, and Australia, while some studies have reported a decrease in China (3) and Japan (4). HCC most commonly occurs as a result of liver disease and cirrhosis, which in turn is most often caused by alcoholic liver disease, viral infections such as hepatitis B and C, and non-alcoholic steatosis hepatis (NASH) (5). While reduction of viral risk factors have been tentatively successful, the emergence of widespread obesity and diabetes has led to a changing epidemiology of liver cancers (1).

1.1.2 Pathology

HCC develops in hepatocytes, most often as a result of oxidative stress and inflammation due to chronic liver disease (1). In western countries, up to 90% of HCC develops in cirrhotic livers (5). Development of HCC without underlying cirrhosis is less well understood, with at least part of these cases arising from malignant transformation of hepatocellular adenomas (6). While a number of genetic and epigenetic changes have been observed in HCC (Figure 1), there has not been a single driver of disease identified (7). HCC can be classified into a proliferative and a nonproliferative group, with the proliferative group often showing changes of signaling activity in the RAS, mTOR and IGF pathways, while the nonproliferative group is more heterogenous (7). A complex network of signaling pathways has been shown to be dysregulated in HCC in general, including the MAPK, Pi3K/AKT, JAK/STAT, TGFBR and WNT/b-catenin pathways (7). Growth factors also play an important role in the development of disease in HCC and many other cancers, and their receptors (such as EGFR (epidermal growth factor receptor) or VEGFR (vascular endothelial growth factor receptor)) have been widely explored as molecular targets in drug design (8).
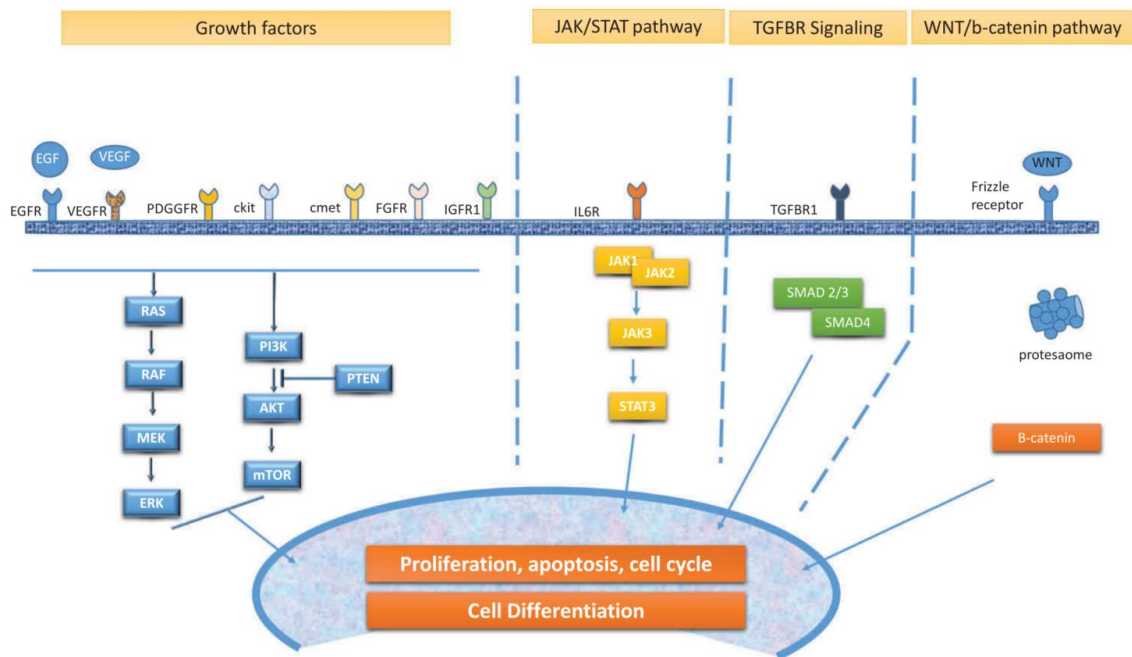
Figure 1. Pathways frequently dysregulated in HCC. Image from de Rosamel et al. (7).

1.1.3 Clinical Presentation and Diagnosis

Symptoms caused by HCC can vary widely. Patients undergoing regular screenings might be completely asymptomatic at time of diagnosis, while other patients can present with abdominal pain, weight loss, early saturation, a palpable mass, decompensation of previously stable liver cirrhosis, and paraneoplastic syndromes (9). These include hypoglycemia, erythrocytosis, hypercalcemia, diarrhea and skin changes, and are often associated with poor prognosis (10).

Regular screening for liver lesions (commonly with ultrasound and serological markers) is generally recommended for patients with liver cirrhosis, as well as those with chronic hepatitis B (11). Other high-risk groups in terms of family history, ethnicity and age may be included in surveillance programs, depending on different national guidelines. The objective is to diagnose patients at an early stage of disease to improve prognosis and applicability of therapeutic options (11).

Diagnosis in high-risk patients can be attempted with imaging methods like dynamic contrast-enhanced computer tomography, magnetic resonance imaging or ultrasound. Depending on the specific characteristics of contrast-enhancement, diagnosis of HCC may be possible without biopsy in this patient group (11). Patients without chronic liver disease are more likely to present with benign lesions or liver metastases of other tumor entities than with HCC (11). Therefore, diagnosis for this group additionally includes

screening for previously undetected liver disease and other malignancies. The final diagnostic option is a liver biopsy, which is generally recommended in order to verify the diagnosis for patients at low-risk for HCC (11). Once HCC is diagnosed, staging is recommended, based on extent of disease, liver function and overall health according to the BCLC (Barcelona-Clinic-Liver Cancer) classification (11).

1.1.4 Therapy and Prognosis

As HCC is frequently diagnosed in advanced stages and the patient's liver function can be reduced due to cirrhosis, treatment options are often limited. While the primary choice of therapy is surgical resection, this is recommended only for patients in the early or very early stage of disease. In the absence of cirrhosis and limited tumor spread (early stage), liver transplantation can also be attempted (11).

If surgery is not an option, there are a number of alternative treatment methods including local approaches (ablation, irreversible electroporation, embolization, radiation therapy and stereotactic radiation therapy) and systemic chemotherapy (with cytotoxic agents, molecularly targeted therapies or immunotherapy) (11, 12). Systemic chemotherapy is currently mainly restricted to cases of unresectable, advanced HCC, when liver-focused treatments such as ablation and embolization are not feasible. The median life expectancy for patients with advanced HCC is 6-8 months without treatment (11), and systemic treatment with conventional cytotoxic chemotherapy is considered mostly ineffective and poorly tolerated by patients with decreased liver function (11, 13).

Only the emergence of the kinase inhibitor (KI) sorafenib (FDA-approved (Food and Drug Administration) for HCC in 2005) – and some others since then – has led to survival benefit as compared to best supportive care in a palliative setting (14). Following the success of the KIs, new research has also shown promise for immune checkpoint inhibitors, with the combination therapy of the monoclonal antibodies atezolizumab and bevacizumab showing improved outcomes for patients with liver cirrhosis no worse than Child-Pugh class A (15) when compared to monotherapy with sorafenib (16).

Individual choice of treatment can be made with algorithms based on liver cirrhosis, tumor size and location, portal vein affectation and other criteria (11). Considering the current surge of systemic therapies under investigation, suitable patients should be given the option to enroll in ongoing studies (12). If that is not possible or desired, patients should receive immune checkpoint inhibitors or kinase inhibitors (12). Prognosis is variable

depending on tumor extent, liver function and overall health, but HCC in general has a very high mortality rate, second only to pancreatic cancer (17).

1.2 Drug Design

1.2.1 Drug Discovery and Development

The process of bringing a new drug to market is considered extremely time and resource demanding. A recent investigation estimated the median investment to bring a single drug to market in the United States at 985.3 million US dollars (18), while other estimations range as high as 2.6 billion US dollars (19). Additionally, getting a new medicine to patients is estimated to take up to 15 years (20). A major cause for this is the failure of projects at different stages due to safety or efficacy shortcomings (19).

Generally, drug discovery approaches can be divided into forward and reverse pharmacology (21). In the classical approach of forward pharmacology, a compound's therapeutic effect is observed first, and in subsequent investigations the mechanism of action is determined. The rational drug discovery approach of reverse pharmacology utilizes the knowledge of disease pathways to identify key proteins which are then specifically targeted with new compounds. After their effect on the intended targets has been established, their functional activity within cells and organisms is investigated. While there is a strong focus on developing more selective drugs to reduce toxicity and side effects with this approach, it has also been used to target multiple connected proteins. This approach – called network pharmacology – takes the interconnectedness of disease pathways into consideration (22).

Drug discovery consists of target identification, high-throughput screening (HTS) for potentially active ligands (hits), and subsequent hit-to-lead optimization (19). After promising drug candidates are identified, they are moved on to the drug development pipeline. Drug development consists of a preclinical phase and four to five clinical phases (23, 24). Preclinical testing and drug discovery are often considered as one process. This includes *in silico*, *in vitro* and *in vivo* experiments to determine the efficacy, toxicity and pharmacokinetics of potential drugs (25). In this phase, human immortalized cell lines (*in vitro*) and model organisms (*in vivo*) are commonly used. Cell lines derived from different tissues are grown, treated with potential drugs and studied for their reactions. This includes not only observation of growth inhibition or cell death, but also changes in the expression or activation of proteins, as well as the modulation of signaling pathways. Drug

effects on subcellular structures can also be studied in cell-free systems, e.g., when looking at enzymatic or protein interactions with specific assays. As a last preclinical step, systemic effects of a drug can be observed in animal studies before it enters clinical studies (25). To start clinical testing, investigational new drug (IND) studies (phase 0 or I) may be performed with very low dosages and small numbers of participants to get early data on bioavailability and pharmacokinetics. Phase I studies have a similar setup, with an increasing subtherapeutic dose range administered to 20-100 healthy volunteers (or cancer patients for cancer drugs). In Phase II studies, the drug is given to 100-300 patients with a specific disease to determine efficacy and side effects at a therapeutic dose. Before a drug can be approved for the market, phase III trials with large numbers of participants must be successfully performed. After a drug has entered the market, surveillance continues in Phase IV studies to detect potential long-term effects (23).

1.2.2   Computer-Aided Drug Discovery (CADD)

As described above, the process of drug discovery and development is time-consuming and costly. In recent decades, computer-based (*in silico*) methods have become an integral part of industrial and academic research (26, 27). Traditionally, new drug candidates had to be chemically synthesized or purchased from chemical libraries (28) and tested *in vitro* to obtain rational information about their efficacy, selectivity and potential toxicity. Computational methods can be applied independently of drug synthesis, and with the increasing computational power of hardware and improved algorithms, a near infinite number of calculations can be performed within reasonable timeframes. This allows the prioritizing of more promising compounds for biological testing prior to synthesis, ideally leading to drug candidates with higher chances of success in subsequent phases of drug discovery. A wide variety of computational methods have been developed to this end. Beyond following the linear process of CADD (Figure 2), many computational methods can be applied at any stage of drug discovery and medical research in general.

Target identification relates to the process of finding potentially druggable targets that are either responsible for the development of a disease, or whose manipulation might influence the symptoms or course of a disease. Once the targets of interest have been identified, ligand- and structure-based drug discovery approaches can be applied.

This step usually consists of the screening of large compound libraries against the target(s) of interest. The results lead to so called hits, or compounds predicted to be

bioactive towards certain targets. These are considered as the most promising molecules to be optimized into drugs. The subsequent stages of lead generation, including compound optimization of potency and selectivity, consideration of ADMET properties (absorption, distribution, metabolism, excretion and toxicity), and *in vitro* verification of *in silico* predictions are often done in parallel.

In the following chapters, the concepts of ligand- and structure-based computational methods will be elucidated (29).
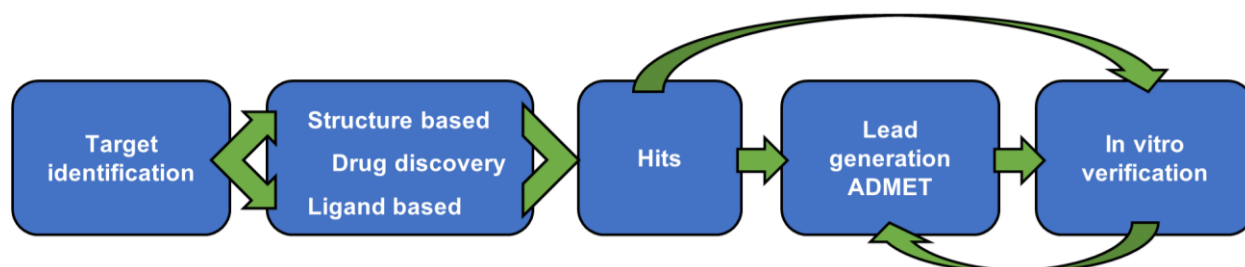
Figure 2. CADD pipeline applied before or in parallel to starting *in vitro* testing. Schematic representation based on Leelananda et al. (19).

1.2.2.1 Structure-based approaches

Structure-based approaches utilize the 3D structures of proteins, most prominently for molecular docking (Figure 3) and scoring (30). This allows for virtual high-throughput screening of potential ligands to a certain protein, as well as inverse screening to detect the potential targets and off-targets of certain drug candidates. Furthermore, the specific ligand-target interactions and structure-activity relationships (SAR) can be studied in more depth. Protein structures are often acquired by x-ray crystallography, and alternative methods include NMR (nuclear magnetic resonance) and electron microscopy (31). If structures have not been determined by experimental methods, computational methods such as homology modelling, fold recognition or de novo modelling can also be useful (19). The acquired structural data of a desired target can then be prepared for use in docking studies. In a first step, the binding site is defined either manually by selecting each amino acid residue involved, or by the docking program based on a (co-crystallized) ligand or automatic detection of empty pockets. Next, compounds under investigation are placed into the binding pocket. Depending on the desired outcome (quantity in high-throughput screening vs. quality in structure-activity relationship (SAR) analysis), algorithms with varying complexity can be used.
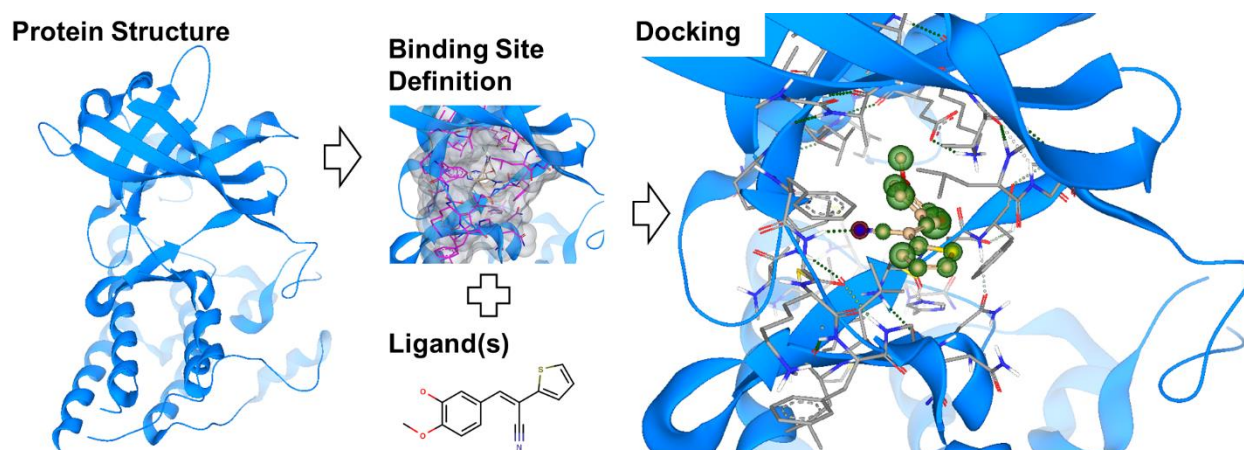
Figure 3. Simplified workflow of the docking process. Example shown with one of the compounds investigated in this work (**Thio-Iva**) and a crystal structure of VEGFR2 (3VHE). Images created with SeeSAR (SeeSAR version 10.2; BioSolveIT GmbH, Sankt Augustin, Germany, 2020 (32, 33)) and MarvinSketch (MarvinSketch 17.02.13.0, 2017, ChemAxon (34)).

During or after docking, the generated poses of the ligand within the binding pocket are scored based on a range of criteria such as hydrogen bonds, hydrophobic interaction, clashes, coverage of the binding pocket and dehydration (29, 33).

Potential shortcomings of current docking software are the limited consideration of protein flexibility as well as the limited availability and quality-differences of crystal structures for more or less 'popular' targets (35). To improve on the former, molecular dynamics simulations attempt to simulate the movements and interactions of an entire protein and its ligands in a solvent (30). While this method takes protein flexibility into account to a certain degree, it requires a lot more computational power than docking.

1.2.2.2 Ligand-based approaches

Ligand-based approaches can be applied independently of the availability of protein structures. In these approaches, public or in-house databases of ligands with known biological activities are utilized, such as ChEMBL (36). All of the following methods are based on the assumption that similar molecules tend to bind to similar targets and/or trigger similar biological effects (37). Depending on the demands of each specific method, the molecules' properties are translated into descriptors, which can then be used to compare the molecules computationally. Figure 4 shows different ways to describe a small molecule using the example of one of the compounds investigated in this work. The ligand can be encoded in sequential text formats like SMILES (Simplified Molecular Input Line Entry Specification) (38), while physiochemical features and molecular fingerprints describe the global or local properties of the molecule. Molecular fingerprints encode substructures of molecules and are often created by starting at one atom and analyzing

its adjacent atoms in a circular (e.g. Morgan fingerprints), path-based (e.g. FP2) or tree-based fashion. This process is then repeated for every atom in the molecule. Another way of generating molecular fingerprints is by creating a list of predefined molecular patterns (e.g. encoded via SMARTS – SMiles ARbitrary Target Specification (39)) which are either present or absent in the query molecule. This type of fingerprint (e.g. MACCS – Molecular ACCess System) is then expressed as a binary bit string. 3D descriptors include conformational information about the ligand as well as additional features rooted in the three-dimensional arrangement such as electrostatic information or lipophilicity (e.g. ES5D – electroshape 5D). Similarity between molecules based on these global properties or substructures can be calculated with different methods. For example, the Tanimoto similarity between two molecules can be calculated by dividing the number of fingerprint patterns present in both compounds by the total number of fingerprint patterns (40).

Sequential Text Formats

Formula	C14H11NO2S
SMILES	OC1=C(OC)C=CC(\C=C(/C#N)C2=CC=CS2)=C1
	...

Global Descriptors

Molecular Weight (MW)	257.31 g/mol
LogP (lipophilicity)	2.91
No. heavy atoms	18
No. H-bond acceptors	3
No. H-bond donors	1
...	

Molecular Fingerprints

Morgan Fingerprints

MACCS fingerprint

00000000000000000000000000000000010000100000000100
00000000000000000001000100001010000100001001001000000
00000001000000000001110000000001010001100000101000010
11111110

SMARTS queries

[a]	"a" is any aromatic atom.
CC	Molecules where an aliphatic carbon is SINGLE BONDED to another aliphatic carbon
[#7,C;+0,+1]	Atoms that (are Nitrogens or are aliphatic Carbons) and (are neutral or positively charged)

3D Properties

...

- Conformation
- Electrostatic information
- Atomic lipophilicity
- ...

Figure 4. Different ways of describing molecules. Shown using the example of **Thio-Iva**, a compound explored in this thesis. Global descriptors based on SwissADME (41), SMARTS queries from Daylight Chemical Information System, Inc. (39). Images created with MarvinSketch (34) and PyMOL (The PyMOL Molecular Graphics System, Version 2.0 Schrödinger, LLC (42)), MACCS fingerprint created with Python RDKit (43).

The most direct ligand-based approach is *similarity search*, which is based on the simple premise that structurally similar compounds will tend to bind to similar targets. For this approach, novel compounds are screened against a database of experimentally tested ligands. Potential activities are identified based on the query ligand's molecular similarity to ligands known to have a specific biological activity or target. Related approaches with increased complexity are *pharmacophore modelling* (44) and *quantitative structure-activity relationship (QSAR) models* (45). QSAR models predict the activity of new compounds by applying a statistical model that relates the molecular descriptors to the (bio)activity. Most *machine learning* applications in drug discovery are also based on ligand information and require training of models with a dataset consisting of – in the classification setting – biologically active and inactive molecules. Once a model has been trained and evaluated (e.g. in cross-validation studies), it can be applied to predict the likelihood of a new compound to be active (19).

One of the main limitations of any ligand-based approach is the availability of data from biologically evaluated ligands against the targets of interest, which can lead to a bias towards more established targets (29).

1.3 Protein Kinase Inhibitors

1.3.1 Human Protein Kinases

Protein kinases are a group of transferases that play a major role in many essential cell processes. Their purpose is to catalyze phosphorylation processes (transfer of a phosphoryl group from adenosine triphosphate (ATP) to substrates) of proteins (often other kinases) (46). Protein kinases are frequently involved in networks of intracellular cascading signaling pathways, serving to amplify the original signal, and also to integrate different signals (47). The roughly 555 human kinases identified so far can be divided into a main class and a smaller group of *atypical* kinases, which lack genetic similarity despite expressing kinase-like activity (46). The commonly used classification into further groups, families, and subfamilies was established by Manning et al. (48), mainly based on the sequence similarity of their catalytic domains. The nine groups of the typical kinases are: *AGC* (PKA-, PKG- and PKC-containing families), *CAMK* (calcium/calmodulin-dependent protein kinase), *CK1* (casein kinase 1), *CMGC* (CDK-, MAPK-, GSK3- and CLK-containing families), *Other*, *RGC* (receptor guanylate cyclase), *STE* (homologues of yeast

sterile 7, sterile 11, sterile 20 kinases), *TK* (tyrosine kinases) and *TKL* (tyrosine-like kinases).

Due to their importance in physiological processes as well as in the development of disease (including cancer) when dysregulated, kinases have become an important area of research for targeted therapies (49).

1.3.2 Definition and Classifications

Most of the clinically approved protein kinase inhibitors (PKIs) are so called small molecule kinase inhibitors, referring to their low molecular weight of under 500 g/mol (50). An example of one of the few non-small molecule kinase inhibiting drugs is the monoclonal antibody Cetuximab used against EGFR-expressing colorectal cancer and head and neck cancer (51).

The first small molecule kinase inhibitor was clinically approved in 1999, and as of the 14th of April 2021, 65 are FDA-approved small molecule PKIs (52). 50 of them have tyrosine kinases as primary targets, four have the dual specificity kinase MEK1/2 as a primary target, and the remaining 11 target serine/threonine kinases (52, 53).

PKIs can be classified into type I to VI as summarized by Roskoski in 2016 (Table 1) (54). Type I and II are designed to bind in the ATP pocket region, while type III and IV bind allosterically. Type V inhibitors can bind to two separate regions at the same time (typically the ATP pocket and an allosteric site) (55). Type VI inhibitors bind covalently to the kinase, as opposed to type I-V, which all bind noncovalently. Of the FDA-approved PKIs, almost half are considered to be type I or II inhibitors. The defining difference between these two classes is the conformation of the DFG motif (D: Aspartate, F: Phenylalanine, G: Glycine). This conserved sequence of amino acids is placed at the beginning of the activation loop of kinases and can be observed in two major conformations: DFG-in and DFG-out. DFG-in occurs mostly in active kinase conformations, while DFG-out is considered an inactive conformation where the Phenylalanine occupies parts of the ATP-binding pocket (56).

While both type I and II PKIs bind in the region of the ATP-binding pocket, type I inhibitors bind kinases in a DFG-in conformation, while type II inhibitors bind to a dormant kinase with a DFG-out conformation.

Table 1. Classification of small molecule protein kinase inhibitors as defined by Roskoski (53).

Type	Binding mode characteristics	FDA approved examples
I	ATP pocket – DFG-in	Gefitinib (2003)
II	ATP pocket – DFG-out	Sorafenib (2005)
III	Allosteric site adjacent to ATP pocket	Trametinib (2013)
IV	Allosteric site distant from ATP pocket	Temsirolimus (2007)
V	Bivalent to two separate areas	–
VI	Covalent	Afatinib (2013)

The main challenges for developing new kinase inhibitors are selectivity and development of resistance. Selectivity of type I and II inhibitors can be challenging due to the high conservation of the ATP-binding pocket. While the potential additional targets can cause unwanted side effects, they may also sometimes work in a synergistic way (22). Targeting one specific target can be especially useful when it has a disease-driving mutation (57). Drug resistance can develop due to mutations within the cancer cells (58, 59). One example of a frequently occurring mutation is the EGFR-mutation T790M, which impairs drug binding of EGFR inhibitors such as Gefitinib or Erlotinib (58). Ways around such mutations are developing type III or IV inhibitors that bind to other sites of EGFR, or type VI inhibitors that bind covalently.

1.3.3 Current Clinical Applications

As dysregulation of protein kinases plays a major role in the development of neoplastic (and many other) diseases, many of them have become the focus of targeted therapies (35). Indications range from solid and nonsolid cancers to rheumatoid arthritis and glaucoma. However, the majority of kinase inhibitors are used against neoplastic disease (60). Current cancer applications of different kinase inhibitors include many forms of leukemia and lymphoma, different forms of lung, breast, colorectal, pancreatic, thyroid, renal, and urothelial, as well as hepatocellular and cholangiocarcinoma, gastrointestinal stromal tumors, melanoma, neuroendocrine tumors, sarcomas and selected brain tumors (60).

The indication for a targeted therapy with a kinase inhibitor is often dependent on the genetic aberrations of the individual cancer, and some (Entrecitinib, Larotrectinib) are even approved for a specific mutation (NTRK (neurotrophic receptor tyrosine kinase) fusion) rather than a specific tumor (52). Depending on the cancer type and mutational status, PKIs can be applied as first line and potentially curative therapy (e.g. chronic

myeloid leukemia (57)), while in other cases only a moderate increase in life expectancy and/or quality of life can be achieved (e.g. advanced HCC (11)).

1.3.4 Novel Potential Tyrosine Kinase Inhibitors

A panel of new potential tyrosine kinase inhibitors (TKIs) was proposed and synthesized by our research partners at the Organic Chemistry Laboratory, University of Bayreuth. The molecular structure was derived from the tyrphostin RG-13022 (Figure 5, A), which has shown inhibitory effects on the EGFR and PDGFR in previous studies (61, 62). Tyrphostins are a group of type I/II TKIs derived from the naturally occurring TKI erbstatin (Figure 5, A) (63). The proposed panel consisted of two subgroups of compounds with distinct core structures (Figure 5, B). For the first subgroup, the pyridine ring of RG-13022 was replaced by a thiophene, for the second set it was replaced by a bromobenzene. The methoxy groups at the benzene ring were replaced by a range of different modifications. In preliminary assessments performed by the chemistry laboratory, **Thio-Iva** and **Briva** appeared to be the most promising members of the thiophene- and bromobenzene derivatives, respectively.

Over the course of this project, more derivates of the thiophene subset were generated (Figure 5, B, compounds **1a**, **1e**, **1i** and **1j**). The entire thiophene subset was examined more deeply by our lab group (64), with some data from this thesis included in the publication (see preface).

A
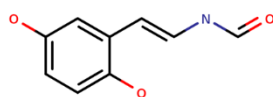
Erbstatin
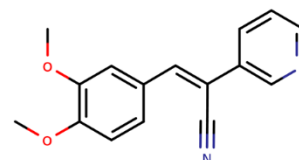
Tyrphostin RG-13022

B
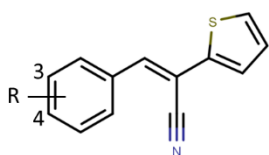
Thio-Iva (1c)	**R = 3-OH, 4-OCH₃**	**Briva**
Thio-Van (1d)	**R = 3-OCH₃, 4-OH**	**Brova**
Thio-Dam (1b)	**R = 4-N(CH₃)₂**	**Bro-Dam**
1a*	R = 4-OMe	
1e*	R = 3-CH₃, 4-OCH₃	
1i*	R = 4-(N-methylpiperazin-1-yl)	
1j*	R = 3-F, 4-OCH₃	
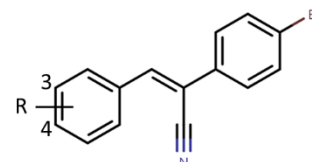
Figure 5. A 2D depictions of naturally occurring TKI Erbstatin and Tyrphostin RG-13022 **B** 2D depictions of the compounds investigated in this work, showing the six initially proposed compounds and four compounds (*) from the appended panel (64). The most promising one from each subgroup (**Thio-Iva** and **Briva**) were investigated more deeply in this work.

1.4 Research Aim

HCC is a disease with poor prognosis, and treatment options for advanced HCC are still very limited. Developing highly effective kinase inhibitors for HCC and understanding their target landscape is therefore an important and current research goal. For this work, newly synthesized compounds with potential tyrosine kinase inhibitory activity were investigated with *in silico* and *in vitro* methods.

The aim of this study was to gather knowledge on the suitability of the new compounds as potential therapeutic agents, and to elucidate their potential molecular (kinase) targets as well as their anticancer efficacy and mode of action in HCC cell models.

This main goal was broken down into several subgoals:

- Investigate how the novel compounds exert their function by identifying key tyrosine kinase targets as well as potential unexpected (off-)targets
- Understand how they inhibit (bind to) the identified target kinases to investigate the structure-activity relationship of the most promising compounds with their respective target structures, and potentially optimize them in the future
- Determine the growth inhibitory activity of the novel compounds in HCC cells
- Predict and evaluate the compounds' potential interaction with cells and organisms, including ADME properties, unspecific and unwanted toxicities and induction or inhibition of signaling pathways including apoptotic pathways

While investigating the potential of the proposed compounds as kinase inhibitors for anticancer therapy, it was also possible to evaluate the transferability of *in silico* predictions to *in vitro* results.

2   Materials and Methods

In this thesis, a panel of ten compounds was investigated with a range of *in silico* and *in vitro* methods. Due to prioritization of the two lead compounds **Thio-Iva** and **Briva** in the initial panel and the later addition of the compounds **1a**, **1e**, **1i** and **1j**, not all methods were applied for all compounds. Table 2 gives a short overview of the different methods applied to each individual compound.

Table 2. Overview of methods used in this work by compound investigated.

	Thio-Iva	Thio-Van	Thio-Dam					Briva	Brova	Bro-Dam
	1c	1d	1b	1a	1e	1i	1j	Briva	Brova	Bro-Dam
SwissTargetPrediction	yes	no	no	no	no	no	no	yes	no	no
@TOME screening	yes	no	no	no	no	no	no	yes	no	no
iRAISE screening	yes	no	no	no	no	no	no	no	no	no
Docking studies	yes	yes	yes	yes	yes	yes	yes	yes	yes	yes
MD simulations	yes	no	no	no	no	no	no	no	no	no
SwissADME	yes	no	no	no	no	no	no	yes	no	no
eMolTox	yes	no	no	no	no	no	no	yes	no	no
Growth inhibition	yes	no*	no*	no*	no*	no*	no*	yes	no	no**
Caspase-3 activity	yes	no	no*	no*	no*	no	no	yes	no	no**
LDH release	yes	no	no*	no*	no	no	no	yes	no	no**
Kinase Assay	yes	no	yes	yes	no	no	no	yes	no	no**

* Similar or identical experiment performed by our lab group in Schaller et. al (64).
** compound not suitable for wet lab evaluation.

2.1   In Silico Studies

2.1.1   Target Prediction

When developing new compounds, *in silico* prediction of potential targets and off-targets assist in identifying potential expected or unexpected therapeutic applications. This helps us to understand biological effects and predict potential side effects due to binding promiscuity. For this process, both ligand- and structure-based approaches can be applied.

In this work, three different tools were used in combination. As a ligand-based method, SwissTargetPrediction was employed, developed by the Swiss Institute of Bioinformatics (65, 66). For structure-based prediction, the inverse screening software iRAISE (RApid Index-based Screening Engine, version 1.0.2, developed by the University of Hamburg, Center for Bioinformatics) (67), and the screening service LIST v3 (Large-scale Inverse Screening Tool for protein kinases (Human)) provided by the @TOME (@utomatic Threading Optimization Modeling and Evaluation) platform (68) were used.

2.1.1.1 Ligand-Based: SwissTargetPrediction

The screening server SwissTargetPrediction investigates the 2D and 3D similarity of input ligands to compounds with known *in vitro* activity data in the ChEMBL Library (ChEMBL23 in the version used (66)). Compound-target data points from ChEMBL are included in the prediction database if the activity against the target is derived from direct binding protein assays and the compound contains less than 80 heavy atoms. Data from five organisms are included (human, mouse, rat, cow and horse). Finally, only active compound-target pairs are of interest for this target prediction method. SwissTargetPrediction considers a compound to be active on a target if the IC50 (inhibitory concentration where activity is reduced to 50%) or comparable value is below 10 μM. To compare the query compounds to this dataset of *known actives* (compounds deposited on the ChEMBL database and classified as active on a specific target), molecular fingerprints (FP2 for 2D and ES5D for 3D) are generated. Acceptable similarity of each known active to the query molecule is determined by a Tanimoto index above 0.65 for 2D similarity and a Manhattan-based similarity of more than 0.85 in 3D (65). For each target in the database, all active compounds similar to the query ligand above the described thresholds are collected and their scores and frequency are compiled to a probability score. The higher the predicted score, the higher the likelihood that this is a potential target for the queried compound. Results from the server include a list of the top 100 potential protein targets, as well as the similar known actives per target found for the query compound.

For this work, the two lead compounds **Thio-Iva** and **Briva** were screened with SwissTargetPrediction (69). The respective SMILES were added as the query input and the species was set to homo sapiens. The list of predicted targets as well as information on the known actives were downloaded and further analyzed manually.

2.1.1.2 Structure-Based: @TOME and iRAISE Screening

@TOME Screening

The @TOME kinase screening service LIST v3 (68, 70), which is based on the previously published KinDOCK server (71), attempts to dock query ligands into kinase structures. The kinase library consists of crystal structures of kinase-ligand complexes and homology models previously created with the @TOME pipeline (68). For the docking, it takes into consideration not only the protein alone, but also the position and contacts of the co-crystallized ligand. Docking poses for the queried compounds are calculated with the

PLANTS docking software, developed by the University of Tuebingen (72), with a weighting applied to favor poses similar to those of the co-crystallized ligands.

A predicted affinity (pKd – predicted dissociation constant) is calculated from a combination of scoring functions (PLANTS, MedusaScore (73), X-score (74) and DSX (75)). The theoretical ligand position error (LPE) is calculated with a machine learning model trained on crystal structures (SVM Torch (76)) as an approximation of reliability of the predicted binding poses. The LPE is a theoretical RMSD (Root-mean-square deviation) between size, shape, position and interactions of the query ligand and ligands from crystallographic homologous complexes (70). The best pKd and LPE for each kinase is given in the results overview, and individual results for each crystal structure can additionally be acquired.

The @TOME kinase screening of **Thio-Iva** and **Briva** was performed with LIST v3 and the database version 'PK_HUMAN_I90_2019M4 (Apr 2019)' (77). All 241 available kinases (Figure 6) were screened with the preset standard parameters, changing only the speed of the PLANTS docking algorithm to highest reliability. The top scoring results returned by the server were analyzed with Excel, while docking poses and multiple other descriptors calculated by LIST v3 were not further investigated for this work.
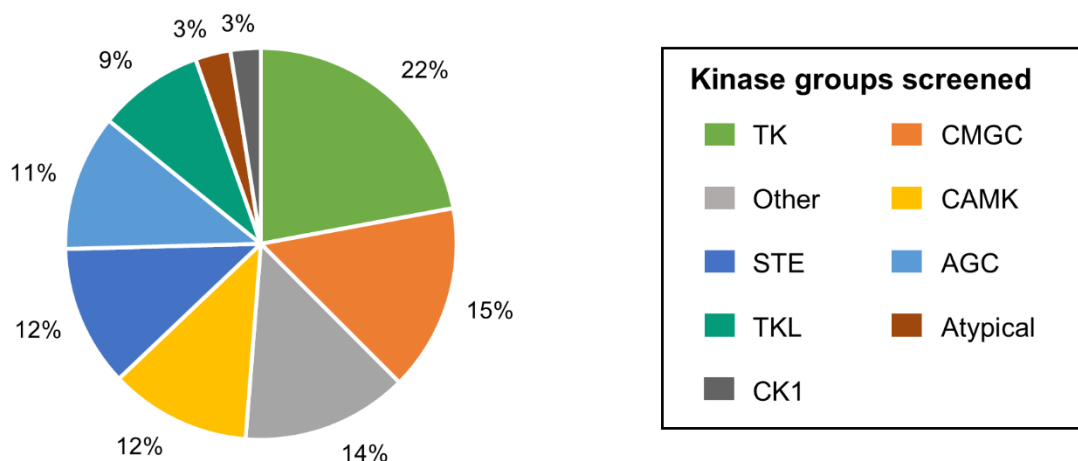
Figure 6. Percentages of kinase groups represented in the kinase library of the @TOME screening service LIST v3. Classification according to KinHub (78).

iRAISE Screening

The iRAISE inverse screening tool is designed to screen a compound of interest against a database of potential targets to identify the targets it will most likely interact with. The target database is prepared by the user according to the structures of interest for the screening. Protein structures in the form of PDB (protein data bank) files are downloaded,

and in a registration procedure the binding sites are defined, usually by the co-crystallized reference ligand(s) with a radius of 6.5 Å. These sites as well as the compound(s) of interest are then described by calculating so called triangle descriptors, which take into consideration steric and pharmacophoric properties. Through this, the representation of both active site and ligand are reduced to their essential properties, allowing for rapid screening. The docking strategy is based on matching the triangle descriptors, superimposing the structures based on this match and scoring the resulting ligand pose in the target protein. The scoring cascade includes steps to filter out unlikely poses based on clashes, reference (ligand) score cut-off and ligand/pocket coverage. Through this, an interaction score is created for each pose.

For this thesis, iRAISE was applied with the support of Pratik Dhakal, MSc Bioinformatics, who was involved in the selection and preparation of crystal structures programmatically, as well as the running of the iRAISE software (which required calculations on an HPC cluster infrastructure). He was not part of the post-screening redocking and analysis of data.

The iRAISE screening was performed for the main compound **Thio-Iva** against tyrosine kinases (TKs), which were the most likely target group (since the investigated compound is derived from a tyrphostin structure) to limit computational load.

Screening database preparation: First, all crystal structures deposited on the human proteome on Uniprot (79, 80) were downloaded from the RCSB Protein Data Bank (81, 82). Next, suitable crystal structures were selected using the kinase information available through the KLIFS database (83). The final database was restricted to contain only crystal structures of kinases from the TK group, which have been co-crystallized with a ligand (to allow for automatic binding site annotation).

This resulted in a final panel of 796 protein structures from 56 different tyrosine kinases grouped into 24 kinase families (Figure 7). They were prepared for screening by splitting the chains and aligning the structures (to allow for ease of comparison in the analysis of results) and entered into the registration procedure as described above.

Compound preparation: The structure of the ligand **Thio-Iva** was drawn with MarvinSketch (MarvinSketch 17.02.13.0, 2017, ChemAxon (34)), transformed into a 3D structure, saved as a spatial data file (SDF) and supplied as input for the iRAISE screening.

iRAISE screening: The screening was performed on Curta, a general-purpose high-performance computer at ZEDAT, Freie Universität Berlin (84), with the standard

parameters as described above. Results of the successfully docked structures were exported as a list reporting predicted energy scores, as well as the SDFs of the best 5 poses per target generated in the inverse screening.

SeeSAR post-screening analysis: For each kinase, the crystal structure with the highest scoring pose was used for redocking of the five top scoring poses with SeeSAR (SeeSAR version 5.5; BioSolveIT GmbH, Sankt Augustin, Germany, 2017; see Chapter 2.1.2 for detailed background of the method) and ten more poses were generated. This was done to increase reliability of the inverse screening. The generated binding modes and estimated affinities were then analyzed manually.
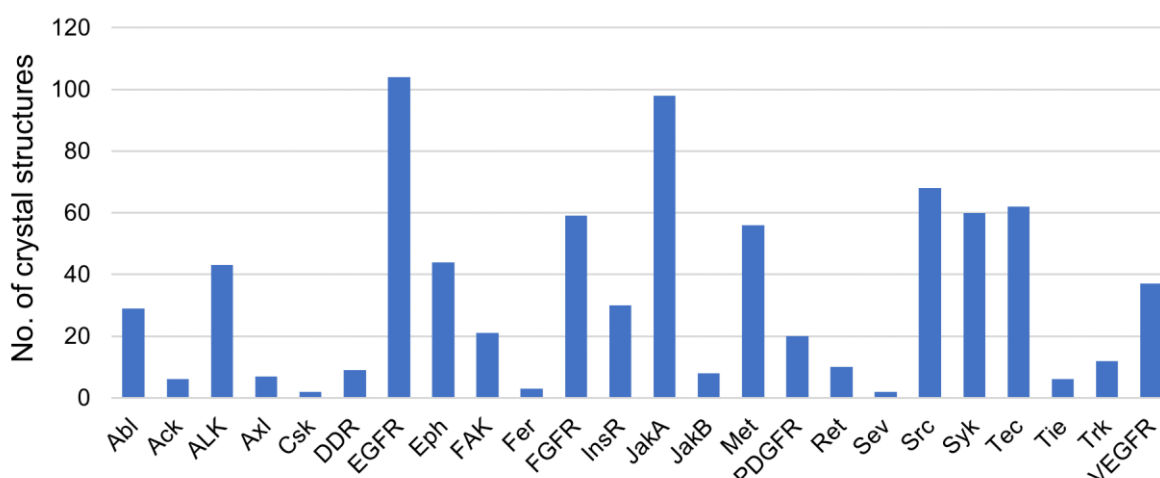
Figure 7. Number of crystal structures per kinase family in the panel screened for targets of **Thio-Iva** with iRAISE.

2.1.2 SeeSAR Docking

After specific targets have been identified, the structure-based approach of protein-ligand docking and scoring can be used to predict possible binding poses and binding affinities (expressed as scores), as well as investigate how the ligand interacts with its target.

Docking studies were performed with the BioSolveIT software SeeSAR (SeeSAR version 10.2; BioSolveIT GmbH, Sankt Augustin, Germany, 2020). As a first step, the target protein structure is loaded and a binding pocket defined, either by automatically detecting empty pockets or by using a ligand (usually the co-crystallized one). SeeSAR's docking strategy is based on the FlexX docking algorithm (32). With this algorithm, the input ligands are split into fragments that are then placed into the binding pocket, after which a pre-scoring takes place. The ligand is then built up from the base fragment by adding one fragment after another, and the individual solutions are continually scored in the binding

site. The best overall solutions for the fully rebuilt molecule poses will then be shown as output to the user. In the most current version of FlexX, an additional algorithm called the single interaction scan has been added (85). Poses from both algorithms are combined in order to increase the diversity of the output.

The evaluation of each docking pose is done with the HYDE scoring function (33). This scoring algorithm takes into account the hydrogen bonds formed between the docked ligand and its protein target, as well as the dehydration energies of the protein-ligand complex. The latter term is based on the fact that both ligand and protein are in an aqueous solution before the binding process. During binding, both are desolvated to a certain degree when encountering each other. While this is considered a disadvantageous effect for the stability of the binding pose, newly established hydrogen bonds and removal of water from hydrophobic areas of protein and ligand can counter that effect and lead to a gain in energy.

Docking studies for this thesis were performed as redocking of iRAISE screening results for target prediction (as detailed in Chapter 2.1.1.2), but more extensively for SAR analysis with all ten compounds on VEGFR2 as the target exhibiting the strongest inhibition by **Thio-Iva** *in vitro* (see Chapter 3.1.2). In the following, the process for the VEGFR2 docking is explained in detail.

Compound preparation: As a first step, the ten new compounds were drawn with MarvinSketch (MarvinSketch 17.02.13.0, 2017, ChemAxon (34)) and transformed into a 3D structure within the same software to represent the compound library.

Structure selection and preparation: First, a search for suitable VEGFR2 structures was performed using the KLIFS database (86, 87). Structures were filtered for VEGFR2 ('KDR') structures with the criteria 'Human', 'Ligand bound', a KLIFS quality score between 7 and 10 and a crystal structure resolution below 2.0 Å. The remaining 13 structures were investigated manually for mutations, chain interruptions (amino acid residues that were not resolved in the X-Ray structure) and DFG conformations. Employing these criteria, the structure 3VHE was chosen (88). Due to the structural similarity of the newly proposed compounds to tyrphostins, it was assumed that they would most likely act as type I/II kinase inhibitors (89). Therefore, the ATP-binding pocket was chosen as the binding site for docking.

Docking and scoring: For initial docking, the structure was prepared in SeeSAR as follows. The binding site of the VEGFR2 structure 3VHE was defined by the co-crystallized ligand 42Q in the ATP-binding-pocket, including amino acid residues within a

radius of 6.5 Å. Docking was performed without pharmacophore restrictions, the number of maximum solutions was increased to 500, and all other settings were left at default. The prepared compound library consisting of the ten new compounds was loaded. Additionally, 42Q was redocked for quality control, and RMSD from the co-crystallized pose was calculated with the PyMOL function pair_fit (42).

The inbuilt HYDE scoring function was applied and used for prioritization of binding poses. *Postprocessing*: For all ten ligands, the 50 highest-ranking binding poses were further analyzed within SeeSAR. Selected high scoring poses together with the crystal structure were imported into LigandScout 4.4, a program specialized in 3D pharmacophore generation and detailed analysis of compounds and their interactions with macromolecules (90). In this project it was used to automatically create pharmacophores (used to analyze and visualize the ligand-protein interactions) and to minimize the energies of the systems using MMFF94 (Merck Molecular Force Field 94).

2.1.3 Molecular Dynamics Simulations

Since most docking methods do not account for the intrinsic flexibility of protein structure, e.g. upon ligand binding, promising binding poses can be further validated with molecular dynamics (MD) simulations. MD simulations were performed with the simulation software Desmond 6.1.013 (Schrödinger Suite 2020-1) (91). Desmond aims for high performance and efficiency by applying parallel algorithms (92) and numerical methods (91, 93). For each simulated time step, the forces for each particle (usually one atom) are calculated with a forcefield (a model specifying the potential energy of a system based on the atomic coordinates). Once this step (called *force computation*) is completed, the resulting changes in position and velocities of the atoms are calculated according to basic laws of physics (Newton's laws of motion) in the step called *integration*.

MD simulations were performed with the help of Dr. David Schaller, who was involved in preparation of the crystal structure and ligand, as well as running the MD simulation programmatically. The simulation was done with **Thio-Iva** and VEGFR2, the most strongly inhibited target in the radiometric kinase assay (see Chapter 3.1.2).

Preparation: To prepare the protein structure 3VHE for the simulation, a python script was used integrating the tools OESpruce, OEChem and OEGrid from the OpenEye toolkit 2020.1.0 (94). In this step, chain interruptions, missing atoms and residues were detected and filled, and the ends of the amino acid chain of the crystallized structure were capped. The prepared structure, together with the predicted docking poses of **Thio-Iva** (generated

with SeeSAR and energy minimized with LigandScout, see Chapter 3.2.1), was then further prepared with Maestro 12.3.013 (Schrödinger Suite 2020-1). The system was set up with the OPLS (Optimized Potential for Liquid Simulations) forcefield (2005) (95). The protein charge was neutralized with 4 Cl$^-$ ions and up to 0.15 M KCl, and a cubic SPC (simple point-charge) water box with 10 Å padding was added.

MD simulation: The simulations were run on Curta, a general-purpose high-performance computer at ZEDAT, Freie Universität Berlin (84). They were performed with periodic boundary conditions, the default equilibration scheme and at a temperature of 300 K. The duration was 100 ns and frames were written every 100 ps, resulting in a total of 1,001 frames. Simulations were performed for three potential binding modes of **Thio-Iva** predicted by SeeSAR. The simulations were evaluated for stability of the binding pose, and the most stable one (starting pose **Thio-Iva_032**) was run two additional times with a change in configuration to account for different random starting points. This was done by changing the seed (used to generate the starting speed of atoms) from the arbitrary number 2007 in the first simulation to 2008 and 2009.

Postprocessing: The most stable simulation was further analyzed with VMD (Visual Molecular Dynamics) version 1.9.3 (96). The inbuilt RMSD Trajectory tool was used to align the results (each timestep) to the backbone of the protein in the first frame, as well as for subsequent analysis of the RMSD of the ligand over time. Key interactions were analyzed by measuring the distance between the interacting atoms over time.

2.1.4 ADMET Prediction Models

2.1.4.1 eMolTox

To predict potential toxicity of the novel compounds, the web server eMolTox was used (97, 98). This server offers a structural alert search for potentially problematic substructures, where the query compound is screened against publicly available structural alert datasets (Figure 8, A). As a more complex prediction method, eMolTox employs machine learning (ML) based models that predict a wide range of toxicities based on molecular descriptors. As described in the introduction, such ML models are trained on a set of compounds with known activity or effect on the investigated toxic endpoints. To build prediction models, eMolTox uses circular fingerprints (2048-bit ECFP4 (extended connectivity fingerprint)) and 196 physiochemical descriptors. Machine

learning models based on random forests and conformational prediction are trained and applied to make predictions for any input ligand.

Notably in this application, a special technique called conformal prediction is applied that allows for confidence estimations of the predictions. In short, the confidence is measured by comparing the predicted scores of a query molecule to the scores of previously seen molecules.

The model compiles extensive toxicology data from 174 publicly available sources, which includes *in vivo* and *in vitro* data ranging from unspecific acute oral toxicity to activities on specific proteins whose inhibition/activation is known to regularly lead to potentially unwanted effects (such as CYP450 interaction) (Figure 8, B).

To apply eMolTox to the novel compounds, SMILES of **Thio-Iva** and **Briva** were given as input information. Toxicity prediction was run for all available alerts and analyzed in detail at a later point. The 169 toxic endpoints available at the time of the screening were defined by an action (e.g. activity on a specific enzyme) and assigned to one or multiple injuries (mostly affected organ systems). For the analysis of the results, toxic endpoints were grouped according to the injuries defined by eMolTox. Exceptions were made for animal experiments, which were all classified according to their action (acute oral toxicity). Lungs and respiratory injuries were grouped together, as were peripheral, central, and nervous systems, carcinogenicity and cancer, as well as the endocrine system and one reproductive injury described as endocrine disruption.
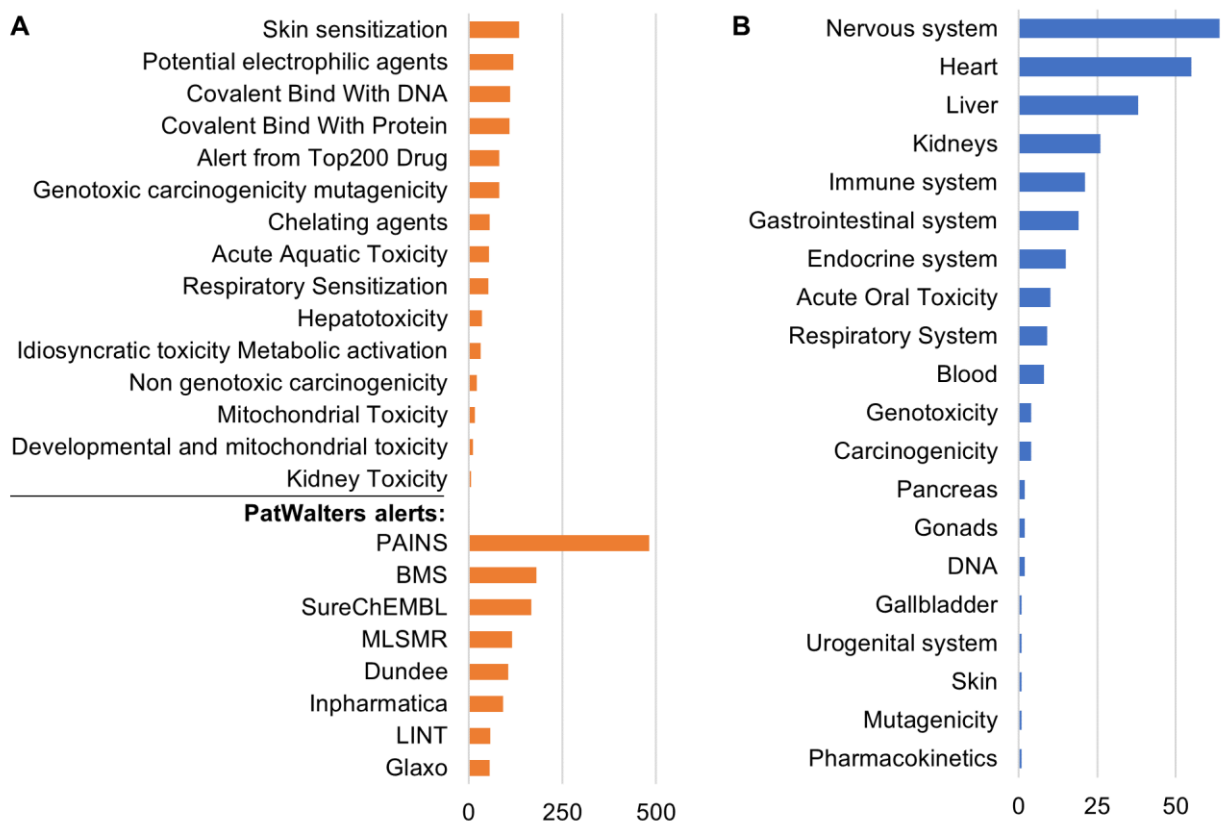
Figure 8. A Distribution of the 2,173 potential toxic substructure alerts detectable with eMolTox **B** Distribution of injury categories of ML based eMolTox toxicity screening.

2.1.4.2 SwissADME

The webservice SwissADME was used to calculate ADME properties and the druglikeness of the lead compounds (41, 99). It is a tool developed by the Swiss Institute of Bioinformatics and compiles a wide range of adapted methodologies from many different sources, as well as models generated by the Swiss Institute for Bioinformatics. Many of these models are based on machine learning, whereby molecules with specific traits are used to train a model to predict the presence of these traits in an unknown compound. Other endpoints are calculated with formulas established in drug discovery based on statistical observation of favorable or unfavorable properties of potential future drugs. The combination of these prediction models allows for the prediction of a wide range of properties, including physiochemical descriptors, parameters concerning druglikeness, chemical accessibility as well as ADME properties and structural alerts. The aim of this tool is to provide a quick overview of these properties for potential drugs without requiring *in vitro* testing.

For this thesis, the SMILES of **Thio-Iva** and **Briva** were used as input files, and selected results were downloaded and analysed further.

35

2.2 In Vitro Studies

2.2.1 Enzymatic Kinase Assay

Enzymatic kinase profiling was performed with a commercial radiometric assay (KinaseProfiler™) by Eurofins. This cell-free kinase assay tests the enzyme inhibitory activity of a compound for a wide selection of kinases. The test was performed in duplicates with an ATP concentration of 10 µM. The compounds were provided to Eurofins at a concentration of 10 mM dissolved in DMSO.

Thio-Iva was screened against a customized panel of 43 targets that were chosen from *in silico* predictions and for HCC relevance (Table 3, see Chapter 3.1.1.3) with a compound concentration of 10 µM. Separately, an IC50 determination for the inhibitory activity of VEGFR2 was performed with nine concentrations of **Thio-Iva** ranging from 0.003 µM to 30 µM. Additionally, **Briva**, **Thio-Dam** and **1a** were screened against VEGFR1 (Flt1), VEGFR2 (KDR), Pim-1, Pim-2, c-Kit, CLK1 and EGFR at a concentration of 10 µM.

Table 3. Targets selected for **Thio-Iva** screening with Eurofins KinaseProfiler™.

Kinase target	In silico	HCC	Kinase target	In silico	HCC	Kinase target	In silico	HCC
KDR(h)	X	X	PDGFRα(h)	X		TGFBR1(h)	X	
Flt1(h)	X		Arg(h)		X	PDK1(h)		X
Pim-1(h)		X	MEK1(h)	X		JNK2α2(h)		X
CLK1(h)		X	BTK(h)		X	mTOR(h)	X	
cKit(h)	X	X	ACK1(h)	X		Tie2 (h)		X
Pim-2(h)		X	B-Raf(h)		X	Bmx(h)	X	
Aurora-B(h)		X	PDGFRβ(h)	X	X	FGFR3(h)		X
TrkA(h)		X	FGFR1(h)	X	X	JNK3(h)		X
cSRC(h)		X	FGFR2(h)	X	X	CSK(h)	X	
Lyn(h)		X	Plk1(h)		X	IGF-1R(h)		X
Abl(h)		X	Tec(h) act.	X		GSK3β(h)		X
EGFR(h)	X		JAK1(h)	X		Met(h)	X	X
CDK2/cyclinA(h)		X	IGF-1R(h) act.	X		EphB4(h)		X
CDK2/cyclinE(h)		X	JAK2(h)	X				
Ret(h)		X	Plk3(h)	X				

In silico: target included due to *in silico* target prediction – **HCC:** target included due to relevance to HCC. **(h)** human.

2.2.2 Cell Culture

All cell-based experiments were conducted with HepG2 (ATCC® HB-8065) and Huh-7 (JCRB#0403) cells, both categorized as epithelial-like hepatocellular carcinoma cell lines by the ATCC® and JCRB cell banks, respectively. However, the HepG2 cell line has been shown to originate from hepatoblastoma cells (100) and can be found with different classifications in literature. Here, both cell lines will be referred to as hepatocellular

carcinoma cells, as the original classification has not officially been changed, and the molecular makeup of both cell lines is quite well researched.

The cells were kept in an incubator (37°C, 5% CO_2 and 95% humidity) in RPMI 1640 medium (Gibco; Thermo Fisher Scientific, Inc., Waltham, MA, USA) supplemented with 100 U/ml penicillin (Gibco), 100 µg/ml streptomycin, 2 mM L-glutamine (Gibco) and 10% fetal bovine serum (Sigma Aldrich, Darmstadt, Germany).

2.2.3 Crystal Violet Assay

Growth inhibition was determined by measuring treatment-induced changes in the cell number of HepG2 and Huh-7 cells using crystal violet assays. The method is based on the staining of cellular DNA with the dye crystal violet. Due to the stable amount of DNA per cell, differences in the amount of DNA in the probes are linear to changes in the in cell numbers. Therefore, staining of the DNA with crystal violet can be used as readout for the determination of growth inhibition (101). For this thesis, 5,000 cells/well were seeded in 96-well plates and maintained for adherence in an incubator for one day before treatment (or at a density of 1,500 cells/well three days before treatment). The cells were then treated with the compounds at different concentrations in sextuplet for each condition. After 0, 24, 48 and 72 hours, the cells were fixated and stained as follows. First, the wells were washed with 200 µl of PBS (phosphate buffered saline), then filled with 100 µl 1% glutaraldehyde solution and incubated for 15 minutes at room temperature to fix the cells in the wells. After washing the wells again with 200 µl of PBS, 100µl of 1g/L crystal violet solution was added to the wells, and the plates were incubated for 30 minutes at room temperature in the dark. After the incubation period, the unbound dye was washed out with moving water for 30 minutes. After thorough drying of the plates, the bound crystal violet was dissolved with 100 µl of 0.2% Triton X-100 (Sigma) solution overnight. The optical density of the wells was then measured at a wavelength of 570 nm with a Dynex MRX^e Microplate Reader.

2.2.4 LDH Assay

The Cytotoxicity Detection Kit (LDH) (Roche, Mannheim, Germany) was used according to the manufacturer's protocol to determine unspecific cytotoxicity of the new compounds after 12 and 24h of treatment. In this test, the release of lactate dehydrogenase (LDH) into the supernatant of the cell culture medium is measured and compared between treated and untreated cells.

Cells were seeded out in 96-well plates at a density of 5,000 cells per well and treated with **Thio-Iva** and **Briva**, as well as with 2% Triton for positive control after 24 hours. For this step, RPMI medium with only 1% fetal bovine serum was used to reduce background noise. After another 12 and 24 hours, respectively, 100 µl of medium was pipetted from the wells containing the cells onto a new plate, and then 100 µl of reaction mixture was added (cytotoxicity dye solution and catalyst solution at a relation of 45:1). The mix was then incubated for 30 minutes at room temperature in the dark. Next, absorbance of the samples at a wavelength of 490 nm was measured with a Dynex MRX^e Microplate Reader.

2.2.5 Caspase-3 Activity Assay

As a marker for apoptotic cell death, activity of caspase-3 in treated cells was measured compared to untreated control cells with the Caspase-3 Cellular Activity Assay Kit (Calbiochem/Merck KgaA, Darmstadt, Germany). For this, the specific substrate acetylated Ac-DEVD (N-acetyl-Aspartate-Glutamine-Valine-Aspartate) was used, which is linked to the Fluorophore AMC (7-amino-4-methylcoumarin). Caspase-3 contained in the samples cleaves the substrate Ac-DEVD-AMC, so that the released AMC becomes fluorescent. In order to put this fluorescence signal into relation to the overall protein concentration in each sample, additional protein determination was performed (Pierce^{TM} BCA Protein Assay Kit, Thermo Fisher, IL, USA).

Cells were seeded out in a range of densities, either in 6-well plates or 10 cm petri dishes, to achieve the desired cell density and volume for the different time points and cell lines. HepG2 cells were seeded out at densities of 50,000-400,000 cells 2 to 4 days before treatment, and Huh-7 cells at densities of 200,000-800,000 cells 2 to 3 days before treatment.

Cells were treated with increasing concentrations of **Thio-Iva** and **Briva**, and after 12, 24 or 48 hours they were harvested and frozen at -20°C. After being frozen for at least 24 hours, cell pellets were lysed with 280 µl lysis buffer for 30 minutes and centrifuged for 15 minutes at high speed. The supernatant was transferred and used for protein determination and caspase-3 Ac-DEVD-AMC reaction.

For protein determination, 20 µl of cell lysate was pipetted onto a 96-well plate in duplicates, and the same was done for a BSA protein standard row (0-2,000 µg/ml). 100 µl of reaction solution (solutions A and B at a relation of 50:1) was added to each well

and incubated for 30 minutes at 37°C. Extinction was then measured at 570 nm with a Dynex MRX^e Microplate Reader.

For caspase-3 activity determination, 100 µl of lysate per well was mixed with substrate solution (1 µg Substrate in 100 µl HEPES-buffer) on a 96-well plate. After mixing, the plate was incubated for 1 hour at 37°C. Fluorescence was measured with a Varioskan Flash 40053 microplate luminometer (Thermo Fisher Scientific, Waltham, MA, USA) with an emission wavelength of 350 nm and an excitation wavelength of 450 nm.

2.2.6 Statistical Analysis

For all cell culture experiments, statistical analysis was performed with the data transformed into percentage of positive/negative control. Dose response curves for inhibitory effects were fitted with nonlinear regression with an inhibitor or (log)inhibitor vs. normalized response model in GraphPad Prism 9.1.0. IC50 values were calculated with this method for crystal violet assays and Eurofins IC50 determination.

3-way-ANOVA was performed for the crystal violet assay and caspase-3 activity assay for each cell line separately with the factors time, dose and compound. As the assumption of homogeneity of variance was not fulfilled according to Levene's test, statistical analysis of these experiments is considered exploratory, not confirmatory. For the LDH assay, the more robust one-way Welch's ANOVA was performed for each time point with Dunnett's T3 multiple comparisons test.

Results were considered significant at a p-value < 0.05. All statistical analyses except the fitting of dose response curves were performed with IBM SPSS Statistics 26.

3 Results

3.1 Target Identification

As a first step, the hypothesis of the compounds being (tyrosine) kinase inhibitors was investigated by performing *in silico* target prediction and subsequent verification with a radiometric assay.

3.1.1 Target Prediction

Target prediction studies were performed from both a ligand- and a structure-based perspective. For the subsequent *in vitro* verification screening, the results from the different tools for our lead structure **Thio-Iva** were combined and the resulting panel was expanded with kinases relevant to the pathomechanism of HCC.

3.1.1.1 Ligand-Based Target Prediction

Potential targets for **Thio-Iva** and **Briva** were predicted using the web server SwissTargetPrediction, which calculates similarities to compounds with known actives based on their molecular structures. The screening took into consideration all protein families with available data of bioactive compounds.

Figure 9 shows an overview of target classes represented in the results (top 100 predicted targets) found for **Thio-Iva** (A) and **Briva** (B). Note that the targets were grouped according to the BRENDA Comprehensive Enzyme Information System (102). The group 'non-enzyme target' includes proteins such as ion channels, structural proteins or G protein-coupled receptors.
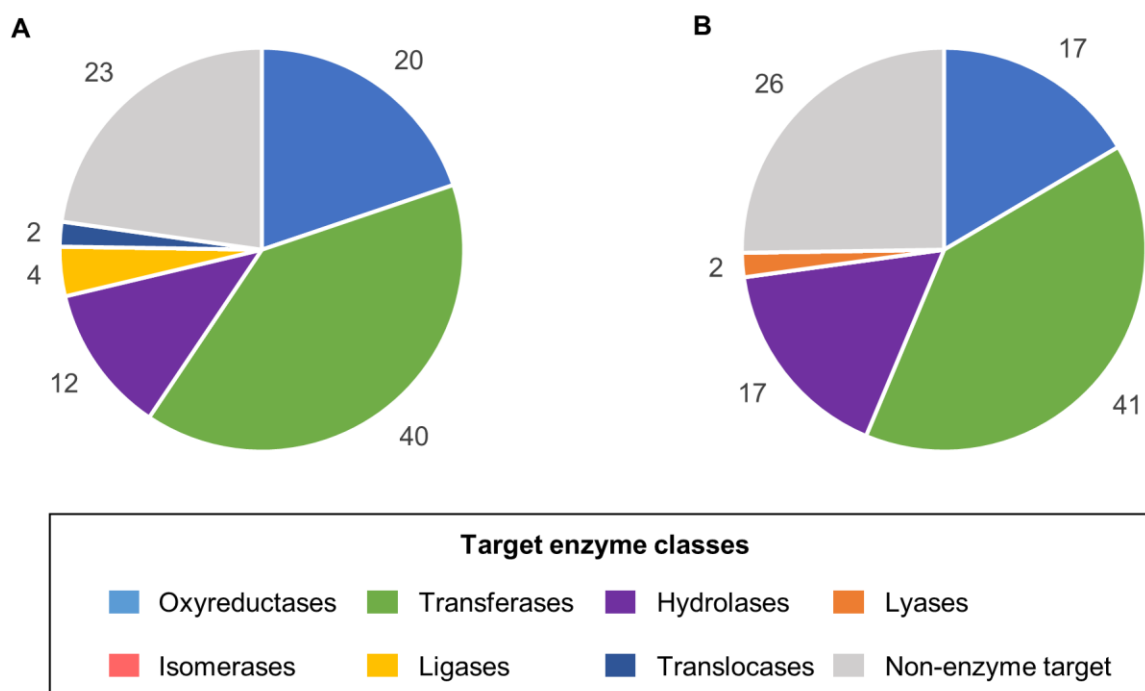
Figure 9. Target classes of top 100 targets predicted by SwissTargetPrediction for **Thio-Iva** (**A**) and **Briva** (**B**), classified according to the BRENDA Comprehensive Enzyme Information System (102). The total number is higher than 100 due to IRE1 being classified as both a transferase and a hydrolase, and GSTA1 as an oxyreductase, transferase and isomerase.

Kinases, a subgroup of transferases, represented the largest predicted target family for both compounds (36 targets for **Thio-Iva** and 34 targets for **Briva**) and were therefore further investigated. Table 4 shows the kinase results for **Thio-Iva** and **Briva**, respectively. 17 of the kinases were predicted as potential targets for both compounds.

Table 4. Prediction by SwissTargetPrediction of potential kinase targets of **Thio-Iva** and **Briva**.
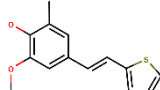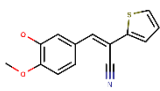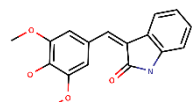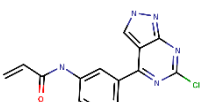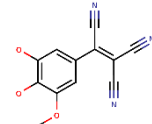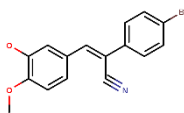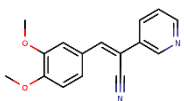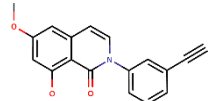
Thio-Iva				Briva			
ABL1	Erk1	KDR	PDHK1	**ABL1**	CLK2	**ILK**	**PLK1**
AKT1	FGFR1	KIT	PIM1	**AKT1**	CLK3	**IRE1**	**PLK4**
AurB	FGFR3	LYN	PIM2	**BRAF**	CLK4	JAK1	RAF1
BRAF	**GSK3A**	MET	PKCa	BRK	DYRK1A	JAK2	**RET**
BTK	**GSK3B**	MSK1	**PLK1**	**CDC2**	DYRK1B	JNK1	smMLCK
CDC2	**ILK**	**p38a**	**PLK4**	**CDK2**	EGFR	**JNK2**	**SRC**
CDK2	**IRE1**	p70S6K	**RET**	CDK5	**GSK3A**	**JNK3**	
CLK1	**JNK2**	PDGFRa	RSK2	CK2a1	**GSK3B**	NEK1	
DAPK3	**JNK3**	PDGFRb	**SRC**	**CLK1**	HGK	**p38a**	

Kinases predicted as targets for both compounds are shown in **bold**. Kinase names unified to naming convention used by KinHub (78) and sorted alphabetically.

Investigation of known actives similar to **Thio-Iva** and **Briva** showed that generally, many more similar 2D structures were found for **Briva** than for **Thio-Iva**, while more similar 3D structures were found for **Thio-Iva** than for **Briva**. For the subgroup of kinases, the amount of 3D similar known actives found was more alike, and 2D similarity was detected

for only one target (35 known actives of EGFR similar to **Briva**). Table 5 shows the known actives with the highest similarity score overall and within the kinase subgroup. Compound CHEMBL67027 (also called RG-13022) is featured in this table despite its low similarity score, as it is the tyrphostin on which the panel of compounds investigated in this thesis is based on.

Table 5. Examples of known actives most similar to **Thio-Iva** and **Briva** in 2D and 3D as predicted by SwissTargetPrediction.

Thio-Iva	Target	2D[1]	Known active		Notes
	ALOX5	0.70	CHEMBL413324		Also inhibits COX, 2nd highest 3D similarity (0.89)
	Target	**3D[2]**	**Known active**		
	DHFR	0.90	CHEMBL2163553		Also inhibits TYSY
	BTK	0.88	CHEMBL3685421		Kinase with highest similarity score
Briva	**Target**	**2D[1]**	**Known active**		
	EGFR	0.74	CHEMBL489147		Highest similarity score overall and in kinases
	EGFR	0.60	CHEMBL67027		Also inhibits PDGF
	Target	**3D[2]**	**Known active**		
	EGFR	0.85	CHEMBL2442327		

[1] 2D similarity shown as Tanimoto index. [2] 3D similarity shown as Manhattan-based similarity score. Images created with MarvinSketch (34).

3.1.1.2 Structure-Based Target Prediction

@TOME Screening

The structure-based target prediction screening with @TOME was performed with all 241 available kinases for **Thio-Iva** and **Briva**. The largest group in the kinase screening library was tyrosine kinases with 22%.

As scores are returned for all available targets, a selection of higher scoring targets – more likely to represent true targets – was made. For **Thio-Iva**, predictions with a predicted affinity of less than 5 nm pKd and an LPE of 3 or higher (indicating a 'dubious' binding mode as suggested on the screening service website (77)) were excluded in this step. These criteria left 94 kinases (Table 6) predicted for **Thio-Iva** for further analysis.

Table 6. Selected @TOME screening results for **Thio-Iva**.

Kinase	pKd	Kinase	pKd	Kinase	pKd	Kinase	pKd	Kinase	pKd
PAK2	6.1	**TRKA**	5.5	CASK	5.4	DAPK2	5.2	JNK2	5.1
PKN1	6.0	**MST1**	5.5	**IRE1**	5.4	**JNK3**	5.1	**ACTR2B**	5.1
FGFR1	5.9	**MAP2K1**	5.5	**ITK**	5.3	**CaMKK2**	5.1	PAK6	5.0
BIKE	5.9	**MST2**	5.5	**MINK**	5.3	**TTK**	5.1	**TAK1**	5.0
CDK2	5.9	**CHED**	5.5	**MAP3K5**	5.3	**KHS2**	5.1	PKACa	5.0
COT	5.9	Wee1B	5.5	AurB	5.3	DRAK2	5.1	GSK3B	5.0
SgK085	5.9	**RET**	5.4	**CRK7**	5.3	**TIE2**	5.1	**EphB4**	5.0
CDK5	5.8	**TNIK**	5.4	**CLK3**	5.3	PHKg2	5.1	RSK2	5.0
DYRK3	5.8	**ABL2**	5.4	JAK1	5.3	**CK1d**	5.1	PKCt	5.0
PLK3	5.8	**HGK**	5.4	**BMX**	5.3	IGF1R	5.1	TBK1	5.0
CK2a2	5.7	**VRK1**	5.4	CDKL2	5.3	**CLK2**	5.1	**LIMK1**	5.0
RIPK1	5.7	PDK1	5.4	**MST3**	5.2	**TGFbR2**	5.1	**Erk2**	5.0
AMPKa2	5.6	PDPK2P[1]	5.4	**SLK**	5.2	**Wnk3**	5.1	PIM2	5.0
CHK2	5.5	**CDKL3**	5.4	**CaMK1g**	5.2	ULK3	5.1	**FYN**	5.0
IRAK4	5.5	**CaMKK1**	5.4	**TGFbR1**	5.2	**FGFR2**	5.1	PCTAIRE	5.0
PIM1	5.5	CLK1	5.4	**CDK6**	5.2	RSK1_b	5.1	AKT2	5.0
AurA	5.5	**ACK**	5.4	TAO2	5.2	**KDR**	5.1	MPSK1	5.0
ULK1	5.5	BMPR1B	5.4	PLK1	5.2	HPK1	5.1	RAF1	5.0
MET	5.5	MAP2K6	5.4	MST4	5.2	**CSK**	5.1		

Kinases appearing in both **Thio-Iva** and **Briva** screening shown in **bold**. Kinase names unified to naming convention used by KinHub (78). [1] Missing in KinHub, HGNC name (103) used instead.
pKD Predicted affinity as calculated by @TOME server.

For **Briva**, a higher pKd was observed for more kinases compared to **Thio-Iva**, with the highest pKd of **Briva** on MYT1 with 7.1, as compared to **Thio-Iva** on PAK2 with 6.1. To achieve a similar rate of most likely targets as for **Thio-Iva** (about 40%), the minimal pKd to include targets in the analysis was increased to 5.8, which lead to 96 included kinases (Table 7).

Table 7. Selected @TOME screening results for **Briva**.

Kinase	pKd	Kinase	pKd	Kinase	pKd	Kinase	pKd	Kinase	pKd
MYT1	7.0	**CK2a2**	6.4	Wee1	6.2	**HGK**	6.0	CK1e	5.9
CDK5	6.8	TYK2	6.4	Haspin	6.2	CK2a1	6.0	**ULK1**	5.9
CaMKK2	6.8	CDK9	6.4	AAK1	6.2	**ITK**	6.0	AMPKa1	5.9
ABL2	6.8	**CDKL3**	6.4	TTBK1	6.2	ZAP70	6.0	**CHK2**	5.8
ABL1	6.8	**AurA**	6.3	PLK4	6.2	DYRK2	6.0	NEK2	5.8
TRKA	6.8	**FGFR2**	6.3	**CLK2**	6.2	VRK2	6.0	CSNK2A3[1]	5.8
PKN1	6.8	RIPK2	6.3	p38g	6.2	**ACTR2B**	6.0	CaMK2g	5.8
COT	6.8	**TIE2**	6.3	**CaMK1g**	6.2	MAPKAPK3	6.0	**TTK**	5.8
BIKE	6.8	**IRE1**	6.3	**PIM1**	6.1	**FYN**	6.0	CaMK2d	5.8
CaMKK1	6.7	**MST1**	6.3	CHK1	6.1	JAK2	6.0	**CK1d**	5.8
CHED	6.7	JAK3	6.3	MELK	6.1	**Wnk3**	6.0	**CSK**	5.8
DYRK3	6.7	p70S6K	6.3	**AMPKa2**	6.1	**TAK1**	5.9	PKCi	5.8
PAK2	6.6	FLT1	6.3	**TGFbR1**	6.1	**EphB4**	5.9	**BMX**	5.8
CRK7	6.6	**IRAK4**	6.2	**CDK6**	6.1	JNK1	5.9	**KDR**	5.8
MAP2K1	6.6	**MST3**	6.2	**MAP3K5**	6.1	**SLK**	5.9	**SgK085**	5.8
TNIK	6.5	**CDK2**	6.2	**CLK3**	6.1	**JNK3**	5.9	ALK4	5.8
MINK	6.5	MAPKAPK2	6.2	DYRK1A	6.1	**Erk2**	5.9		
FGFR1	6.5	MNK2	6.2	**VRK1**	6.0	**LIMK1**	5.9		
TGFbR2	6.5	ZAK	6.2	**RET**	6.0	**ACK**	5.9		
MST2	6.5	**KHS2**	6.2	EphA3	6.0	PKCa	5.9		

Kinases appearing in both **Thio-Iva** and **Briva** screening shown in **bold**. Kinase names unified to naming convention used by KinHub (78). [1] Missing in KinHub, HGNC name (103) used instead.
pKD Predicted affinity as calculated by @TOME server.

Of the potentially targeted kinases predicted, 59 were for both compounds, 35 were only for **Thio-Iva** and 37 were only for **Briva**. To determine if some kinase families were more prevalent in the prediction for **Thio-Iva** and **Briva** compared to the complete screened dataset, distribution of predicted targets was analyzed (Figure 10). A deviation of more than 10% from the average prediction rate (~40%) over all groups was observed for *atypical* kinases (with none of the seven available kinases predicted as a target), as well as for *AGC*, where only 27% were predicted as potential targets for **Thio-Iva**, and only 15% for **Briva**. Targets from the group *STE* were enriched compared to the overall results for **Thio-Iva** (61%). For **Briva**, the enriched groups were *CMGC* (51%) and *CK1* (83%). Note that the representation of some groups in this screening is quite small, such as *atypical* kinases (eight members) and *CK1* (six members).
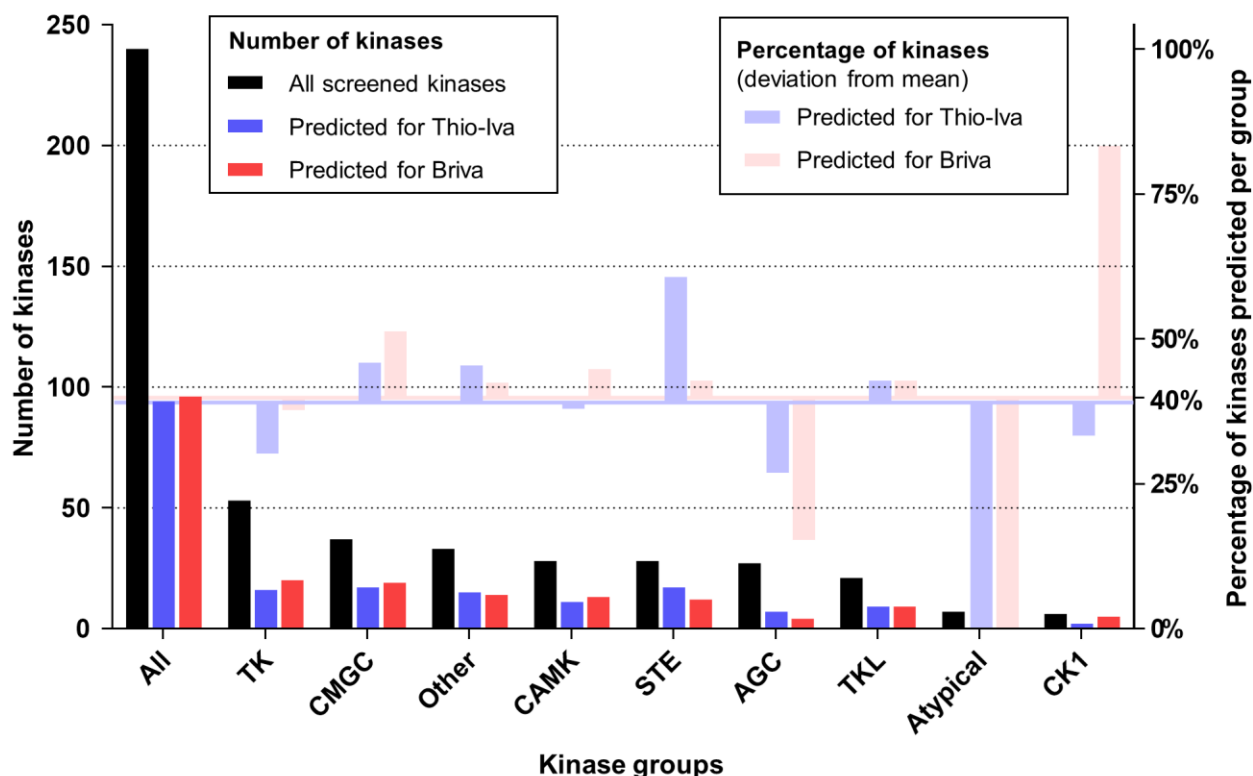
Figure 10. Results of @TOME target prediction by kinase families. **Left axis:** Absolute numbers of kinases screened and predicted for **Thio-Iva** and **Briva – Right axis:** Percentage of kinases predicted for each compound per kinase family, shown as deviation from the mean of predicted kinases.

iRAISE Screening

A screening of **Thio-Iva** against 796 crystal structures from 56 tyrosine kinases was performed with iRAISE. For 714 crystal structures from 54 TKs, poses and their scores could be obtained with this method. Subsequent SeeSAR redocking was performed for the structure with the highest scoring pose per kinase and evaluated according to the inbuilt HYDE scoring function. Results showed a range of estimated affinities (Table 8). While HYDE scores (the lower, the better) varied strongly across kinases, plausible binding modes could be generated in almost all visually inspected crystal structures.

Table 8. Results of iRAISE screening and SeeSAR redocking for **Thio-Iva**.

Kinases	PDB	EA (in µM)	Kinases	PDB	EA (in µM)	Kinases	PDB	EA (in µM)
FMS	4R7H	0.10 - 8.89	TYK2_b	3ZON	2.08 - 206.70	**FYN**	2DQ7	10.58 - 1051
KIT	3G0F	0.17 - 16.48	**FLT1**	3HNG	2.10 - 208.63	FES	3BKB	10.66 - 1059
EphA7	3DKO	0.18 - 17.42	**SRC**	1YOL	2.69 - 267.20	IGF1R	3QQU	12.25 - 1217
ErbB2	3RCD	0.21 - 21.16	**BMX**	3SXR	2.80 - 278.64	**DDR1**	4CKR	13.71 - 1362.
ErbB4	3BBT	0.33 - 32.84	**LYN**	3A4O	3.14 - 312.16	JAK3	4QT1	21.19 - 2106
TRKA	4PMM	0.36 - 35.52	SYK	4I0T	3.34 - 331.87	TYK2	3LXN	30.28 - 3008
TRKC	3V5Q	0.36 - 35.88	**INSR**	5E1S	3.48 - 345.55	EphA2	1MQB	31.67 - 3147
MET	3CTH	0.46 - 45.16	**ACK**	4ID7	3.76 - 373.82	**FAK**	4GU9	31.67 - 3147
BRK	5DA3	0.49 - 48.64	CSK	1BYG	3.95 - 392.81	JAK1	4K6Z	61.27 - 6087
TIE2	2WQB	0.53 - 52.99	**ErbB3**	3LMG	3.97 - 394.24	RON	3PLS	210.92 - 20957

ALK	3LCS	0.88 - 87.26	**FGFR1**	4UWB	4.64 - 460.63	**EphA3**	4G2F	216.88 - 21549
KDR	3U6J	0.96 - 95.09	**FGFR2**	2Q0B	4.73 - 469.47	ROS	3ZBF	314.24 - 31221
LCK	2HCK	0.97 - 96.06	**EphB4**	3ZEW	5.35 - 531.09	FGFR4	4TYI	385.33 - 38285
PDGFRb	3LCD	0.97 - 96.65	TRKB	4AT3	5.77 - 573.26	ITK	4PPB	446.28 - 44341
FLT3	4RT7	1.09 - 108.18	**MER**	4MH7	7.63 - 758.39	RET	2IVT	450.21 - 44731
PYK2	3FZT	1.23 - 122.31	ABL2	2XYN	8.58 - 852.72	JAK2	4BBE	459.51 - 45655
BTK	4ZLY	1.30 - 128.72	**ABL1**	2G2F	8.69 - 863.38	ZAP70	4K2R	$2.7 \times 10^5 - 2.7 \times 10^7$
HCK	3VS7	1.31 - 129.70	EGFR	5CAP	10.21 - 1013	FGFR3	4K33	$2.1 \times 10^6 - 2.1 \times 10^8$

EA Estimated Affinity as calculated with the HYDE scoring function by SeeSAR.
Kinases with favourable binding pose as highest scoring pose shown in **bold**. Kinase names unified to naming convention used by KinHub (78).

Manual investigation of the binding poses showed that in 41 out of the 54 screened kinases the top scoring pose formed a hydrogen bond at the hinge region (Figure 11). In 23 of these targets, the top scoring pose formed this hydrogen bond with the nitril group of **Thio-Iva**, which was considered the most favorable binding pose (104). In 13 kinases, the top scoring pose did not express an interaction with the hinge region at all. Of the 31 targets where the top scoring pose did not show an interaction between the nitril and the hinge region, alternative poses were investigated. For 14 of these targets, a lower scoring pose existed that formed a hydrogen bond with the nitril at the hinge region. Only for the six targets with the lowest scoring top pose (Table 8) was there also no pose interacting at the hinge region.
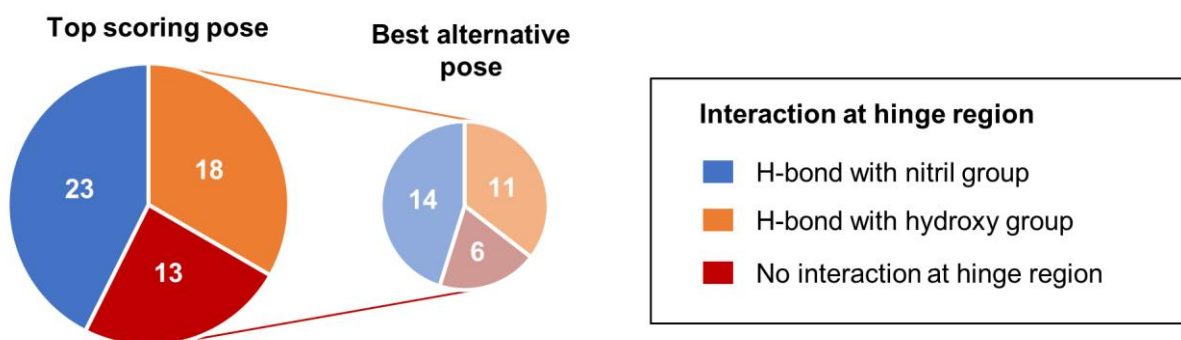

Figure 11. Observed poses (SeeSAR) of **Thio-Iva** in crystal structures of 54 different kinase targets. Binding properties are shown for the top scoring pose (left pie). For the 31 kinases where the top pose's interaction at the hinge region was not a hydrogen bond with the nitril group of **Thio-Iva**, interactions of the best alternative pose were investigated (right pie).

3.1.1.3 Correlation of In Silico Target Predictions

To increase the reliability of our computational target predictions, the results for the lead compound **Thio-Iva** from all three *in silico* prediction methods were combined.
Figure 12 shows the selected results on a human kinome tree generated by KinMap (78). The following targets were included from each method: (i) 35 targets from the iRAISE

screening that passed subsequent manual evaluation with SeeSAR, exhibiting an estimated affinity of below 10 – 1000 µM; (ii) 94 out of the 241 kinases screened with @Tome that fulfilled the two thresholds of a minimum of 5 nm pKd and a LPE of less than 3; (iii) Using the ligand-based similarity approach with SwissTargetPrediction, all kinases with any known actives above the similarity thresholds were included.

All targets that were suggested by more than one method were included in the final list. The ranking within each method was not taken into consideration. This resulted in a final list of 29 computationally predicted targets. Note that due to irregularities within the different naming conventions used in the screening methods, IRE1 and RSK2 were accidentally not included in the final list, despite appearing in more than one method, and PDK1 was included needlessly.

Furthermore, 20 targets known to be relevant for HCC were identified from literature (7), 14 of which were not already represented in the correlated *in silico* target prediction list (however, 9 of the 14 appeared in exactly one of the computational target prediction methods). They were therefore added to the final list of 43 targets, which were subsequently experimentally evaluated by radiometric kinase assays (see Chapter 3.1.2).
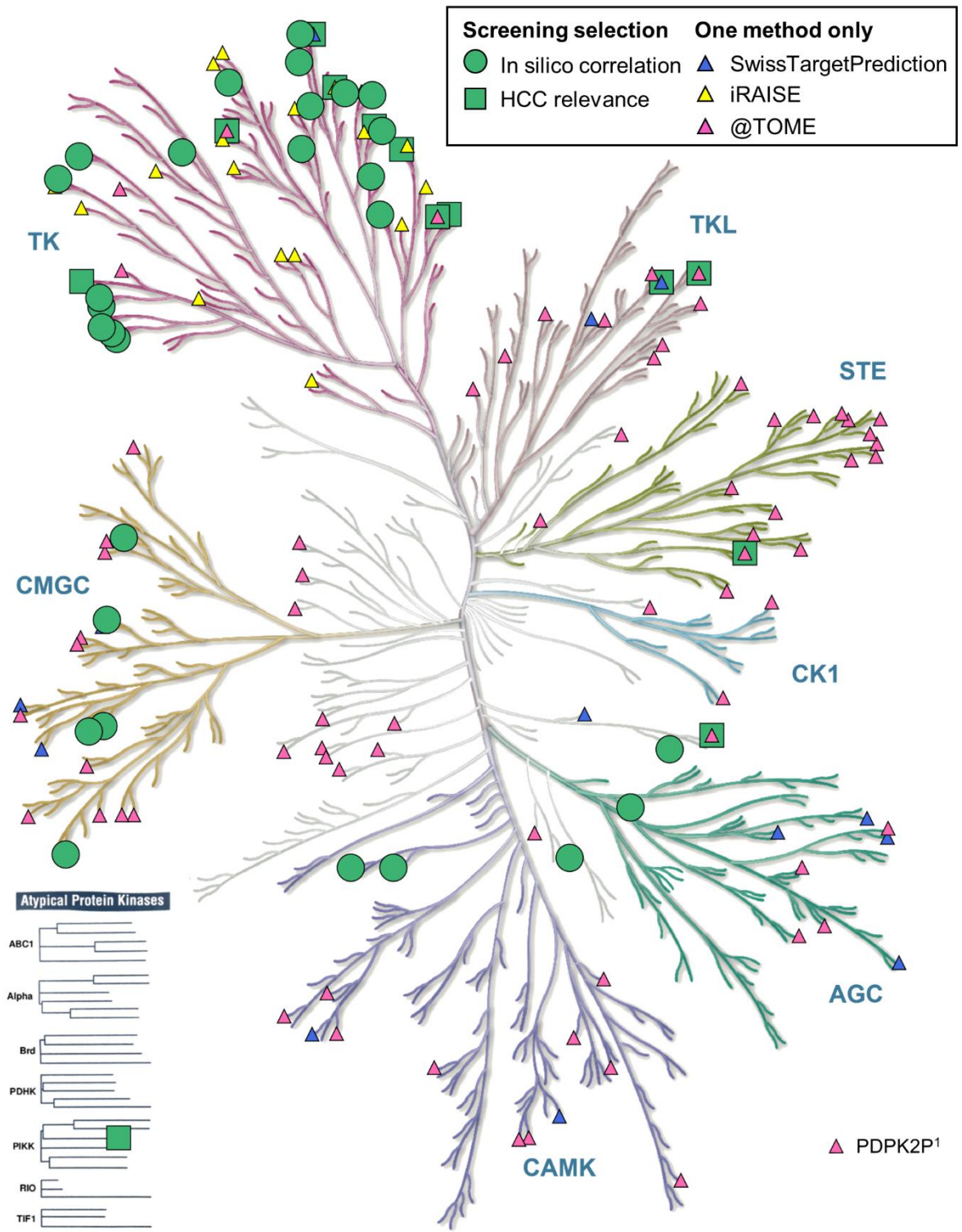
Figure 12. Visual representation of **Thio-Iva** targets selected for *in vitro* testing (green), predicted by more than one prediction method (circles), targets included due to relevance to HCC (squares), and targets predicted by one screening method only (triangles). [1] Kinase not present on KinMap.
Source: KinMap. Illustration reproduced courtesy of Cell Signaling Technology, Inc. (www.cellsignal.com).

3.1.2 Kinase Profiling

A set of 43 targets (see Chapter 3.1.1.3) was screened with the KinaseProfiler™ to identify **Thio-Iva's** targets and to evaluate the prediction power of the *in silico* methods. Results showed more than 50% inhibition of kinase activity by 10 µM **Thio-Iva** for six out of the 43 tested kinases (Figure 13 and Figure 14).
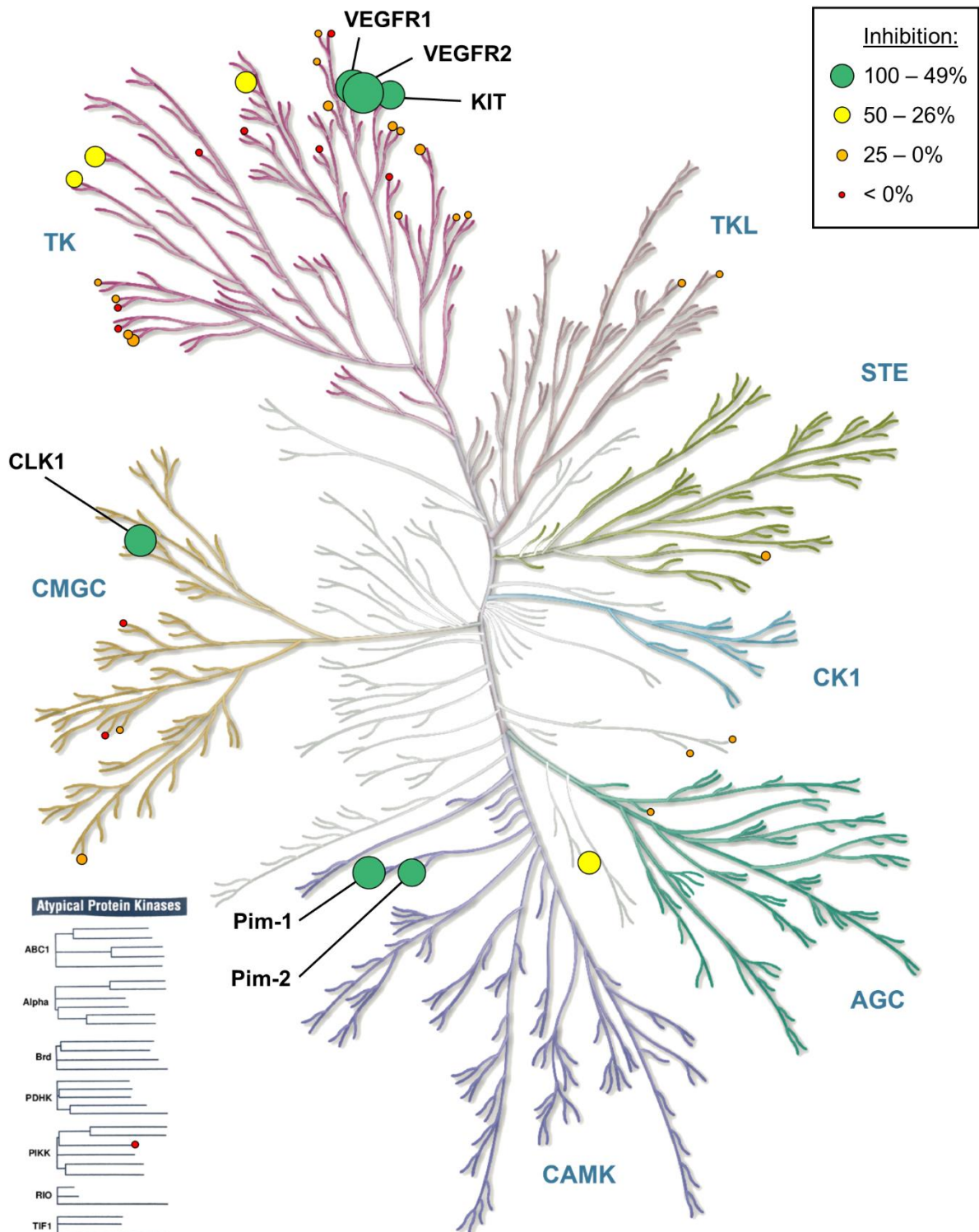
Figure 13. Visual representation of Eurofins KinaseProfiler™ results for **Thio-Iva** at 10 µM (43 Kinases). Source: KinMap. Illustration reproduced courtesy of Cell Signaling Technology, Inc. (www.cellsignal.com).

The strongest inhibition was observed for VEGFR2 (89%) and VEGFR1 (75%). The other four strongly inhibited kinases were Pim-1 (71%) and Pim-2 (60%), as well as CLK1 (69%) and c-Kit (61%). These six targets, as well as EGFR, were then also screened for the inhibitory effects of **Thio-Dam**, **1a** and **Briva** (Figure 14). Interestingly, **Thio-Dam** showed strong inhibition of VEGFR2 (86%), while not inhibiting the other six kinases by more than 50%. **1a** exhibited no effect on VEGFR2, and only inhibited CLK1 by more than 50% (68%). For **Briva** the effects were less pronounced than **Thio-Iva**, with only three (VEGFR2 (56%), CLK1 (67%) and c-KIT (62%)) of the seven targets inhibited by more than 50%.
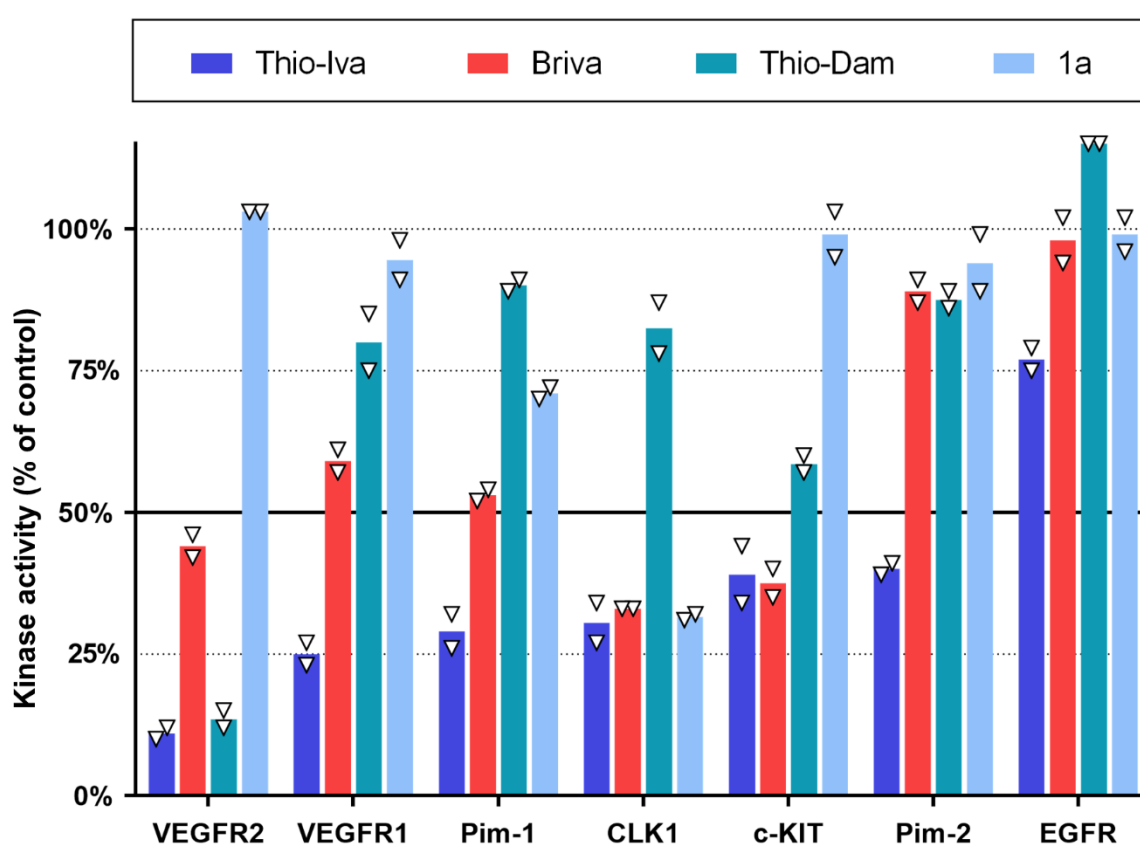
Figure 14. Eurofins KinaseProfiler™ results for **Thio-Iva**, **Thio-Dam**, **1a** and **Briva** at a concentration of 10 µM. Kinase selection based on **Thio-Iva** results, with EGFR added independently. Data given as percentage of uninhibited control (mean with individual data points).

An additional concentration row for IC50 determination of **Thio-Iva** on the most strongly inhibited kinase VEGFR2 (Figure 15) was performed by Eurofins. The calculated IC50 amounted to 2.81 µM.
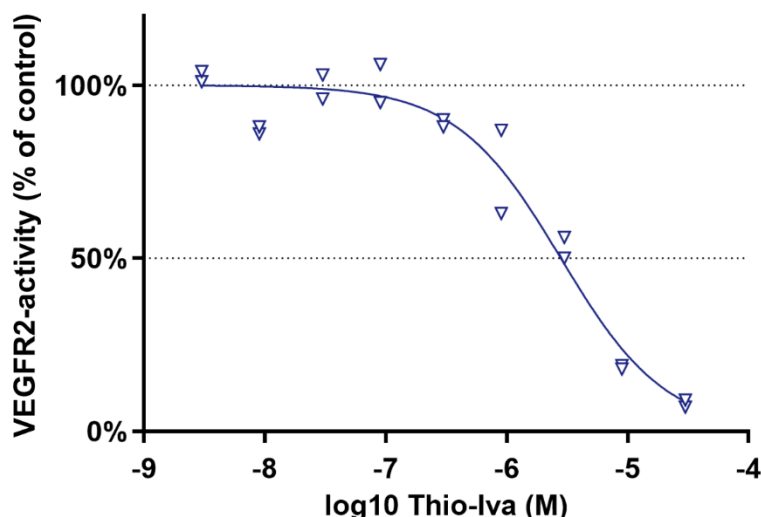
Figure 15. VEGFR2 activity in relation to concentration of **Thio-Iva**. Data shown as individual data points and curve fitted with nonlinear regression.

3.2 Structure-Activity Relationship

3.2.1 Docking Studies

To better understand how the compounds exhibit their effect on **Thio-Iva's** potential main target VEGFR2, molecular docking was performed for all ten proposed compounds shown in Figure 5, B, i.e., the thiophenes **Thio-Iva**, **Thio-Van**, **Thio-Dam**, **1a**, **1e**, **1i** and **1j**, as well as the bromobenzenes **Briva**, **Brova** and **Bro-Dam**. VEGFR2 was chosen following the results of the computational target prediction and subsequent kinase-assay evaluation for the lead compound **Thio-Iva** (see Chapter 3.1.2).

As a proof of concept for the docking tool (SeeSAR), the co-crystallized ligand of the crystal structure 3VHE (42Q) was redocked and showed a stable predicted pose with an RMSD of 2.2 Å when compared to the co-crystallized ligand position.

Results of the docking studies for the ten compounds against VEGFR2 (on the crystal structure 3VHE) were investigated according to estimated affinities predicted by HYDE scoring, as well as by visual inspection. The highest scoring docking poses for each compound are shown in Table 9. Additional poses for **Thio-Iva** were included to illustrate some of the observed variable binding modes. The 2nd highest scoring pose of **Thio-Dam** and the 6th for **Bro-Dam** were also included, as for these compounds, these were the highest scoring poses with a hydrogen bond formed between the compound's nitril and the backbone nitrogen of cysteine 919. Interaction with the hinge region is an essential feature of ATP binding, and often observed in clinically successful inhibitors (104).

Table 9. Selected docking results for 3VHE.

Compounds	EA (SeeSAR)	H-bonds
Thio-Iva_075	14.60 – 1450.19 nM	**Cys919**
Thio-Iva_111	29.27 – 2908.34 nM	**Cys919**, Asp1046
Thio-Iva_032	35.37 – 3514.07 nM	**Cys919**, Asp1046
Thio-Van_115	48.96 - 4864.40 nM	**Cys919**
Thio-Dam_104	33.14 - 3292.22 nM	Gly841
Thio-Dam_47	46.28 - 4598.48 nM	**Cys919**
1a_69	194.53 - 19327.59 nM	**Cys919**
1e_31	0.41 - 40.67 nM	**Cys919**
1j_12	23.51 - 2336.11 nM	**Cys919**, Phe1047
1i_28	24.87 - 2470.97 nM	**Cys919**, Glu885
Briva_17	26.04 – 2587.05 nM	**Cys919**, **Leu840**
Brova_25	34.27 - 3404.51 nM	**Cys919**
Bro-Dam_107	9.20 - 913.62 nM	(H_2O-Asp1046)
Bro-Dam_106	13.70 – 1361.65 nM	**Cys919**, Glu885

Numbering of compounds according to SeeSAR generated pose (random). **EA** Estimated Affinities according to HYDE scoring function in SeeSAR – H-bonds predicted by both SeeSAR and LigandScout shown in **bold**. H-bond in () only predicted by SeeSAR.

Figures 16 and 17 show 3D and 2D depictions of the highest scoring binding pose interacting at the hinge region for each compound. For some compounds (**Thio-Iva**, **Thio-Van**, **Brova** and **1e**), this pose was also the most frequent orientation among the 50 highest scoring poses. In others (notably **1a**, **1i** and **1j**), the top scoring pose was not frequent at all. The top poses of only two compounds (**Thio-Dam** and **Bro-Dam**) had no hinge region interaction, while the top scoring poses of all the others formed a hydrogen bond with their nitril to cysteine 919.
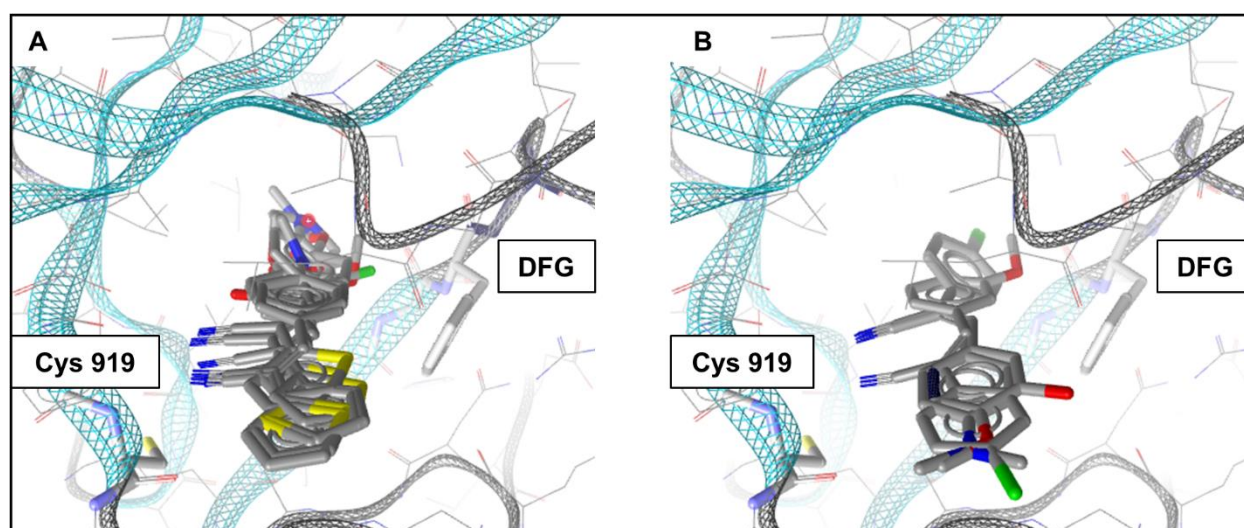
Figure 16. Overlay of all thiophenes (**A**) and all bromobenzenes (**B**) in their highest scoring pose interacting with the hinge region of VEGFR2. Images created with LigandScout.
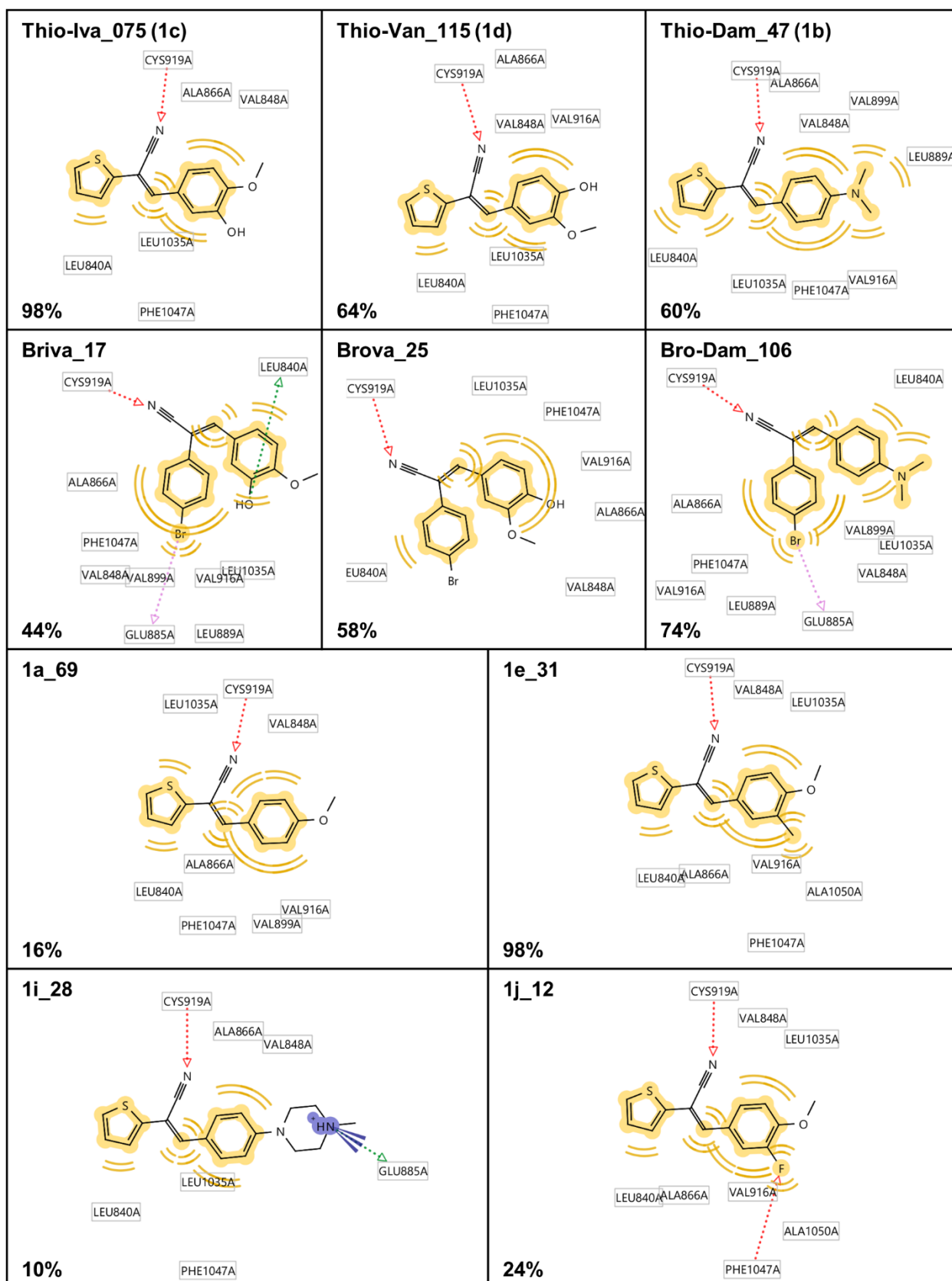
Figure 17. 2D images of highest scoring binding pose for each compound in VEGFR2 (3VHE). Frequency of pose in the 50 highest scoring poses shown in percentage at the bottom left. Images created with LigandScout. Arrows indicate hydrogen bonds (green: donor, red: acceptor), yellow indicates hydrophobic interaction, blue a positive ionizable area.

In Figure 18 predicted high scoring binding poses of **Thio-Iva** are shown to illustrate the variations of this compound's most frequent pose. The three binding poses depicted were later used as starting positions for molecular dynamics simulations (see Chapter 3.2.2).
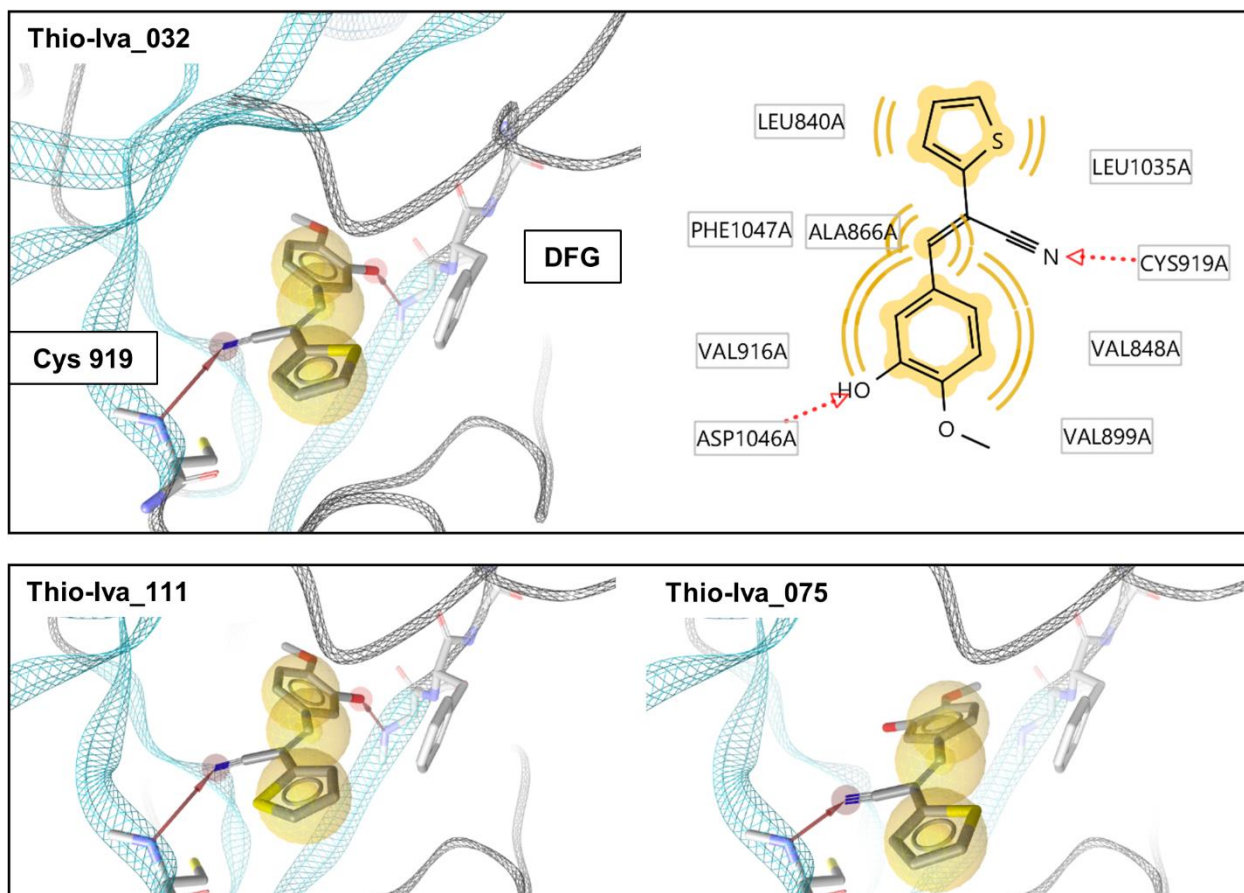

Figure 18. ATP-binding pocket of VEGFR2 (3VHE) with predicted binding poses of **Thio-Iva**. Images created with LigandScout**.**

A detailed analysis of the 50 highest scoring poses for all ten compounds is summarized in Table 10. Results show that of all the compounds investigated, **Thio-Iva** and **1e** were docked most consistently, with 49 of 50 poses forming a hydrogen bond between the nitril group of the ligand and the backbone nitrogen of cysteine 919 at the hinge region of VEGFR2. For **Thio-Iva**, 33 out of 50 poses formed a hydrogen bond of the nitril group with the backbone nitrogen of cysteine 919 at the hinge region, and the thiophene ring turned towards the solvent (Figure 18). 16 poses still formed the same hydrogen bond, but the entire molecule was flipped by 180°, with the thiophene ring oriented towards the back pocket. Only one of the top 50 poses of **Thio-Iva** formed no hydrogen bond at the hinge region.

Thio-Van and **Thio-Dam** also showed the majority of the first 50 poses docking in this orientation. However, for these compounds more poses than for **Thio-Iva** and **1e** were

predicted to have no interaction to the hinge region. For the compounds **1a**, **1i** and **1j**, the majority of the top 50 generated poses showed no interaction at the hinge region. The compound group with the bromobenzene showed less consistent binding modes compared to **Thio-Iva** overall, with **Bro-Dam** showing most consistent results and a preference to turn the bromine towards the solvent to a similar extent as the thiophene in **Thio-Dam**. Meanwhile, almost half of the top 50 predicted poses for **Briva** and **Brova** showed no interaction at the hinge region, and the remaining ones showed a preference to turn the bromine towards the back pocket. Only two compounds, **Briva** and **Thio-Van**, presented some poses with their hydroxy group forming a hydrogen bond with the hinge region.

Table 10. Analysis of top 50 docking poses according to SeeSAR for all ten investigated compounds.

Interaction at Hinge region	Thio-Iva	Thio-Van	Thio-Dam	1a	1e	1i	1j	Briva	Brova	Bro-Dam
H-bond with nitril group	**49**	**32**	**30**	8	**49**	5	12	22	29	**37**
S/Br towards solvent	**33**	**19**	**30**	8	**32**	5	12	4	11	**31**
S/Br towards back pocket	**16**	**13**	0	0	**17**	0	0	18	18	6
H-bond with hydroxy group	**0**	**7**	**0**	0	**0**	0	0	5	0	**0**
No interaction	**1**	**11**	**20**	42	**1**	45	37	23	21	**13**

Poses of compounds with high consistency (> 30 poses in same position) marked in **bold**.

3.2.2 Molecular Dynamics Simulations

To analyze the interaction of the lead compound **Thio-Iva** with the target protein VEGFR2, molecular dynamics simulations were performed with Desmond 6.1.013 (91). Of the three investigated binding modes of **Thio-Iva** (075, 111 and 032) previously created with SeeSAR, **Thio-Iva_032** stayed most consistently in the binding pocket, and two more repeats with random starting speeds were performed. Results of the most stable MD in terms of RMSD of protein and compound (**Thio-Iva_032_2**) were further investigated. Figure 19 shows an overlay of pictures taken every 10 ns as a visual representation of a stable binding pose with **Thio-Iva** remaining consistently in the same orientation inside the binding pocket over the entire time simulated.
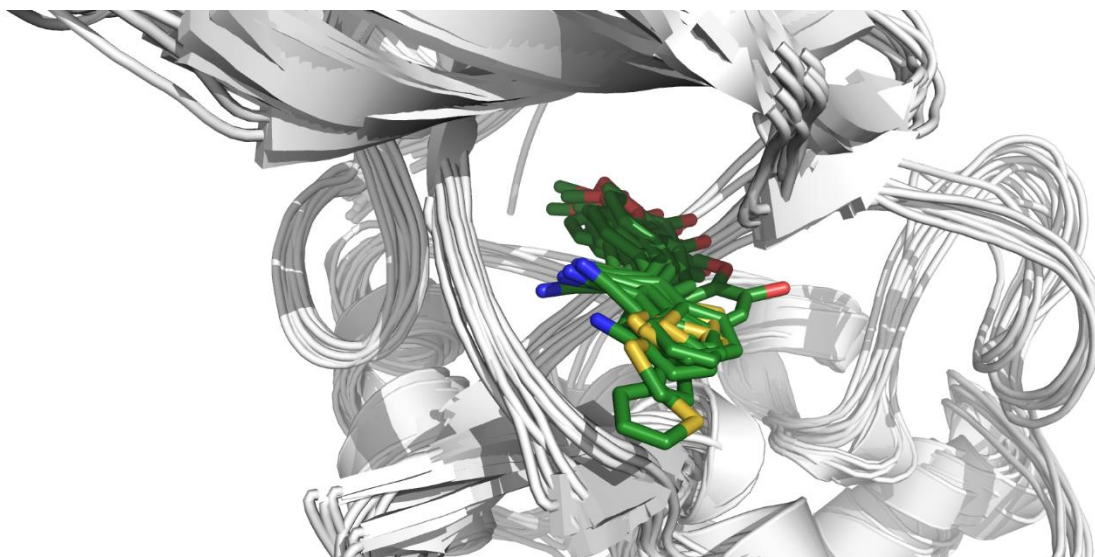
Figure 19. Overlay of snapshots taken every 10 ns from MD simulation of **Thio-Iva_032_2** in the structure 3VHE. Image created with PyMOL (42).

The RMSD of the protein and the ligand over time is shown in Figure 20, A. This is a measure of the average distance between atoms when superimposed onto the first frame of the MD simulation, thereby quantitatively describing the change in position over time. After a first jump in RMSD (correlating to the start increase in temperature of the simulated system) the RMSD of 3VHE stayed very stable. The ligand **Thio-Iva** also remained below a deviation of 4 Å over 97.2% of frames. However, at frame 497 there is a notable increase in RMSD, which corresponds to a change in position of **Thio-Iva** while remaining in the binding pocket. Within 2 ns, the molecule reverts to its initial position, with only the thiophene ring flipped by 180° for the remainder of the simulation.

The distance of **Thio-Iva's** nitril group to the cysteine 919 of 3VHE, corresponding to the essential hydrogen bond at the hinge region of VEGFR2, is illustrated in Figure 20, B. The distance remained below 3.8 Å over 99% of the simulation, the maximum distance proposed by Wolber et al. (90) to allow for a stable hydrogen bond interaction in crystal structures. The other hydrogen bond predicted for the binding pose used for the simulation was between **Thio-Iva's** hydroxy group and the backbone nitrogen of the aspartate 1046 (Figure 18). This bond appeared less stable over the time simulated, with only 2 frames where the distance between the interaction partners was below 3.8 Å. When investigating the distance to potential alternative interacting atoms in the region, the most consistent proximity was observed between the oxygen of the hydroxy group and the backbone oxygen of aspartate 1046 (Figure 20, B, Asp1046:O-1). There, the distance remained below 3.8 Å for 77% of frames.
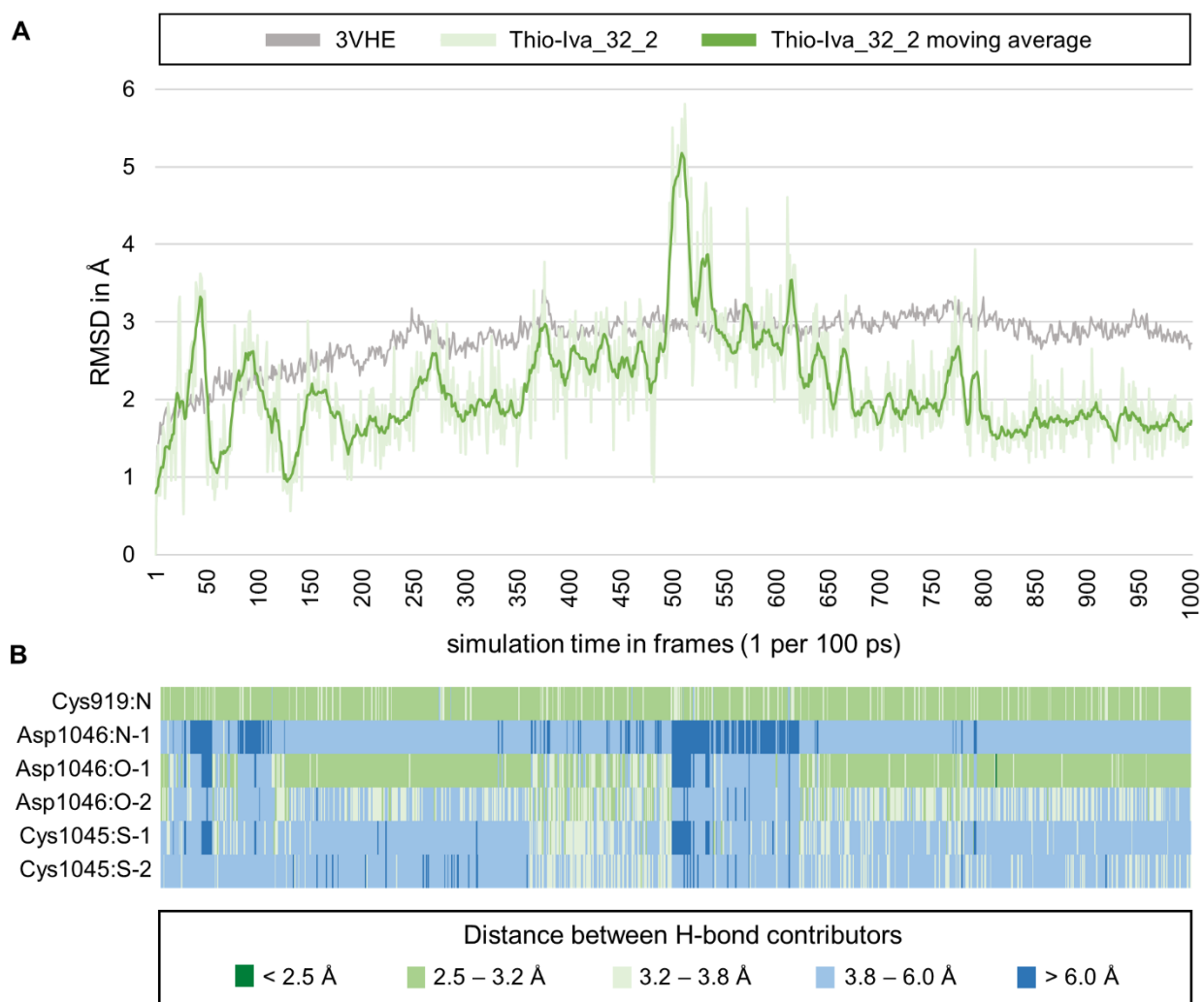
Figure 20. Analysis of MD simulation. **A** Graph showing the RMSD over time for 3VHE (grey) and **Thio-Iva** (green, showing each individual data point as well as the moving average over 10 frames). **B** Distance of donor and acceptor in the critical H-bond at the hinge region and a second potential interaction area close to the DFG motif. Nomenclature: **Cys**: Cysteine, **Asp**: Aspartate, **N:** Nitrogen, **1**: Oxygen of the hydroxy group, **2:** Oxygen of methoxy group.

3.3 Cell Growth Inhibition

The growth inhibitory effects of **Thio-Iva** and **Briva** on HepG2 and Huh-7 cells were studied with crystal violet assays over a total of 72 hours. Results showed a strong time- and dose-dependent inhibitory effect of both substances in both cell lines (Figure 21). Exploratory 3-way ANOVA tests showed a significant difference in means depending on the factors of time, dose, and compound in both cell lines. The difference in compound efficacy is illustrated by **Briva** needing to be dosed twice as high as **Thio-Iva** to achieve the same effect at most time points and for both cell lines.
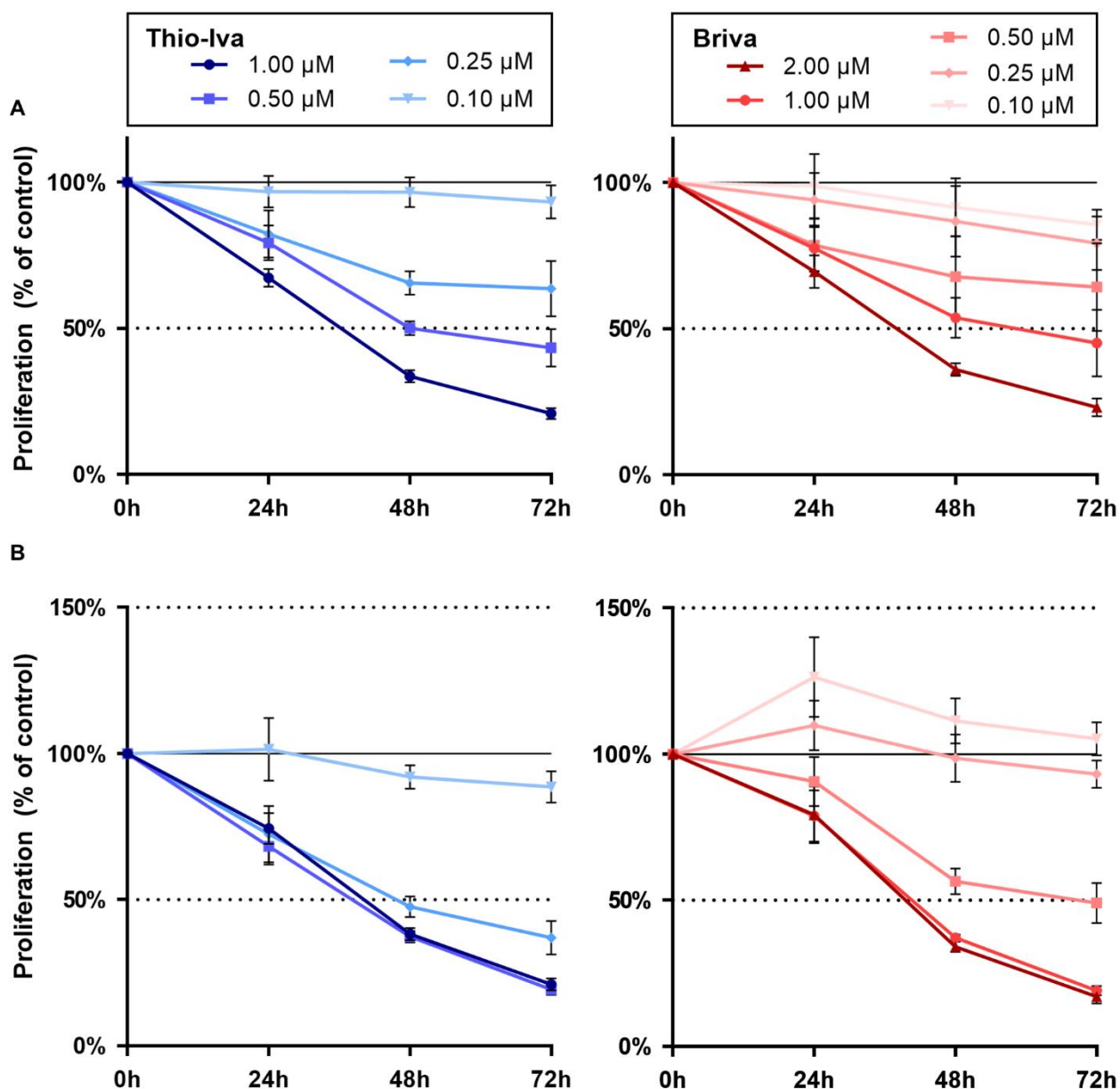
Figure 21. Growth inhibition of HepG2 (**A**) and Huh-7 (**B**) cells treated with **Thio-Iva** and **Briva**, shown as percentage of untreated control (mean ± SEM of at least n=4).

Table 11 shows the IC50 values (concentration at which 50% inhibition of proliferation was achieved) after 48 hours. The growth inhibitory effect of **Thio-Iva** was more pronounced than that of **Briva**, with IC50 values in the submicromolar range after 48 hours.

Briva's IC50 values were close to 1 µM, and interestingly, the compound seemed to have a growth stimulatory effect at very low concentrations after 24 hours in Huh-7 cells (Figure 21, B). As a model for non-malignant liver cells, our partner laboratory at the Johannes Gutenberg University investigated the growth inhibitory effects of **Thio-Iva** and **Briva** on the AML-12 cell model (Table 11). Growth inhibitory effects in these non-malignant liver

cells were less pronounced than in the HCC models HepG2 and Huh-7. The IC50 value for **Thio-Iva** was more than threefold higher in the nonmalignant cells than the highest from the cancer cell lines, while for **Briva** it was almost sixfold higher.

Table 11. IC50 values (in µM) after 48 hours.

	HepG2	Huh-7	AML-12
Thio-Iva	0.54 ± 0.06	0.38 ± 0.05	1.81 ± 0.31[1]
Briva	1.16 ± 0.24	0.97 ± 0.18	6.78 ± 1.37[2]

Results shown as mean ± SEM of at least n=4. [1] Data taken from Schaller et. al (64), [2] Unpublished data acquired by the same methods as for **Thio-Iva**.

3.4 Mode of Action and ADMET properties

3.4.1 In Silico ADME Evaluation

To get an overview of the lead compounds' properties relevant to their processing in the body, SwissADME was applied. SwissADME's bioavailability radar (Figure 22) shows a quick summary of six important physiochemical properties. Lipophilicity, size, polarity, solubility, and flexibility were all within the ranges of desired drug properties. The only property outside the desired range for both compounds was saturation. This measurement indicates the fraction of sp^3 hybridized carbons of total carbons. It has been shown that this fraction increases in drugs from preclinical stages to drug approval, and is thus assumed favorable (above 0.25 in SwissADME) for developing successful compounds (105). The fractions reported for **Thio-Iva** and **Briva** correspond to one carbon in each compound being sp^3 hybridized, indicating the carbon in the hydroxymethyl group of the two lead compounds.
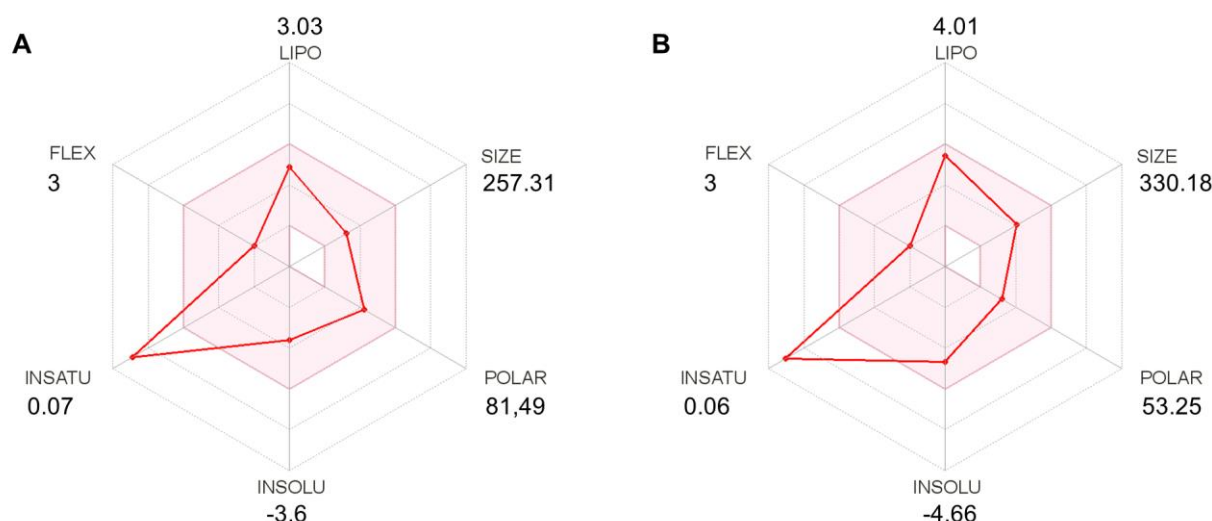
LIPO	(Lipophilicity)	$-0.7 < XLOGP3 < +5.0$	INSOLU (Insolubility)	Log S (ESOL) < 6
SIZE		150g/mol < MW < 500g/mol	INSATU (Insaturation)	$0.25 < Fracion\ Csp^3 < 1$
POLAR	(Polarity)	$20Å^2 < TPSA < 130Å^2$	FLEX (Flexibility)	#Rotable bonds < 9

Figure 22. Bioavailability radar for **Thio-Iva** (A) and **Briva** (B) provided by SwissADME.

Table 12 shows the most relevant additional results provided by SwissADME. The pharmacokinetics analysis predicted high absorption in the gastrointestinal tract for both compounds, while only **Briva** was predicted to pass the blood brain barrier. Neither compound was predicted to be a substrate of the P-glycoprotein, but some members of the Cytochrome P450 family were predicted to be inhibited by the compounds.

Leadlikeness is defined as 250-350 g/mol molecular weight, a XLOGP below or equal to 3.5 and a maximum of seven rotatable bonds (106). **Thio-Iva** fulfilled all those criteria, while **Briva's** XLOG3 was considered too high.

Table 12. Selected results from SwissADME for **Thio-Iva** and **Briva**, evaluated further in this thesis.

Physiochemical Properties	Thio-Iva	Briva	Pharmacokinetics	Thio-Iva	Briva
#Heavy atoms	18	20	GI absorption	High	High
#Aromatic heavy atoms	11	12	BBB permeant	No	Yes
#H-bond acceptors	3	3	Pgp substrate	No	No
#H-bond donors	1	1	CYP1A2 inhibitor	Yes	Yes
Molar Refractivity	72.76	82.58	CYP2C19 inhibitor	Yes	Yes
Lipophilicity			CYP2C9 inhibitor	Yes	Yes
iLOGP	2.61	3	CYP2D6 inhibitor	No	No
XLOGP3	3.03	4.01	CYP3A4 inhibitor	No	Yes
WLOGP	3.42	4.12	**Druglikeness**		
MLOGP	1.56	3.05	Lipinski	Yes	Yes
Silicos-IT Log P	3.92	3.98	Ghose	Yes	Yes
Consensus Log P	**2.91**	**3.63**	Veber	Yes	Yes
Water Solubility			Egan	Yes	Yes
ESOL Log S	-3.6	-4.66	Muegge	Yes	Yes
ESOL Class	Soluble	Mod. Sol.	Bioavailability Score	0.55	0.55

			Medicinal Chemistry		
Ali Log S	-4.41	-4.83			
Ali Class	Mod. Sol.	Mod. Sol.	Brenk #alerts [1]	1	2
Silicos-IT LogSw	-3.92	-5.47	Leadlikeness #violations [2]	0	1
Silicos-IT class	Soluble	Mod. Sol.	Synthetic Accessibility	2.62	2.36

[1] Brenk alerts: conjugated nitrile group, stilbene (**Briva** only) – [2] Leadlikeness violation: XLOGP3>3.5
Mod. Sol.: Moderately soluble

3.4.2 In Silico Toxicity Prediction

The new compounds were investigated for potential toxic effects with the tools of the eMolTox server, providing a structural alert screening as well as several machine learning models based on fingerprint similarity.

Screening for structural alerts of the two compounds showed alerts from 14 of the 23 alert sources (Table 13), but the majority of problematic substructures were found in more than one source. Including these redundant alerts, only 1.6% of all 2,173 potential alerts were found in any of the two compounds. There were 14 potentially toxic substructures detected in **Thio-Iva** and 17 in **Briva** (Table 14). 12 of them were identical substructures present in both compounds.
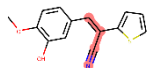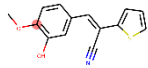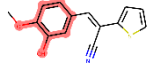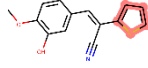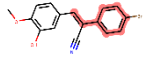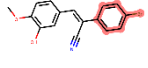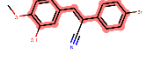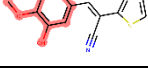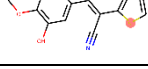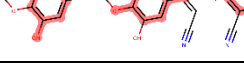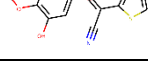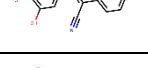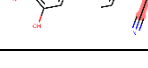
Table 13. Alert sources of eMolTox screening for toxic substructure alerts.

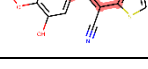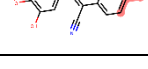| Alert source	Thio-Iva	Briva		Thio-Iva	Briva
Chelating agents	X	X	**Pat Walters**		
Acute Aquatic Toxicity	X	X	Glaxo	-	-
Covalent Bind With Protein	X	X	Dundee	X	X
Respiratory Sensitization	-	-	BMS	X	X
Mitochondrial Toxicity	-	-	PAINS	-	-
Non genotoxic carcinogenicity	-	X	SureChEMBL	-	-
Skin sensitization	X	X	MLSMR	X	X
Alert from Top200 Drug	X	X	Inpharmatica	-	X
Genotoxic carcinogenicity mutagenicity	-	-	LINT	-	X
Kidney Toxicity	-	-			
Hepatotoxicity	X	X			
Developmental and mitochondrial toxicity	-	-			
Covalent Bind With DNA	X	X			
Idiosyncratic toxicity Metabolic activation	X	X			
Potential electrophilic agents	X	X			

X at least one structural alert detected, - no structural alerts detected.

The most frequently appearing structural alerts from the different segments of the **Thio-Iva** and **Briva** concerned the nitril group, the thiophene and the bromobenzene, as well as variations of the benzene ring with different substituents.

Table 14. Substructure alerts detected by eMolTox for **Thio-Iva** and **Briva**.

Substructure	Detected in Database	Compound
	Potential electrophilic agents, Covalent Bond With Protein, Covalent Bond with DNA, Dundee, Acute aquatic toxicity	Both
	Potential electrophilic agents, Covalent Bond With Protein, Covalent Bond with DNA	Both
	Hepatotoxicity, Top200 Drug, Skin sensitization	Both
	Idiosyncratic toxicity metabolic activation, Top200 Drug	Thio-Iva
	Top200 Drug, Potential electrophilic agents	Both
	Top200 Drug, Non genotoxic carcinogenicity	Briva
	Top200 Drug, Dundee	Briva
	Chelating agents, Skin sensitization	Both
	BMS	Thio-Iva
	Top200 Drug	Both
	Idiosyncratic toxicity/metabolic activation	Both
	MLSMR	Both
	LINT	Briva
	Inpharmatica	Briva
	Skin sensitization	Both

In the machine learning based toxic prediction model of eMolTox, only 5% of the 169 potentially toxic endpoints tested were predicted to be possibly relevant for **Thio-Iva**, and for **Briva** it was 8% (Figure 23, A, B). While almost half of the screened toxic endpoints could not be confidently predicted by the server ('inconclusive'), 46% for **Thio-Iva** and 44% for **Briva** were predicted to be unaffected by the respective ligand. These results are comparable to clinically approved kinase inhibitors such as sorafenib or gefitinib (data not

shown). For **Thio-Iva**, six of the nine positive (toxic) injury predictions concerned liver toxicity (Figure 23, C). For **Briva**, eight out of 15 concerned the liver, while three potential toxicities were related to the endocrine system (Figure 23, D). There was no potential toxicity predicted for kidneys, immune, blood, gastrointestinal or respiratory system.
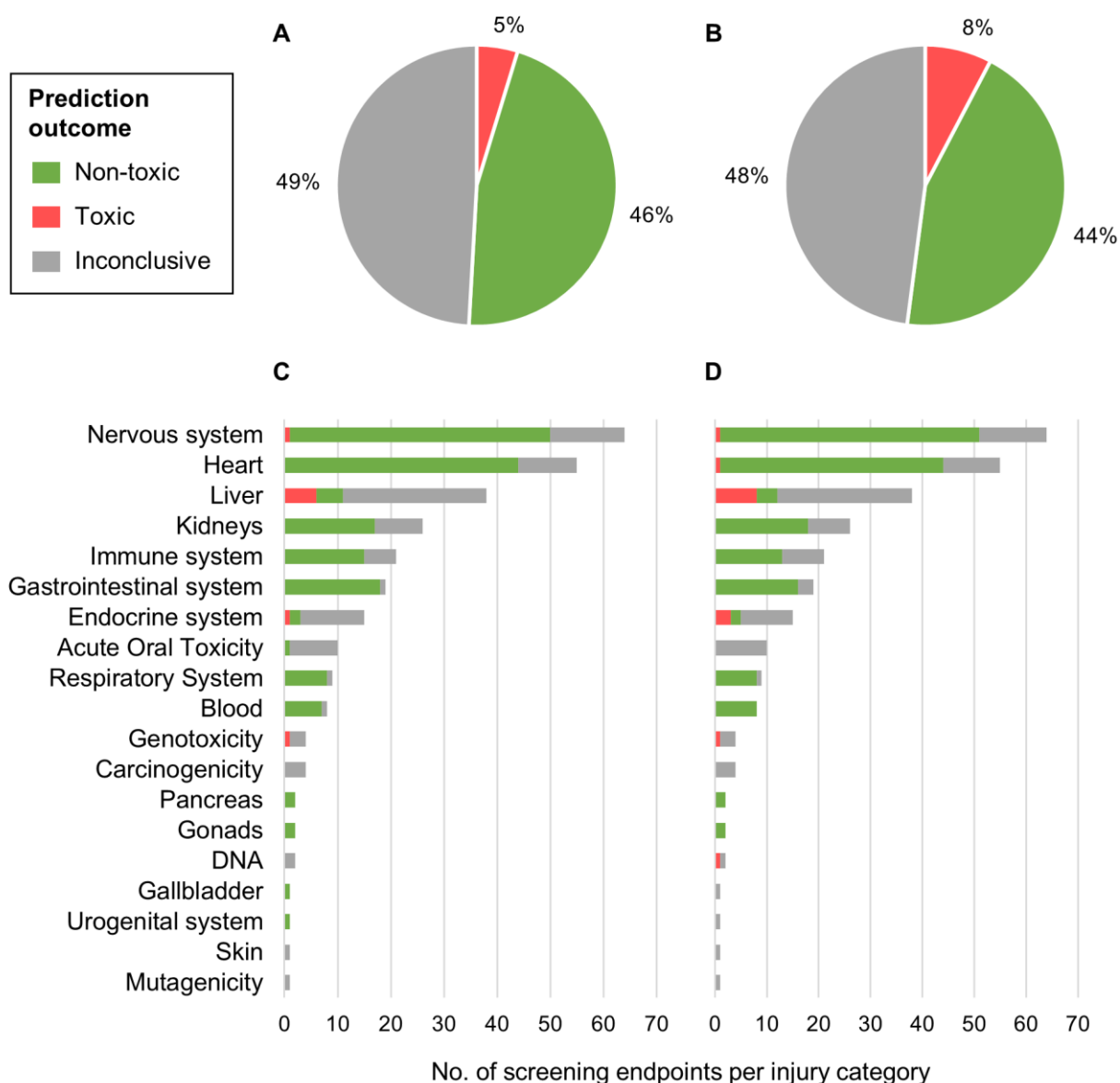
Figure 23. Potential toxicity of **Thio-Iva** (**A**, **C**) and **Briva** (**B**, **D**) as predicted by eMolTox. **A** and **B** show percentages of toxic endpoints, **C** and **D** show absolute numbers of predictions for each injury category.

3.4.3 Acute Cytotoxicity

Unspecific toxicity of the new compounds was examined with a cellular assay measuring LDH (lactate dehydrogenase) release. LDH is an enzyme ubiquitously present in the cytosol and gets released from cells when the cell membrane loses its integrity. Cells treated with **Thio-Iva** or **Briva** (with concentrations ranging from 0.5 to 10 µM) for up to 24h did not show significantly increased LDH release as compared to untreated controls (Figure 24). The lack of meaningful increase of LDH in the medium of the treated samples suggests that there is no immediate unspecific cytotoxicity caused by the two compounds.
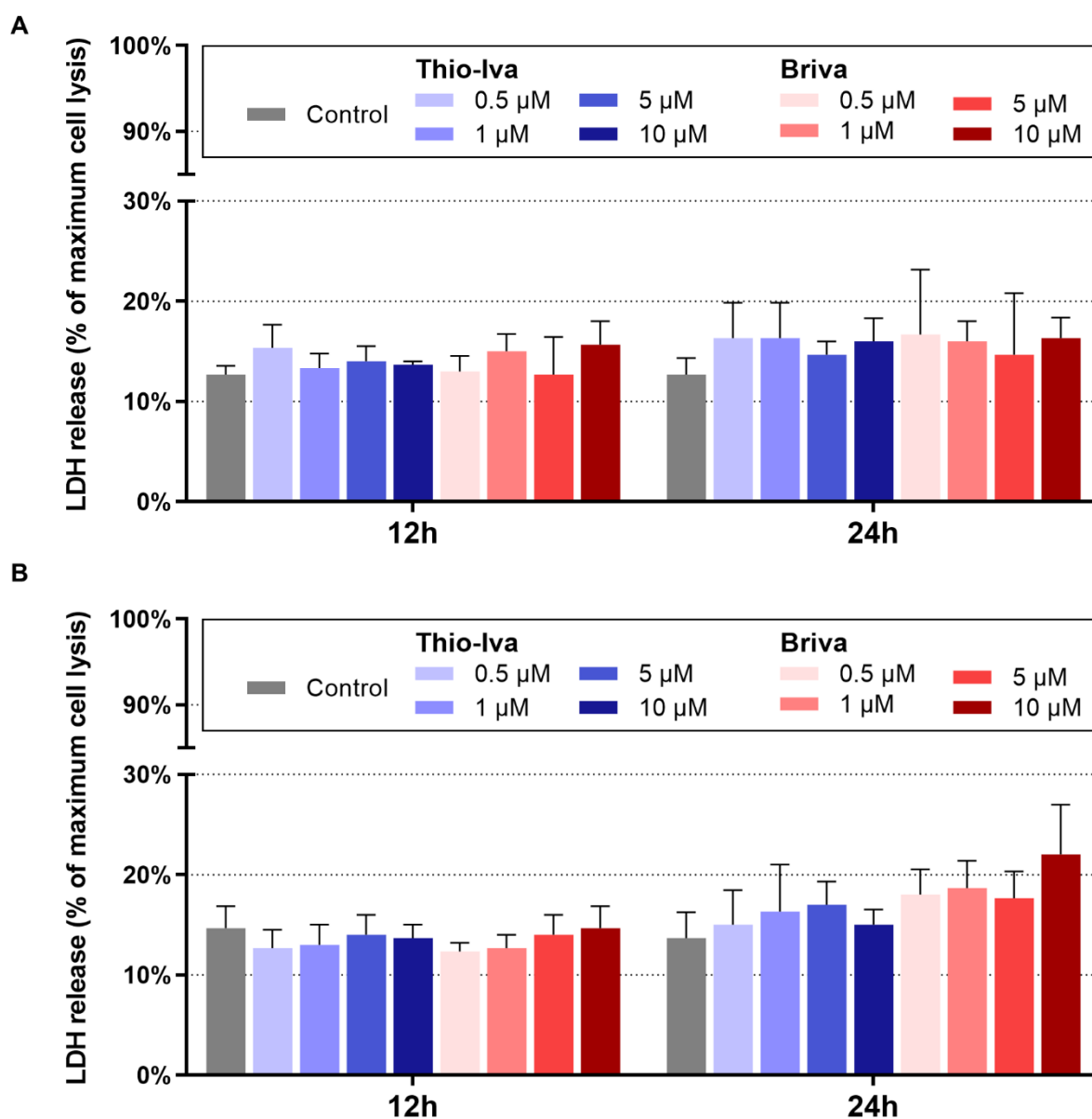
Figure 24. LDH release of HepG2 (**A**) and Huh-7 (**B**) cells treated with **Thio-Iva** and **Briva**, shown as percentage of maximum cell lysis (mean ± SEM of n=3).

3.4.4 Induction of Apoptosis

To investigate alternative modes of cell death, involvement of apoptotic pathways in the growth inhibitory effect of the compounds was determined by measuring caspase-3 activity after treatment with **Thio-Iva** or **Briva**. Results showed a strong increase in caspase-3 activity in the treated cells compared to base activity detected in untreated controls (Figure 25). The effect was time- and dose-dependent for both tested compounds and both cell lines. Statistical analysis with a 3-way ANOVA test for each cell line showed significance for the factor time and dose, but not the different compounds.

This may point to the process of apoptosis playing a role in the growth inhibitory effects observed.
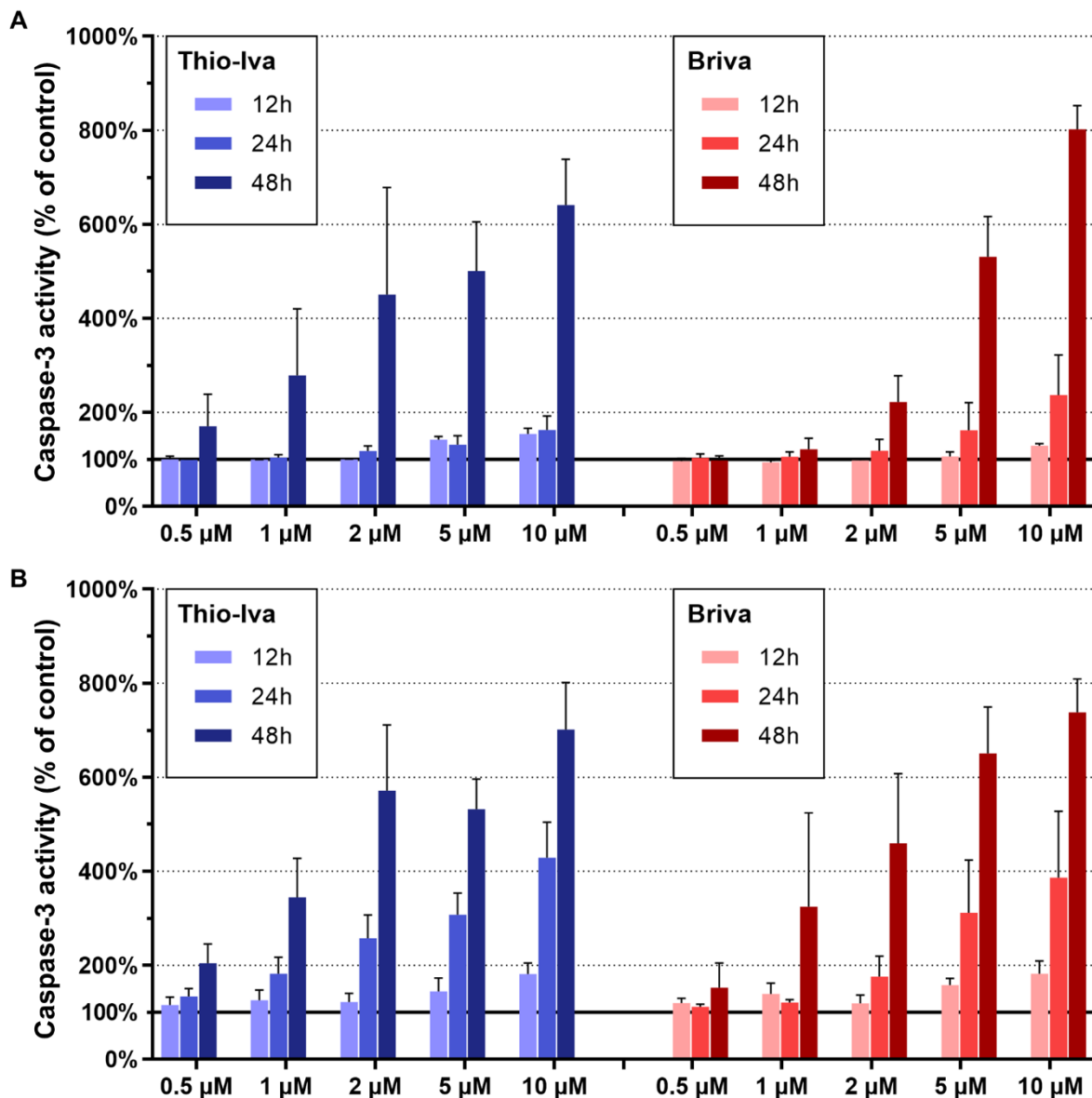

Figure 25. Caspase-3 activity of HepG2 (**A**) and Huh-7 (**B**) cells treated with **Thio-Iva** and **Briva.** Results shown as percentage of untreated controls (mean ± SEM of n=3).

4 Discussion

In this thesis, a panel of potential new kinase inhibitors was investigated for their target selectivity and anticancer potential. The two lead compounds from each subset – the thiophene **Thio-Iva** and the bromobenzene **Briva** – were investigated more in detail. First data on these two compounds suggest that they act as multi-kinase inhibitors with strong growth inhibitory effects on HCC cells and a promising toxicity profile.

Thio-Iva strongly inhibited six kinases (most notably VEGFR2) in a kinase activity assay of 43 targets preselected by computational screenings and HCC relevance. **Briva** inhibited five of **Thio-Iva's** main targets, and inhibition of these kinases could explain the strong growth-inhibitory and apoptosis-inducing effects observed for both compounds *in vitro*. Pronounced differences in VEGFR2 inhibition between some members of the panel were rationalized with *in silico* docking studies. Some of the compounds also exhibited inhibition of targets outside the tyrosine kinase family including Pim kinases, which have been suggested as promising co-targets to potentially interrupt escape mechanisms over the Pim pathway and delay resistance (107).

For both **Thio-Iva** and **Briva** there were few *in silico* predicted toxicities, and *in vitro* immediate unspecific toxicity in HCC cells was low. Additional predicted ADME properties – such as pharmacokinetics, lipophilicity, solubility and druglikeness – showed favorable anticancer drug potential.

4.1 Kinase Targets

To gain a better understanding of how the novel compounds function on a protein level, a process was employed consisting of *in silico* target identification and subsequent *in vitro* verification. This was done extensively for **Thio-Iva**, the lead compound of the thiophene subgroup, and to a lesser extent for **Briva**, the lead compound of the bromobenzene subgroup.

A panel of 43 potential targets of **Thio-Iva** was created for *in vitro* testing, including 29 computationally predicted targets, complemented with 14 additional targets relevant for HCC biology. Results of the subsequent radiometric kinase assay showed six kinases to be inhibited by **Thio-Iva** at a concentration of 10 µM by more than 50%. This indicates a selective kinase inhibition by **Thio-Iva**. Of the six identified targets, three were tyrosine kinases (TK) (VEGFR2 (89% inhibition), VEGFR1 (75%) and c-Kit (61%)), two were

Ca^{2+}/calmodulin-dependent protein kinases (CAMK) (Pim-1 (71%) and Pim-2 (60%)) and one was a CDC-like kinase (CLK) (CLK1 (69%)).

Two more thiophenes (**Thio-Dam** and **1a**) and the bromobenzene **Briva** were tested on seven targets, including **Thio-Iva's** top targets and EGFR (a known target of Tyrphostin RG-13022, from which the compound panel was originally derived). Results for **Thio-Dam** and **1a** showed that despite their high molecular similarity, they displayed distinctly different – and mostly lower – inhibitory activities on these kinases compared to **Thio-Iva**. **Thio-Dam** showed a similarly strong inhibition of VEGFR2 as **Thio-Iva**, but no inhibition below 50% kinase activity for the other six targets. **1a** showed no effect on VEGFR2, and only showed moderate inhibition below 50% for CLK1. While **Briva** showed some effects on five of **Thio-Iva's** six main targets (notably VEGFR2, CLK1 and c-KIT), they were mostly less pronounced, with the strongest inhibition being on CLK1 (67%).

Interestingly, none of the tested compounds inhibited EGFR to below 50% activity, which was unexpected since the compounds were derived from the EGFR-inhibiting Tyrphostin RG-13022.

Differences in VEGFR2 inhibition are further discussed in the results of the docking studies, where the compounds most active on VEGFR2 also showed the most consistent binding poses over the top scored 50 poses (see Chapter 4.3).

The strongest effect of **Thio-Iva** was observed for the two VEGF receptors VEGFR2 and VEGFR1. VEGF and its receptors play an important role in tumor growth and angiogenesis, and VEGFR2 is often overexpressed in solid tumors, including HCC (108). When a tumor exceeds a few millimeters in size, its center becomes hypoxic and increased levels of VEGF are released (109). Depending on the speed of tumor growth, the center can become necrotic, and induce proliferation of blood vessels via immune and inflammatory processes (110). VEGFR2 has been identified as the most relevant to angiogenesis in physiological as well as pathological processes, including blood-vessel formation in tumors (111). VEGFR1 plays a major role in hematopoietic cells and normal blood vessel development (109). However, cross-talk of VEGFR1 with VEGFR2 and a potential involvement in pathological angiogenesis has been suggested and is still under investigation (109, 112). Due to these reasons, VEGFR2 has become a target of high interest for anticancer drugs (96), and happens to be a main target of all four small molecule KIs which are currently FDA-approved for medical treatment of HCC (52, 113).

Another target that was strongly inhibited by **Thio-Iva** is c-Kit (mast/stem cell growth factor receptor), a TK relevant for cell proliferation and survival. Upregulation as well as mutations of c-KIT are expressed in some cancers, and thus c-Kit is under investigation as a target for cancer therapy. Currently, one TKI (Ripretinib) targeting c-KIT and PDGFR has already been approved by the FDA for treatment of gastrointestinal stromal tumors (52).

The proto-oncogene serine/threonine-protein kinases Pim-1 and Pim-2 belong to the kinase family CAMK. They are relevant for many cellular processes such as cell cycle regulation, inflammation, and cell death. Pim kinases are strongly expressed in several tumors and appear to serve as an escape mechanism from other targeted therapies. Pim-1 has been shown to be overexpressed in HCC (114) and was associated with higher metastatic potential. Consequently, Pim has emerged as an interesting target for combination treatment approaches with other targeted therapies to overcome drug resistance and immune evasion of cancer cells (107).

CLK1 (CDC2-like kinase 1) is a dual specificity protein kinase involved in the regulation of RNA splicing in the nucleus, and has been suggested as a target for the treatment of various diseases such as Alzheimer's disease (115) or Duchenne muscular dystrophy (116). There has been some research conducted into CLK1 inhibitors as anticancer drugs (117), with the CLK inhibitor SM08502 recently entering clinical trials for advanced solid tumors (118).

Taken together, all these kinase targets have some relevance in the search for new anticancer therapy, and **Thio-Iva's** pronounced inhibition of VEGFR and Pim kinases appears especially promising and relevant for targeted therapy of HCC and solid tumors in general.

4.2 Evaluation of In Silico Target Prediction

Assessing the predictive value of computational screening for potential targets of **Thio-Iva** revealed that five out of the six strongly inhibited kinases were predicted by *in silico* screening methods. Each of the kinases was predicted by one ligand-based method (SwissTargetPrediction) and at least one structure-based method (@TOME, iRAISE).

Of the 23 targets selected only by *in silico* methods, three (Pim-1, Pim-2, CLK1) were inhibited *in vitro*, while of the 14 targets selected only for HCC relevance, one (VEGFR1) was inhibited *in vitro*. Of the six targets included based on both computational and

biological investigation, two (VEGFR2, c-Kit) were inhibited *in vitro*. This shows that while a combined approach appears most effective, *in silico* target prediction not only recognizes the more established targets but has the potential to point towards less expected targets.

As the lead compound from the bromobenzene subgroup, **Briva** was also investigated with the *in silico* target prediction methods SwissTargetPrediction and @TOME. The predicted targets differed strongly to those of **Thio-Iva**, with four of **Thio-Iva's** top targets predicted by one of the methods, but none of them by both. This was in part reflected by the initial *in vitro* verification of **Briva** activity on **Thio-Iva's** top targets and EGFR. It seems likely that there are other targets relevant for **Briva's** notable anticancer effect in cell culture experiments. Further investigations, including a full *in silico* target prediction with subsequent *in vitro* verification would be necessary to get a sufficient profile on **Briva**.

4.3   Interaction with VEGFR2

After protein targets were identified, the next aim was to investigate the structure-activity relationship of the compounds and their target(s). To elucidate a binding hypothesis that can explain the experimental findings, docking studies were performed on VEGFR2 as **Thio-Iva's** most strongly inhibited target. All compounds were docked to study how the difference in compound structures across the panel could affect the inhibitory effects on VEGFR. To verify the most prominent binding mode for the most potent inhibitor **Thio-Iva**, additional molecular dynamics simulations were performed.

The most favorable predicted binding pose of **Thio-Iva** in the ATP-binding pocket of VEGFR2 formed a consistent hydrogen bonding pattern between the nitril of the compound and the backbone nitrogen of the cysteine 919 at the hinge region (throughout the investigated top 50 poses and the 100 ns MD simulation). Hydrogen bonding interaction with the hinge region of kinases is a feature of ATP-binding (also common among successful inhibitors) that helps to anchor the molecule in the binding site (104). Generally, hydrogen bonds formed with the rigid backbone of the protein are considered more stable and less influenced by side chain mutations than bonds formed with the more flexible sidechains (119).

The additional hydrophilic interaction of the hydroxy group of **Thio-Iva** with the aspartate 1046 close to the DFG motif was shown to be more variable between docking with SeeSAR and analysis in LigandScout, as well as over time in the MD simulation. This

interaction could also be strongly dependent on the conformation of the DFG motif in the crystal structure used (DFG-out). As high-quality crystal structures of DFG-in (considered active) conformations were not available at the time of investigation, reliable dockings with this alternative could not be performed. This made it impossible to explore further if our compounds could be potential type I rather than type II KIs. However, it has been shown that many VEGFR2 inhibitors bind to the DGF-out (inactive) kinase conformation (120).

Analysis of the docking results of the other nine compounds showed consistency of preferable binding modes, especially for the thiophene **1e**, but also for **Thio-Van** and **Thio-Dam**. Calculated binding modes for **1a**, **1i** and **1j** were more variable, suggesting that VEGFR2 may not be one of their main targets. The bromobenzenes (**Briva**, **Brova** and **Bro-Dam**) showed less consistent results overall, with **Bro-Dam** showing the highest consistency within this subgroup.

These results matched the results of the radiometric kinase assay for the tested compounds **Thio-Iva**, **Thio-Dam**, **1a** and **Briva**. The compounds with more consistent binding modes (**Thio-Iva** and **Thio-Dam**) also showed higher inhibitory effect on VEGFR2 *in vitro*.

To further decipher the SAR of the compounds based on the generated docking poses and measured inhibitory activity, the differences in functional groups of the compounds were analysed. **Thio-Iva** and **Briva** both have a hydroxy group with potential for additional hydrogen bonding towards the DFG motif, while **Thio-Dam** has a dimethylamine group that could account for additional hydrophobic contacts in the back pocket. The compound that did not show any inhibition of VEGFR2 is **1a**, which is missing the hydroxy group of the two lead compounds, and with it the ability to form hydrogen bonds towards the DFG motif. Looking at the difference between **Thio-Iva's** and **Briva's** activity on VEGFR2, their defining feature (thiophene vs. bromobenzene rings) is oriented towards the solvent in the favored binding pose. The bigger hydrophobic bromobenzene could be disadvantageous for binding affinity in the investigated structure. Depending on the depth and makeup of the entrance area of the ATP-binding pocket in different kinases, this feature could strongly influence overall fit. This is supported by **Briva** showing some – but less – activity on most of **Thio-Iva's** targets.

Overall, the docking results together with *in vitro* verification indicate that **Thio-Iva** is a VEGFR2 inhibitor with potential to be optimized for an even more specific fit by extending it towards the back pocket.

4.4 Growth Inhibitory Effects and Modes of Action

In addition to determining the compounds' kinase inhibitory effects, this thesis aimed to determine the anticancer effects on HCC cell lines and the potential contributions of apoptosis and unspecific toxicity. Regarding the further development of the novel compounds into drugs, additional properties influencing the compounds' suitability in terms of absorption, distribution, metabolism, excretion, and toxicity (ADMET) were bioinformatically investigated.

Thio-Iva and **Briva** showed strong growth inhibitory effects on HCC cells, while their effect on normal liver cells was comparably low, indicating a tumor-selective mode of action of the compounds. While unspecific cytotoxic effects of the compounds remained low, there was a substantial induction of caspase-3 activity. This may indicate that apoptosis plays a role as an underlying mode of action against HCC cells, while unspecific cytotoxic effects may not be a prominent factor in the cell death-inducing effects of the compounds.

Unspecific toxicity is an unwanted feature in anticancer drugs as it causes tissue necrosis and accompanying inflammatory processes, which puts a greater strain on the organism (121). Apoptosis is a physiological process of the body to dispose of dysfunctional cells, and generally leads to less inflammatory reactions than necrosis. During cancer development tumor cells often lose their ability to undergo apoptosis due to changes in the expression and balanced regulation of pro- and anti-apoptotic proteins. The reinitiation of apoptosis is therefore a desirable feature for effective anticancer drugs with reduced side effects (122). In this regard, **Thio-Iva** and **Briva** showed promising results, with pronounced dose- and time-dependent growth inhibitory and apoptosis-inducing effects in the investigated HCC cell models.

VEGFR2 stimulation has been shown to lead to anti-apoptotic signaling, and inhibition of this pathway has been suggested to play a role in the clinical efficacy of VEGFR2 inhibitors (123). The observed effects of growth inhibition in general and induction of apoptosis specifically may therefore be related to the inhibition of VEGFR2 and other kinases. However, further investigations are needed to clarify the specific mode of apoptosis induction (intrinsic/extrinsic apoptosis) and related signaling events in terms of mitochondrial involvement by the novel compounds.

Evaluation of ADMET properties showed an overall positive property profile for both compounds, but especially for **Thio-Iva**. Of the general criteria for druglikeness established by the screening tool SwissADME, both investigated compounds fulfilled requirements on size, lipophilicity, solubility, polarity, and flexibility. Only the saturation of the compounds (specified by fraction of sp3 hybridized carbons) was considered too low. A rate of over 25% has been specified as favorable for potential drugs (105). This could be addressed when further developing and optimizing the compounds in the future.

In the screening for toxic substructure alerts, the most frequently detected potentially problematic one was the conjugated nitril group. While the concept of avoiding such substructures in drug design and thereby eliminating toxicity is appealing, these warnings are not necessarily based on proven causality. While being aware of problematic substructures and their potential effects is valuable, avoiding all alerts does not seem to be a feasible approach. At least one structural alert can be found in many recently approved small molecule inhibitors (124).

Bioinformatic screening for toxicities based on fingerprint similarity revealed no increased indication for potential toxic side effects of **Thio-Iva** and **Briva** compared to clinically approved KIs.

4.5   Conclusions

A combined *in silico* and *in vitro* strategy was explored to identify and characterize kinase inhibitory and antineoplastic effects of novel potential tyrosine kinase inhibitors.

When screening for kinases inhibited by the novel compounds, targets were successfully narrowed down for **Thio-Iva** by applying a combination of *in silico* prediction methods. Six of the 43 kinases suggested were experimentally verified as major targets of **Thio-Iva**. This showcases how a combination of *in silico* and *in vitro* methods can be a time- and cost-efficient strategy in drug discovery when applied with care.

Testing the successful targets with the similar, yet slightly different members of the panel (**Thio-Dam**, **1a** and **Briva**) revealed that despite their molecular similarity, they expressed distinctly different activities.

The structure-activity relationship of the compounds to the most strongly inhibited kinase VEGFR2 was further investigated in computational docking studies. This offered an opportunity to investigate and visualize the differences in interactions formed with VEGFR2 caused by small modifications of the molecules. At the same time, **Thio-Iva's**

specific binding mode – and its stability over time – was analyzed in depth. This knowledge can serve as a basis for potential compound optimization in the future, as both investigated lead compounds are well below the maximum threshold of 500 g/mol for small molecule inhibitors. Potential optimization could address druglikeness issues such as the compounds' saturation, target selectivity and potency. Increased selectivity and potency could be achieved by extending the molecules towards the back pocket to create a better and more selective fit with certain kinases.

As there is still a strong need for highly effective therapy for advanced HCC, the data of this work may serve as a promising starting point for further development of novel therapeutic compounds based on a combined approach of bioinformatical analysis and biological evaluation.

First testing of the novel compounds on HCC cells showed their strong growth inhibitory potential, low unspecific toxicity, and induction of apoptosis. Nevertheless, further experiments should be performed to identify the involved pathways and mode of action of the promising new compounds in more depth.

V.   References

1.   Petrick JL, McGlynn KA. The changing epidemiology of primary liver cancer. Curr Epidemiol Rep. 2019;6(2):104-11.
2.   Dasgupta P, Henshaw C, Youlden DR, Clark PJ, Aitken JF, Baade PD. Global Trends in Incidence Rates of Primary Adult Liver Cancers: A Systematic Review and Meta-Analysis. Front Oncol. 2020;10:171.
3.   Gao S, Yang WS, Bray F, Va P, Zhang W, Gao J, Xiang YB. Declining rates of hepatocellular carcinoma in urban Shanghai: incidence trends in 1976-2005. Eur J Epidemiol. 2012;27(1):39-46.
4.   Tanaka H, Imai Y, Hiramatsu N, Ito Y, Imanaka K, Oshita M, Hijioka T, Katayama K, Yabuuchi I, Yoshihara H, Inoue A, Kato M, Takehara T, Tamura S, Kasahara A, Hayashi N, Tsukuma H. Declining incidence of hepatocellular carcinoma in Osaka, Japan, from 1990 to 2003. Ann Intern Med. 2008;148(11):820-6.
5.   Forner A, Reig M, Bruix J. Hepatocellular carcinoma. Lancet. 2018;391(10127):1301-14.
6.   Liu T-C, Vachharajani N, Chapman WC, Brunt EM. Noncirrhotic hepatocellular carcinoma: derivation from hepatocellular adenoma? Clinicopathologic analysis. Modern Pathology. 2014;27(3):420-32.
7.   de Rosamel L, Blanc JF. Emerging tyrosine kinase inhibitors for the treatment of hepatocellular carcinoma. Expert Opin Emerg Drugs. 2017;22(2):175-90.
8.   Kaufman NEM, Dhingra S, Jois SD, Vicente MDGH. Molecular Targeting of Epidermal Growth Factor Receptor (EGFR) and Vascular Endothelial Growth Factor Receptor (VEGFR). Molecules. 2021;26(4):1076.
9.   Bialecki ES, Di Bisceglie AM. Diagnosis of hepatocellular carcinoma. HPB. 2005;7(1):26-34.
10.   Luo JC, Hwang SJ, Wu JC, Lai CR, Li CP, Chang FY, Chiang JH, Lui WY, Chu CW, Lee SD. Clinical characteristics and prognosis of hepatocellular carcinoma patients with paraneoplastic syndromes. Hepatogastroenterology. 2002;49(47):1315-9.
11.   Galle PR, Forner A, Llovet JM, Mazzaferro V, Piscaglia F, Raoul J-L, Schirmacher P, Vilgrain V. EASL Clinical Practice Guidelines: Management of hepatocellular carcinoma. Journal of Hepatology. 2018;69(1):182-236.
12.   Gordan JD, Kennedy EB, Abou-Alfa GK, Beg MS, Brower ST, Gade TP, Goff L, Gupta S, Guy J, Harris WP, Iyer R, Jaiyesimi I, Jhawer M, Karippot A, Kaseb AO, Kelley RK, Knox JJ, Kortmansky J, Leaf A, Remak WM, Shroff RT, Sohal DPS, Taddei TH, Venepalli NK, Wilson A, Zhu AX, Rose MG. Systemic Therapy for Advanced Hepatocellular Carcinoma: ASCO Guideline. Journal of Clinical Oncology. 2020;38(36):4317-45.
13.   Nagahama H, Okada S, Okusaka T, Ishii H, Ikeda M, Nakasuka H, Yoshimori M. Predictive Factors for Tumor Response to Systemic Chemotherapy in Patients With Hepatocellular Carcinoma. Japanese Journal of Clinical Oncology. 1997;27(5):321-4.
14.   Llovet JM, Ricci S, Mazzaferro V, Hilgard P, Gane E, Blanc J-F, De Oliveira AC, Santoro A, Raoul J-L, Forner A, Schwartz M, Porta C, Zeuzem S, Bolondi L, Greten TF, Galle PR, Seitz J-F, Borbath I, Häussinger D, Giannaris T, Shan M, Moscovici M, Voliotis D, Bruix J. Sorafenib in Advanced Hepatocellular Carcinoma. New England Journal of Medicine. 2008;359(4):378-90.
15.   Durand F, Valla D. Assessment of the prognosis of cirrhosis: Child-Pugh versus MELD. J Hepatol. 2005;42 Suppl(1):S100-7.
16.   Finn RS, Qin S, Ikeda M, Galle PR, Ducreux M, Kim T-Y, Kudo M, Breder V, Merle P, Kaseb AO, Li D, Verret W, Xu D-Z, Hernandez S, Liu J, Huang C, Mulla S, Wang Y,

Lim HY, Zhu AX, Cheng A-L. Atezolizumab plus Bevacizumab in Unresectable Hepatocellular Carcinoma. New England Journal of Medicine. 2020;382(20):1894-905.

17.   Jemal A, Ward EM, Johnson CJ, Cronin KA, Ma J, Ryerson B, Mariotto A, Lake AJ, Wilson R, Sherman RL, Anderson RN, Henley SJ, Kohler BA, Penberthy L, Feuer EJ, Weir HK. Annual Report to the Nation on the Status of Cancer, 1975-2014, Featuring Survival. J Natl Cancer Inst. 2017;109(9).

18.   Wouters OJ, McKee M, Luyten J. Estimated Research and Development Investment Needed to Bring a New Medicine to Market, 2009-2018. JAMA. 2020;323(9):844.

19.   Leelananda SP, Lindert S. Computational methods in drug discovery. Beilstein J Org Chem. 2016;12:2694-718.

20.   Prada-Gracia D, Huerta-Yepez S, Moreno-Vargas LM. Application of computational methods for anticancer drug discovery, design, and optimization. Bol Med Hosp Infant Mex. 2016;73(6):411-23.

21.   Takenaka T. Classical vs reverse pharmacology in drug discovery. BJU International. 2008;88:7-10.

22.   Hopkins AL. Network pharmacology: the next paradigm in drug discovery. Nature Chemical Biology. 2008;4(11):682-90.

23.   National Comprehensive Cancer Network. Phases of clinical trials. 2020 www.nccn.org/patients/resources/clinical_trials/phases.aspx. accessed August 8, 2020.

24.   Yamashita S, Sugiyama Y. New strategy for drug development with exploratory IND studies: Scientific basis and future directions. Advanced Drug Delivery Reviews. 2011;63(7):493.

25.   Shegokar R. Preclinical testing—Understanding the basics first. Elsevier; 2020. p. 19-32.

26.   Macalino SJY, Gosu V, Hong S, Choi S. Role of computer-aided drug design in modern drug discovery. Archives of Pharmacal Research. 2015;38(9):1686-701.

27.   Jorgensen WL. The Many Roles of Computation in Drug Discovery. Science. 2004;303(5665):1813-8.

28.   Springer Nature Limited. Chemical libraries. 2021 www.nature.com /subjects/chemical-libraries. accessed January 23, 2021.

29.   Sydow D, Burggraaff L, Szengel A, Van Vlijmen HWT, Ijzerman AP, Van Westen GJP, Volkamer A. Advances and Challenges in Computational Target Prediction. Journal of Chemical Information and Modeling. 2019;59(5):1728-42.

30.   Pinzi L, Rastelli G. Molecular Docking: Shifting Paradigms in Drug Discovery. International Journal of Molecular Sciences. 2019;20(18):4331.

31.   Kuhlbrandt W. Biochemistry. The resolution revolution. Science. 2014;343(6178):1443-4.

32.   Rarey M, Kramer B, Lengauer T, Klebe G. A Fast Flexible Docking Method using an Incremental Construction Algorithm. Journal of Molecular Biology. 1996;261(3):470-89.

33.   Schneider N, Lange G, Hindle S, Klein R, Rarey M. A consistent description of HYdrogen bond and DEhydration energies in protein–ligand complexes: methods behind the HYDE scoring function. Journal of Computer-Aided Molecular Design. 2013;27(1):15-29.

34.   ChemAxon. Marvin. 2021 https://chemaxon.com/products/marvin. accessed April 16, 2021.

35.   Kooistra FAJ, Volkamer A, Jr RAG, Press A. Kinase-Centric Computational Drug Development2017. 197-236 p.

36.   Gaulton A, Hersey A, Nowotka M, Bento AP, Chambers J, Mendez D, Mutowo P, Atkinson F, Bellis LJ, Cibrián-Uhalte E, Davies M, Dedman N, Karlsson A, Magariños MP, Overington JP, Papadatos G, Smit I, Leach AR. The ChEMBL database in 2017. Nucleic Acids Research. 2017;45(D1):D945-D54.

37.   Maggiora G, Vogt M, Stumpfe D, Bajorath J. Molecular similarity in medicinal chemistry. J Med Chem. 2014;57(8):3186-204.

38.   Daylight Chemical Information Systems Inc. SMILES - A Simplified Chemical Language. 2019   https://www.daylight.com/dayhtml/doc/theory/theory.smiles.html. accessed September 6, 2020.

39.   Daylight Chemical Information Systems Inc. SMARTS - A Language for Describing Molecular Patterns. 2019   www.daylight.com/dayhtml/doc/theory/theory.smarts.html. accessed April 16, 2021.

40.   Bajusz D, Rácz A, Héberger K. Why is Tanimoto index an appropriate choice for fingerprint-based similarity calculations? Journal of Cheminformatics. 2015;7(1).

41.   Daina A, Michielin O, Zoete V. SwissADME: a free web tool to evaluate pharmacokinetics, drug-likeness and medicinal chemistry friendliness of small molecules OPEN. 2017.

42.   Schrödinger. The PyMOL Molecular Graphics System, Version 2.0 Schrödinger, LLC. 2021 www.pymol.org. accessed April 16, 2021.

43.   Github S. RDKit: Open-Source Cheminformatics Software. 2021 www.rdkit.org/. accessed April 16 2021.

44.   Vuorinen A, Schuster D. Methods for generating and applying pharmacophore models as virtual screening filters and for bioactivity profiling. Methods. 2015;71:113-34.

45.   Zvinavashe E, Murk AJ, Rietjens IM. Promises and pitfalls of quantitative structure-activity relationship approaches for predicting metabolism and toxicity. Chem Res Toxicol. 2008;21(12):2229-36.

46.   Kanev GK, De Graaf C, De Esch IJP, Leurs R, Würdinger T, Westerman BA, Kooistra AJ. The Landscape of Atypical and Eukaryotic Protein Kinases. Trends in Pharmacological Sciences. 2019;40(11):818-32.

47.   Heinrich P, Müller M, Graeve L. Biochemie und Pathobiochemie / Löffler;Petrides. 9th ed. Heidelberg,, Springer Medizin; 2014.

48.   Manning G. The Protein Kinase Complement of the Human Genome. Science. 2002;298(5600):1912-34.

49.   Bhullar KS, Lagaron NO, McGowan EM, Parmar I, Jha A, Hubbard BP, Rupasinghe HPV. Kinase-targeted cancer therapies: progress, challenges and future directions. Mol Cancer. 2018;17(1):48.

50.   Lipinski CA, Lombardo F, Dominy BW, Feeney PJ. Experimental and computational approaches to estimate solubility and permeability in drug discovery and development settings 1PII of original article: S0169-409X(96)00423-1. The article was originally published in Advanced Drug Delivery Reviews 23 (1997). Advanced Drug Delivery Reviews. 2001;46(1-3):3-26.

51.   European Medicines Agency. Erbitux. 2021 www.ema.europa.eu/en/medicines /human/EPAR/erbitux. accessed March 3, 2021.

52.   Roskoski R. There are 65 FDA-approved small molecule protein kinase inhibitors as of 30 March 2021 as compiled by Robert Roskoski Jr. 2021 www.brimr.org /PKI/PKIs.htm. accessed April 12, 2021.

53.   Roskoski R. Properties of FDA-approved small molecule protein kinase inhibitors: A 2020 update. Pharmacological Research. 2020;152.

54.   Roskoski R. Classification of small molecule protein kinase inhibitors based upon the structures of their drug-enzyme complexes. Pharmacological Research. 2016;103:26-48.

55.   Lamba V, Ghosh I. New directions in targeting protein kinases: focusing upon true allosteric and bivalent inhibitors. Curr Pharm Des. 2012;18(20):2936-45.

56.   Modi V, Dunbrack RL, Jr. Defining a new nomenclature for the structures of active and inactive kinases. Proc Natl Acad Sci U S A. 2019;116(14):6818-27.

57.   Hochhaus A, Baccarani M, Silver RT, Schiffer C, Apperley JF, Cervantes F, Clark RE, Cortes JE, Deininger MW, Guilhot F, Hjorth-Hansen H, Hughes TP, Janssen JJWM, Kantarjian HM, Kim DW, Larson RA, Lipton JH, Mahon FX, Mayer J, Nicolini F, Niederwieser D, Pane F, Radich JP, Rea D, Richter J, Rosti G, Rousselot P, Saglio G, Saußele S, Soverini S, Steegmann JL, Turkina A, Zaritskey A, Hehlmann R. European LeukemiaNet 2020 recommendations for treating chronic myeloid leukemia. Leukemia. 2020;34(4):966-84.

58.   Holohan C, Van Schaeybroeck S, Longley DB, Johnston PG. Cancer drug resistance: an evolving paradigm. Nat Rev Cancer. 2013;13(10):714-26.

59.   Tang Z, Du R, Jiang S, Wu C, Barkauskas DS, Richey J, Molter J, Lam M, Flask C, Gerson S, Dowlati A, Liu L, Lee Z, Halmos B, Wang Y, Kern JA, Ma PC. Dual MET-EGFR combinatorial inhibition against T790M-EGFR-mediated erlotinib-resistant lung cancer. Br J Cancer. 2008;99(6):911-22.

60.   Roskoski R, Jr. Properties of FDA-approved small molecule protein kinase inhibitors: A 2021 update. Pharmacol Res. 2021:105463.

61.   Ogasawara S, Mihara Y, Kondo R, Kusano H, Akiba J, Yano H. Antiproliferative Effect of Lenvatinib on Human Liver Cancer Cell Lines In Vitro and In Vivo. Anticancer Res. 2019;39(11):5973-82.

62.   Maguire MP, Sheets KR, McVety K, Spada AP, Zilberstein A. A new series of PDGF receptor tyrosine kinase inhibitors: 3-substituted quinoline derivatives. J Med Chem. 1994;37(14):2129-37.

63.   Umezawa H, Imoto M, Sawa T, Isshiki K, Matsuda N, Uchida T, Iinuma H, Hamada M, Takeuchi T. Studies on a new epidermal growth factor-receptor kinase inhibitor, erbstatin, produced by MH435-hF3. J Antibiot (Tokyo). 1986;39(1):170-3.

64.   Schaller E, Ma A, Gosch LC, Klefenz A, Schaller D, Goehringer N, Kaps L, Schuppan D, Volkamer A, Schobert R, Biersack B, Nitzsche B, Höpfner M. New 3-Aryl-2-(2-thienyl)acrylonitriles with High Activity Against Hepatoma Cells. International Journal of Molecular Sciences. 2021;22(5):2243.

65.   Gfeller D, Grosdidier A, Wirth M, Daina A, Michielin O, Zoete V. SwissTargetPrediction: a web server for target prediction of bioactive small molecules. Nucleic Acids Research. 2014;42.

66.   Daina A, Michielin O, Zoete V. SwissTargetPrediction: updated data and new features for efficient prediction of protein targets of small molecules. Nucleic Acids Research. 2019;47:357-64.

67.   Schomburg KT, Bietz S, Briem H, Henzler AM, Urbaczek S, Rarey M. Facing the challenges of structure-based target prediction by inverse virtual screening. J Chem Inf Model. 2014;54(6):1676-86.

68.   Pons JL, Labesse G. @TOME-2: a new pipeline for comparative modeling of protein-ligand complexes. Nucleic Acids Res. 2009;37(Web Server issue):W485-91.

69.   Swiss Institute of Bioinformatics. SwissTargetPrediciton. 2019 www.swisstargetprediction.ch. accessed September 14 2020.

70.   http://atome.cbs.cnrs.fr/ATOME_V3/DOC/Atome3.pdf, (last accessed 03.03.2021, 06:54 pm)

71.   Martin L, Catherinot V, Labesse G. kinDOCK: a tool for comparative docking of protein kinase ligands. Nucleic Acids Res. 2006;34(Web Server issue):W325-9.

72.   Korb O, Stutzle T, Exner TE. Empirical scoring functions for advanced protein-ligand docking with PLANTS. J Chem Inf Model. 2009;49(1):84-96.

73.   Yin S, Biedermannova L, Vondrasek J, Dokholyan NV. MedusaScore: an accurate force field-based scoring function for virtual drug screening. J Chem Inf Model. 2008;48(8):1656-62.

74.   Wang R, Lai L, Wang S. Further development and validation of empirical scoring functions for structure-based binding affinity prediction. Journal of Computer-Aided Molecular Design. 2002;16(1):11-26.

75.   Neudert G, Klebe G. DSX: a knowledge-based scoring function for the assessment of protein-ligand complexes. J Chem Inf Model. 2011;51(10):2731-45.

76.   Collobert R, Bengio S. SVMTorch: support vector machines for large-scale regression problems. The Journal of Machine Learning Research. 2000;1:143-60.

77.   CBS, ABCIS, ATOME. Inverse Screening @tome server. 2020 http://atome.cbs.cnrs.fr/ATOME_V3/SERVER/LIST_PK.html. accessed September 24, 2020.

78.   Eid S, Turk S, Volkamer A, Rippmann F, Fulle S. KinMap: a web-based tool for interactive navigation through human kinome data. BMC Bioinformatics. 2017;18(1):16.

79.   UniProt Consortium. UniProt: the universal protein knowledgebase in 2021. Nucleic Acids Research. 2021;49(D1):D480-D9.

80.   UniProt Consortium. UniProt. 2002 www.uniprot.org. accessed February 8, 2017.

81.   Berman H, Henrick K, Nakamura H. Announcing the worldwide Protein Data Bank. Nature Structural & Molecular Biology. 2003;10(12):980-.

82.   Research Collaboratory for Structural Bioinformatics. RSCB PDB. 1998 www.rcsb.org. accessed February 14, 2017.

83.   van Linden OP, Kooistra AJ, Leurs R, de Esch IJ, de Graaf C. KLIFS. 2016 www.klifs.net. accessed February 21, 2017.

84.   Bennett L, Melchers B, B P. Curta: A General-purpose High-Performance Computer at ZEDAT, Freie Universität Berlin. 2020 https://dx.doi.org/10.17169/refubium-26754. accessed April 6, 2021.

85.   Schneider N, Hindle S, Lange G, Klein R, Albrecht J, Briem H, Beyer K, Claußen H, Gastreich M, Lemmen C, Rarey M. Substantial improvements in large-scale redocking and screening using the novel HYDE scoring function. 2012;26(6):701-23.

86.   van Linden OP, Kooistra AJ, Leurs R, de Esch IJ, de Graaf C. KLIFS. 2020 www.klifs.net. accessed December 8, 2020.

87.   Kooistra AJ, Kanev GK, van Linden OP, Leurs R, de Esch IJ, de Graaf C. KLIFS: a structural kinase-ligand interaction database. Nucleic Acids Res. 2016;44(D1):D365-71.

88.   Oguro Y, Miyamoto N, Okada K, Takagi T, Iwata H, Awazu Y, Miki H, Hori A, Kamiyama K, Imamura S. Design, synthesis, and evaluation of 5-methyl-4-phenoxy-5H-pyrrolo[3,2-d]pyrimidine derivatives: novel VEGFR2 kinase inhibitors binding to inactive kinase conformation. Bioorg Med Chem. 2010;18(20):7260-73.

89.   Lolli G, Cozza G, Mazzorana M, Tibaldi E, Cesaro L, Donella-Deana A, Meggio F, Venerando A, Franchin C, Sarno S, Battistutta R, Pinna LA. Inhibition of protein kinase CK2 by flavonoids and tyrphostins. A structural insight. Biochemistry. 2012;51(31):6097-107.

90.   Wolber G, Langer T. LigandScout: 3-D pharmacophores derived from protein-bound ligands and their use as virtual screening filters. J Chem Inf Model. 2005;45(1):160-9.

91.   Bowers KJ, Chow DE, Xu H, Dror RO, Eastwood MP, Gregersen BA, Klepeis JL, Kolossvary I, Moraes MA, Sacerdoti FD, Salmon JK, Shan Y, Shaw DE, editors. Scalable Algorithms for Molecular Dynamics Simulations on Commodity Clusters. SC '06: Proceedings of the 2006 ACM/IEEE Conference on Supercomputing; 2006 11-17 Nov. 2006.

92.   Shaw DE. A fast, scalable method for the parallel evaluation of distance-limited pairwise particle interactions. J Comput Chem. 2005;26(13):1318-28.

93.   Lippert RA, Bowers KJ, Dror RO, Eastwood MP, Gregersen BA, Klepeis JL, Kolossvary I, Shaw DE. A common, avoidable source of error in molecular dynamics integrators. The Journal of Chemical Physics. 2007;126(4):046101.

94.   OpenEye Scientific Software. OpenEye Toolkits 2020.1.0. 2020 www.eyesopen.com. accessed December 2, 2020.

95.   Jorgensen WL, Tirado-Rives J. The OPLS [optimized potentials for liquid simulations] potential functions for proteins, energy minimizations for crystals of cyclic peptides and crambin. J Am Chem Soc. 1988;110(6):1657-66.

96.   Humphrey W, Dalke A, Schulten K. VMD: visual molecular dynamics. J Mol Graph. 1996;14(1):33-8, 27-8.

97.   Ji C. eMolTox. 2018 http://xundrug.cn/moltox. accessed September 14, 2020.

98.   Ji C, Svensson F, Zoufir A, Bender A. Structural bioinformatics eMolTox: prediction of molecular toxicity with confidence.

99.   Swiss Institute of Bioinformatics. SwissADME. 2017 www.swissadme.ch. accessed March 26 2021.

100.   López-Terrada D, Cheung SW, Finegold MJ, Knowles BB. Hep G2 is a hepatoblastoma-derived cell line. Human Pathology. 2009;40(10):1512-5.

101.   Feoktistova M, Geserick P, Leverkus M. Crystal Violet Assay for Determining Viability of Cultured Cells. Cold Spring Harb Protoc. 2016;2016(4):pdb prot087379.

102.   Jeske L, Placzek S, Schomburg I, Chang A, Schomburg D. BRENDA in 2019: a European ELIXIR core data resource. Nucleic Acids Research. 2019;47(D1):D542-D9.

103.   Tweedie S, Braschi B, Gray K, Jones TEM, Ruth, Yates B, Bruford EA. Genenames.org: the HGNC and VGNC resources in 2021. Nucleic Acids Research. 2020.

104.   van Linden OP, Kooistra AJ, Leurs R, de Esch IJ, de Graaf C. KLIFS: a knowledge-based structural database to navigate kinase-ligand interaction space. J Med Chem. 2014;57(2):249-77.

105.   Lovering F, Bikker J, Humblet C. Escape from flatland: increasing saturation as an approach to improving clinical success. J Med Chem. 2009;52(21):6752-6.

106.   Teague SJ, Davis AM, Leeson PD, Oprea T. The Design of Leadlike Combinatorial Libraries. Angew Chem Int Ed Engl. 1999;38(24):3743-8.

107.   Malone T, Schäfer L, Simon N, Heavey S, Cuffe S, Finn S, Moore G, Gately K. Current perspectives on targeting PIM kinases to overcome mechanisms of drug resistance and immune evasion in cancer. Pharmacology & Therapeutics. 2020;207:107454.

108.   Modi SJ, Kulkarni VM. Vascular Endothelial Growth Factor Receptor (VEGFR-2)/KDR Inhibitors: Medicinal Chemistry Perspective. Medicine in Drug Discovery. 2019;2:100009.

109.   Cébe-Suarez S, Zehnder-Fjällman A, Ballmer-Hofer K. The role of VEGF receptors in angiogenesis; complex partnerships. Cellular and Molecular Life Sciences. 2006;63(5):601-15.

110.   Lee SY, Ju MK, Jeon HM, Jeong EK, Lee YJ, Kim CH, Park HG, Han SI, Kang HS. Regulation of Tumor Progression by Programmed Necrosis. Oxidative Medicine and Cellular Longevity. 2018;2018:1-28.

111.   Musumeci F, Radi M, Brullo C, Schenone S. Vascular Endothelial Growth Factor (VEGF) Receptors: Drugs and New Inhibitors. Journal of Medicinal Chemistry. 2012;55(24):10797-822.

112.   Hiratsuka S, Maru Y, Okada A, Seiki M, Noda T, Shibuya M. Involvement of Flt-1 tyrosine kinase (vascular endothelial growth factor receptor-1) in pathological angiogenesis. Cancer Res. 2001;61(3):1207-13.

113.   U.S. Food and Drug Administration. Drugs@FDA: FDA-Approved Drugs. 2021 www.accessdata.fda.gov/scripts/cder/daf/index.cfm. accessed April 13, 2021.

114.   Leung CO, Wong CC, Fan DN, Kai AK, Tung EK, Xu IM, Ng IO, Lo RC. PIM1 regulates glycolysis and promotes tumor progression in hepatocellular carcinoma. Oncotarget. 2015;6(13):10880-92.

115.   Jain P, Karthikeyan C, Moorthy NS, Waiker DK, Jain AK, Trivedi P. Human CDC2-like kinase 1 (CLK1): a novel target for Alzheimer's disease. Curr Drug Targets. 2014;15(5):539-50.

116.   Sako Y, Ninomiya K, Okuno Y, Toyomoto M, Nishida A, Koike Y, Ohe K, Kii I, Yoshida S, Hashimoto N, Hosoya T, Matsuo M, Hagiwara M. Development of an orally available inhibitor of CLK1 for skipping a mutated dystrophin exon in Duchenne muscular dystrophy. Scientific Reports. 2017;7(1):46126.

117.   Martín Moyano P, Němec V, Paruch K. Cdc-Like Kinases (CLKs): Biology, Chemical Probes, and Therapeutic Potential. International Journal of Molecular Sciences. 2020;21(20):7549.

118.   Tam BY, Chiu K, Chung H, Bossard C, Nguyen JD, Creger E, Eastman BW, Mak CC, Ibanez M, Ghias A, Cahiwat J, Do L, Cho S, Nguyen J, Deshmukh V, Stewart J, Chen CW, Barroga C, Dellamary L, Kc SK, Phalen TJ, Hood J, Cha S, Yazici Y. The CLK inhibitor SM08502 induces anti-tumor activity and reduces Wnt pathway gene expression in gastrointestinal cancer models. Cancer Lett. 2020;473:186-97.

119.   Fischer A, Smiesko M, Sellner M, Lill MA. Decision Making in Structure-Based Drug Discovery: Visual Inspection of Docking Results. J Med Chem. 2021.

120.   McTigue M, Murray BW, Chen JH, Deng YL, Solowiej J, Kania RS. Molecular conformations, interactions, and properties associated with drug efficiency and clinical performance among VEGFR TK inhibitors. Proceedings of the National Academy of Sciences. 2012;109(45):18281-9.

121.   Fink SL, Cookson BT. Apoptosis, Pyroptosis, and Necrosis: Mechanistic Description of Dead and Dying Eukaryotic Cells. Infection and Immunity. 2005;73(4):1907-16.

122.   Lim, Greer, Lipkowitz, Takebe. Novel Apoptosis-Inducing Agents for the Treatment of Cancer, a New Arsenal in the Toolbox. Cancers. 2019;11(8):1087.

123.   Harmey JH, Bouchier-Hayes D. Vascular endothelial growth factor (VEGF), a survival factor for tumour cells: implications for anti-angiogenic therapy. Bioessays. 2002;24(3):280-3.

124.   Stepan AF, Walker DP, Bauman J, Price DA, Baillie TA, Kalgutkar AS, Aleo MD. Structural Alert/Reactive Metabolite Concept as Applied in Medicinal Chemistry to Mitigate the Risk of Idiosyncratic Drug Toxicity: A Perspective Based on the Critical Examination of Trends in the Top 200 Drugs Marketed in the United States. Chemical Research in Toxicology. 2011;24(9):1345-410.

VI.   Statutory Declaration

"I, Lisa Chiara Gosch, by personally signing this document in lieu of an oath, hereby affirm that I prepared the submitted dissertation on the topic: *In silico and in vitro investigations on the antiproliferative efficacy of novel tyrosine kinase inhibitors in hepatocellular carcinoma – In silico und in vitro Untersuchungen zur antiproliferativen Wirksamkeit neuartiger Tyrosinkinase-Inhibitoren bei hepatozellulärem Karzinom* independently and without the support of third parties, and that I used no other sources and aids than those stated.

All parts which are based on the publications or presentations of other authors, either in letter or in spirit, are specified as such in accordance with the citing guidelines. The sections on methodology (in particular regarding practical work, laboratory regulations, statistical processing) and results (in particular regarding figures, charts and tables) are exclusively my responsibility.

Furthermore, I declare that I have correctly marked all of the data, the analyses, and the conclusions generated from data obtained in collaboration with other persons, and that I have correctly marked my own contribution and the contributions of other persons (cf. declaration of contribution). I have correctly marked all texts or parts of texts that were generated in collaboration with other persons.

My contributions to any publications to this dissertation correspond to those stated in the below joint declaration made together with the supervisor. All publications created within the scope of the dissertation comply with the guidelines of the ICMJE (International Committee of Medical Journal Editors; www.icmje.org) on authorship. In addition, I declare that I shall comply with the regulations of Charité – Universitätsmedizin Berlin on ensuring good scientific practice.

I declare that I have not yet submitted this dissertation in identical or similar form to another Faculty.

The significance of this statutory declaration and the consequences of a false statutory declaration under criminal law (Sections 156, 161 of the German Criminal Code) are known to me."

Date   Signature

<u>Declaration of your own contribution to any publications</u>

Lisa Chiara Gosch contributed the following to the below listed publications:

Publication 1: Schaller E, Ma A, Gosch LC, Klefenz A, Schaller D, Goehringer N, Kaps L, Schuppan D, Volkamer A, Schobert R, Biersack B, Nitzsche B, Höpfner M, **New 3-Aryl-2-(2-thienyl)acrylonitriles with High Activity Against Hepatoma Cells**, International Journal of Molecular Sciences, 2021;22(5):2243.

Contribution:

Planning and target selection for the kinase assay performed by Eurofins:

- Screening of 43 kinases with 10 µM **1c** (**Figure 5**)
- IC50 determination of **1c** on VEGFR2
- Screening of 6 kinases (VEGFR2, VEGFR1, Pim-1, CLK1, c-KIT, Pim-2) with 10 µM **1a** and **1b** (**Figure 5**)

In silico studies:

- Docking studies of the compounds **1a**, **1b** and **1c** (**Figure 6**)
- Molecular dynamics simulation of **1c** (**Figure 7**) together with Dr. David Schaller

_____

Signature, date and stamp of first supervising university professor / lecturer

_____

Signature of doctoral candidate

VII.   Curriculum Vitae

My curriculum vitae does not appear in the electronic version of my paper for reasons of data protection.

VIII. List of Publications

Journal Publications:

Schaller E, Ma A, **Gosch LC**, Klefenz A, Schaller D, Goehringer N, Kaps L, Schuppan D, Volkamer A, Schobert R, Biersack B, Nitzsche B, Höpfner M. **New 3-Aryl-2-(2-thienyl)acrylonitriles with High Activity Against Hepatoma Cells.** International Journal of Molecular Sciences. 2021;22(5):2243.

Schmitt F, **Gosch LC**, Dittmer A, Rothemund M, Mueller T, Schobert R, Biersack B, Volkamer A, Hopfner M. **Oxazole-Bridged Combretastatin A-4 Derivatives with Tethered Hydroxamic Acids: Structure-Activity Relations of New Inhibitors of HDAC and/or Tubulin Function.** Int J Mol Sci. 2019;20(2).

Conference Poster:

Gosch LC, Schmitt F, Biersack B, Volkamer A, Höpfner M. **Bioinformatic and functional evaluation of novel EGFR-TKIs for the treatment of hepatocellular carcinoma.** Frankfurt Cancer Conference. 2018.

IX.   Acknowledgments